University

of Cyprus

DEPARTMENT OF MECHANICAL AND MANUFACTURING ENGINEERING

POLYMER NANOCOMPOSITES

PREPARED BY ULTRASONIC WELDING

DOCTOR OF PHILOSOPHY DISSERTATION

ANNA CHRISTOU CHRISTOPHIDOU

2015

University

of Cyprus

DEPARTMENT OF MECHANICAL AND MANUFACTURING ENGINEERING

POLYMER NANOCOMPOSITES

PREPARED BY ULTRASONIC WELDING

ANNA CHRISTOU CHRISTOPHIDOU

A Dissertation Submitted to the University of Cyprus in Partial Fulfillment of the requirements for the Degree of Doctor of Philosophy

May 2015

VALIDATION PAGE

Doctoral Candidate: Anna Christou Christophidou

Doctoral Thesis Title: Polymer Nanocomposites Prepared by Ultrasonic Welding

The present Doctoral Dissertation was submitted in partial fulfillment of the requirements for the Degree of Doctor of Philosophy at the **Department of Mechanical and Manufacturing Engineering** and was approved on the August 13, 2015 by the members of the **Examination Committee.**

Examination Committee:

Research Supervisor: Associate Professor Claus Rebholz

_____

(Name, position and signature)

Committee Member: Assistant Professor Andreas Kyprianou

_____

(Name, position and signature)

Committee Member: Associate Professor Theodora Krasia

_____

(Name, position and signature)

Committee Member: Professor Nicolae Crainic

_____

(Name, position and signature)

Committee Member: Dr. Vladislav Ryzhkov

_____

(Name, position and signature)

DECLARATION OF DOCTRORAL CANDIDATE

The present doctoral dissertation was submitted in partial fulfillment of the requirements for the degree of Doctor of Philosophy of the University of Cyprus. It is a product of original work of my own, unless otherwise mentioned through references, notes, or my other statements.

Anna Christou Christophidou

……………………………………….....

Περίληψη

Ο κύριος στόχος της παρούσας διδακτορικής διατριβής είναι η ανάπτυξη και ο χαρακτηρισμός μιας νέας τεχνολογίας, βασισμένη στη συγκόλληση υπερήχων, για την κατασκευή νανοσύνθετων φύλλων πολυμερών (ραφών) που αποτελούνται από στρωματικές διατάξεις με ομοιόμορφα διασκορπισμένα στρώματα διαφόρων νανοσωματίδιων και μικρο-ινών.

Η διδακτορική διατριβή περιλαμβάνει τη σχεδίαση, την κατασκευή και την ανάλυση τεσσάρων διαφορετικών τύπων νάνο και μικρο-σύνθετων πολυμερών υλικών, με διάφορες συγκεντρώσεις ενσωματωμένων σωματιδίων. Για τους σκοπούς του πειραματικού μέρους, χρησιμοποιήθηκαν φύλλα πολυ-βινυλοχλωριδίου (PVC) και κυτταρίνης (CA). Τα ενσωματωμένα σωματίδια περιλάμβαναν οξείδια του σιδήρου, νανοσωληνίσκους άνθρακα και σωματίδια παλλαδίου σταθεροποιημένα σε διάφορους διαλύτες συμβατούς με την πολυμερική μήτρα, καθώς και πλέγματα ηλεκτροκλωσμένων μικροϊνών κυτταρίνης. Η προτεινόμενη διεργασία σύνθεσης των σύνθετων φύλλων πολυμερούς αποτελείται από δύο βασικά στάδια καθώς, αρχικά τα αιωρήματα των νανοσωματίδιων και οι μικρο-ίνες κατανέμονται ομοιόμορφα στις επιφάνειες των φύλλων πολυμερούς ενώ στη συνέχεια ακολουθεί συγκόλληση ραφής υπερήχων. Τα σύνθετα υλικά μελετήθηκαν αναφορικά με τη μικροσκοπική τους δομή και την έκταση της διάχυσης των σωματιδίων μέσα στην μήτρα του πολυμερούς, ενώ στη συνέχεια ακολούθησε ανάλυση άλλων ιδιοτήτων όπως μαγνητικές και μηχανικές ιδιότητες συμπεριλαμβανομένης και της ιξωδοελαστικής τους παραμόρφωσης. Ιδιαίτερα προχώρησε η έρευνα αναφορικά με την ανάλυση των υλικών νανοσύνθετων φύλλων πολυμερικής μήτρας με ενσωματωμένα μαγνητικά νανοσωματίδια. Οι προκύπτουσες ιδιότητες των νέων νανοσύνθετων υλικών δύναται να χρησιμοποιηθούν για ποικιλία εφαρμογών. Είναι σημαντικό να αναφερθεί ότι τα παραχθέντα υλικά αξιολογήθηκαν από την εταιρεία Elysee Irrigation Ltd και ένα εξ αυτών θεωρήθηκε ως χρήσιμο για περαιτέρω

έρευνα και χρήση σε αγωγούς αποχέτευσης και προστασίας καλωδίων στο έδαφος, καθώς λόγω των μαγνητικών του ιδιοτήτων μπορεί να ανιχνευθεί η θέση των αγωγών στο υπέδαφος.

Περαιτέρω, αναπτύχθηκαν δυο μαθηματικά μοντέλα για την κατανόηση βασικών διεργασιών που λαμβάνουν χώρα κατά τη διάρκεια της σύνθεσης των υλικών αυτών με την εν λόγω μέθοδο. Τα μαθηματικά μοντέλα αυτά αποτελούν τη βάση για υπολογιστική προσομοίωση αναφορικά με τον έλεγχο των διεργασιών και των ιδιοτήτων των παραγόμενων με τη μέθοδο της συγκόλλησης υπερήχων, νάνο και μικρο-πολυμερών υλικών.

Abstract

The main objective of this thesis is to develop and characterize a novel production process, based on ultrasonic welding, for manufacturing polymer nanocomposite foils/joints with intermediate "sandwiched" layers of nanoparticles and micro-fibers uniformly dispersed.

The thesis includes the design, fabrication and analysis of four different types of polymer nano- and micro-composite materials with various concentrations of embedded particles. For purposes of the experimental part of this thesis, poly-vinyl chloride and cellulose acetate foils are used. The embedded particles include iron oxides, carbon nanotubes, and palladium nanoparticles stabilized in various liquid carries compatible with the polymeric matrix, as well as electrospun micro-fibers. The proposed synthesis process of polymer nano/micro-composite foils consists of two basic steps; at first the nanoparticle suspensions and micro-fibers are uniformly distributed over the surfaces of the polymer foils, while the second step follows; this is the ultrasonic seam welding. The nano/micro-polymer composites were studied with regards to their microscopic structures (e.g. the dispersion of the nanoparticles and micro-fibers within their matrix), followed by the analysis of their magnetic and mechanical properties, including their response to viscoelastic deformation. Particularly research progress was achieved in the manufacture and analysis of the polymer nanocomposite foils with embedded magnetic nanoparticles. The resulting properties of those novel nanocomposite materials could be potentially used for a variety of applications. It is important to mention that the produced materials were evaluated by Elysee Irrigation Ltd, and the magnetic-containing series was considered to be useful for further research and use in sewage pipes and underground cable protection, since due to their magnetic properties their position can be detected in the subsoil.

Further, two mathematical models were developed for understanding basic processes that take place during the synthesis of such materials with the proposed method. Mathematical models could be used as the basis for further computational simulations in the control of processes and properties of the produced micro and nano-polymer materials.

Acknowledgements

This is supposed to be the end of my long trip to the mysterious path of research. A road which was not smooth and flattened with rose petals but full of exciting memories with opportunities to travel, meet wonderful people, discover new research environments, ways of life and thinking. A road which gave me food for thought, enlarged my horizons, changed the way I think and live, and made me see things from a different point of view.

First I would like to thank my PhD advisors. Associate Professor Claus Rebholz for giving me the opportunity to finish this thesis, as well as my former advisor Professor Charalabos Doumanidis for supporting and guiding me during those years. I have learned many interesting things from them as they gave me the freedom to pursue various projects without objection. They fulfilled me with a deep sense of responsibility which enriches my knowledge and my personality.

I am grateful to Assistant Professor Andreas Kyprianou, member of my thesis committee, for his continue support over all these years and especially for advising my research and giving me his valuable guidance to this final thesis. His advice to the computational part of this thesis was also significant. I am grateful also to the other members of my committee; Associate Professor Theodora Krasia, Professor Nicolae Crainic and Dr. Vladislav Ryzhkov, for giving practical guidance to my PhD thesis and providing me with the nanoparticles I have enclosed in my composite matrices.

I would like to give many thanks to Dr. Zaharias Viskadourakis for his willingness to help out with the magnetic experiments and results. Also, a big thank to Assistant Professor Ioannis Ioannou, Department of Civil and Environment Engineering, for allowing me admission to his lab to carry out mechanical property measurements on my samples.

*I dedicate this thesis to
my parents, my husband, and my daughters
for their constant support and unconditional love.*

Table of Contents

List of Figures

xvi

List of Tables

Chapter 1.   Introduction

1.1 Thematic context

The basic tenet of Material Science and Engineering relevant to technological and engineering applications is that material properties are derived from their structure. Historically, the evolution of "Material Science and Engineering" subject has been governed by the human motivation to understand the structure of materials, unveil the relationship between structure and properties, manipulate the structure to achieve desired properties, synthesise new materials with novel properties and fabricate devices. This thesis describes the research undertaken to experimentally establish whether ultrasound welding, a manufacturing process, could be exploited to fabricate polymeric nano/micro-composites. Moreover, two initial theoretical models have been developed in order to perceive which phenomena occur during the manufacturing process and trigger further investigation.

Materials and their development have been used to label major historical periods such as the so called Stone Age, Copper Age, Bronze Age and Iron Age, which indicates the importance materials have on human lives and the evolution of nature. With the industrialization, around the 1900s, the research for lighter alloys and stronger materials, aluminium, magnesium, titanium, nickel, etc. was made possible. Almost simultaneously with the polymer revolution, which had its beginnings also in the early 20th century, this led to the rapid development of polymer science (1940-1960s) and growth of the sector of composite materials in the mid-1940s when glass-fibre reinforced polymer components were used in the aircraft industry. However, the real transformation of

polymers into high-performance structural materials came with the development of aramid and carbon fibres in the 1960s [1]. Since then, composite materials have been studied extensively and have found diverse applications in engineering.

During the 20th century it was realized by researchers and industry that the behavior of composite materials depended significantly on scale. Polymer nanocomposites (PNCs) open a new dimension for plastics and composites at the beginnings of 21st century [2], as after nanomaterials discovery, it was realized that this dependence was most evident when the scale of the reinforced phase was that of nanometers. PNCs (and materials in general), differ from conventional polymer composites due to the exceptionally high surface to volume ratio of the reinforcing phase and its exceptionally high aspect ratio. It is a fact that the interface area between the polymer matrix and the reinforcement phase is typically an order of magnitude greater than for conventional polymer composites, while the matrix material properties are significantly affected in the vicinity of the reinforcement nanomaterial [3]. The reinforcing materials can vary between nanoparticles, nano-sheets or nano-fibers.

The enormous progress being made worldwide on the standard of living, working, and travelling nowadays has increased the needs for improved and advanced materials. Efficient materials with well-defined and exact properties, such as being stronger but lighter, as small as possible, multi-functional, superparamagnetic, superconducting, biodegradable, able to save recourses at developing stage, to have lower wastes and emissions, with convenient manufacturing and customizable, constitute a very small part of the actual current needs. Accumulating all those needs, science and technology of nanoscale structures is one of the most promising areas for development in the 21st century, and the one that could be described as the nowadays revolution on industrial production route [2-4].

Compared with other matrices, polymers are considered as excellent hosts for nano materials, resulting in nanocomposites that combine the properties of the consisted phases; i.e. the properties of the polymer matrix as well as the properties of the embedded nanoparticles. Several advanced PNCs have been synthesized in recent years, with a wide variety of nano-inclusions, such as metals, semiconductors, carbon

2

nanotubes, and magnetic nanoparticles [5-7]. The developed polymer nanocomposite materials combine the attractive properties of polymers, such as light weight, high conformability, easy processing, low cost, non-corrosiveness and dielectric tunability, along with mechanical (stiffness, strength, dimensional stability), electrical, thermal, optical, biological, chemical, electrochemical properties of the nanoparticles [8-10]. Moreover, the PNCs have the potential for upgrading their properties regarding information storage, heat resistance, resistance to wear and damage, resulting to the development of totally new materials with unforeseen capabilities.

1.2 Proposed research - Originality and innovation

The long-term goal of this research is to develop and characterize a manufacturing process that introduces a novel technology for manufacturing multifunctional PNCs, combining various functionalities with structural integrity. For that purpose a processing method has been developed to fabricate polymeric nanocomposites reinforced with iron oxide (Fe_3O_4) and palladium (Pd) nanoparticles, carbon nanotubes (CNTs) and cellulose acetate (CA) microfibers uniformly dispersed in a poly(vinyl chloride) (PVC) and cellulose acetate (CA) resins, respectively. The new materials were characterised by different testing methods.

PVC was chosen as polymer matrix in this thesis, since it is suitable for various industrial applications, because it has good mechanical properties, resistance to different environments (acidic and basic), fire retardancy, easy processibility and low cost [11-12]. Also, inclusion of magnetic nanoparticles in polymers is especially important, as such nanoparticles have shown promise in various potential applications such as hard disk drives, magnetic random access memory, magnetic bearings and biomedical actuation devices [13-14]. Pd nanoparticles are also promising elements for the development of chemical sensors as they can selectively detect different kinds of gases and liquids [15-17]. CNTs on the other hand can enhance the mechanical properties of those polymers [18].

CA as well as CA/polyaniline (PAni) microfibers are the other materials employed

in this study, since they attract the interest of many research teams and of this project also in order to manufacture biodegradable micro composite foils. This is because of their renewable, biodegradable and environmentally benign nature, as they are polymeric excipients; such as films, membranes and fibers. CA membrans are widely used in pharmaceutical dosage forms of controlled liquid release and test masking, while it is one of the most suitable polymer membranes for osmotic drug delivery system [19-21]. Moreover, CA microfibers have outstanding mechanical properties and are useful for a wide range of applications, such as filters, protective clothing, artificial tissue (skin), and in many other high-tech applications [22-24].

Ultrasonic welding is a very effective technology, both technically and economically, for joining polymer parts. It is the most commonly used welding process for thermoplastics, because it is very fast with low cycle times, is easily automated, and it repeatable produces high quality joints. It finds plentiful applications in industry, including consumer products, automotive parts, appliances, electrical products, toys, packaging and medical products [25-26]. Moreover, and despite the fact that the ultrasonic welding process is widely spread in the industry, there are limited references in the literature that concern ultrasonic welding of polymer composite materials [27-35]. Furthermore, there are no papers available on the in-situ production of polymer composite or polymer nanocomposite materials with the method of ultrasonic welding.

Research hypothesis - Originality. A proper combination of the above mentioned materials and method has as a result a novel technology for manufacturing nano and micro-composites, from stacked polymer foils with intermediate sandwiched layers of uniformly dispersed nanoparticles and micro-fibers, by means of solid-state ultrasonic welding. This is a new method to obtain technologically advanced polymeric foils with good mechanical properties, low-cost equipment and raw materials, short production cycle, consequently short manufacturing time, and based on first time using ultrasonic welding procedure for production of nanocomposite structures [36-38]. Furthermore, two initial computational models have been developed. The first model's aim was to describe/examine the dispersion/movement of nanoparticles into the polymer matrix due to the ultrasonic welding vibratory forced motion in order to determine the final distribution of nanoparticles into the heat affected zone (the weld). The second model's

4

aim was to examine interfacial velocity of CNTs and PVC with molecular dynamics, in order to investigate the phenomena occurring while manufacturing those nanocomposites.

Chapter 2.   Literature survey and motivation

2.1 Polymer nanocomposites

PNCs are multiphase systems that consist of polymers or copolymers (e.g. thermoplastics, thermosets, or elastomers), having inorganic or/and natural particles as additives/fillers with at least one dimension in nanoscale; that means less than 100 nanometers, dispersed in the polymer matrix. The final product can be on the nano-, micro- or macro-scale. Nanoparticles or "nanofillers" may be of different shapes, typically layers, fibers and spheres, and different than polymer materials such as carbon, graphite, metal, and clays. The different parts remain distinct from each other after joining and the nanocomposites exhibit properties of all individual phases.

There are many factors that affect polymer nanocomposite properties [39]. Selecting a proper synthesis method is one of the most important one in order to achieve the best and optimum properties of the final nanocomposite products. Their properties are also strongly depended on the compatibility between the polymer matrix and the reinforcing nanomaterial. Critically important are also the properties of the constituent phases such as the polymers chain morphology, its crystallinity, molecular weight and chemical composition, if the polymer is thermoplastic or thermosetting, in conjunction with the size, type, shape, geometry and the surface of the dispersed phase [3, 40]. In order to achieve the optimum result, their relative amounts should be also considered. Usually the smaller, symmetrical and properly distributed in the matrix the nanoparticles are, better properties are achieved, since the final product becomes more homogeneous.

PNCs offer significant advances and remarkable changes in their properties when compared with traditional polymer composites, since they exhibit multifunctional and high-performance characteristics. This happens due to the fact that the transition to nano-sized particles leads to dramatic changes in their physical, as well as their chemical properties and enhance their performance [41-42]. The enormous increase in the ratio of the surface area to volume of the two consisting parts, as a result of the nano size of the particles, in combination with the particular properties of the nanoparticles is the reason for this [43]. However, the smaller the reinforcing materials are, the larger is their internal surface and as a consequence their tendency to agglomerate rather than to disperse homogeneously in the polymer matrix. Good and proper dispersion of the nanomaterial must be achieved in order to have the optimum properties [44]. Poor dispersion of the reinforced nanomaterial will degrade the properties of the final product. Moreover, nanoparticles can also significantly affect the glass transition temperature (Tg) of the nanocomposites, since nanoparticles influence the mobility due to the bonding between them and the polymer matrix, as well as due to changes of the polymer chains morphology.

A relatively small concentration of nanoparticles can have a perceptible effect on the properties of the nanocomposite. Actually, PNCs can achieve the desired properties usually with very low concentrations in the order of 0.5-5 wt.% reinforced nanoparticles, compared to those achieved by conventional loadings, which is in the order of 15-40 wt.% of traditional fillers [39]. This is an additional reason for lower cost, lighter and more delicate final products.

2.2 Polymer nanocomposite evolution - From laboratory to industrial production

Over the last three decades investigations are turning to new materials that could be synthesized easily and economically, with improved properties or combinations of properties that best suit the target of each different use. The development of polymer nanocomposite materials, as discussed in the previous section, has solved the need for even more improved materials, with better, more specific and finally unique properties. It is important to recognize that laboratory research on PNCs resulted in applications in a

broad range of consumer products, in areas such as electronics, computing, data storage, communications, aerospace engineering, sporting goods, products of the health sector, medicines, energy efficient, environmental and transportation. Furthermore, numerous products utilizing nanoscale materials are currently available in many applications in the automotive, textile, cosmetics, paints, food packaging and other fields [5].

By making a brief historical review, in 1991 Toyota Central Research Laboratories in Japan, reported work on a nylon-6/clay nanocomposite [45]. That was the time when commercialization of PNCs started and were first introduced in the market, in order to produce timing belt covers as a part of the engine for Toyota Camry cars, in collaboration with Ube industries [45]. Those first nanocomposites had a very small amount of reinforced nanoparticles that resulted in a pronounced improvement of thermal and mechanical properties. Following Toyota, a number of other companies also began investigating nanocomposites for use in certain applications. About the same period, Unitika Co. of Japan introduced a nylon-6 nanocomposite for engine covers on Mitsubishi GDI, manufactured by injection molding, which offered a 20% weight reduction and excellent surface finish [46]. In 2002, General Motors, in collaboration with LyondellBasell Industries, launched a step-assist automotive component made of polyolefin reinforced with 3 wt.% nanoclays, for GM's Safari and Chevrolet Astro vans, followed by the application of these nanocomposites in the doors of Chevrolet Impalas [47]. Since then, nanocomposites have gained tremendous acceptance in the automotive market, for the production of external and interior body parts, various coatings, fuel lines and fuel system components, in order to reduce vehicle's weight, improve engine efficiency and fuel saving, reduce CO_2 emissions, upgrade cars safety, increase their comfort, achieve better drivability and superior car performance [48].

The aerospace industry was the other major user of nanocomposites, searching for advanced structural materials, with high performance and light weight. The aerospace industry began taking advantage of the high strength-to-weight ratio associated with composites by replacing aluminum parts with composites about 50 years ago. The main aim of the introduction of lighter and stronger materials into airplanes was to reduce aircraft weight, and increase their efficiency, by saving fuel and therefore costs. In addition to lower weight, composites were also attractive to aircraft engineers because

8

their resistance to corrosion, fatigue performance, better design, flexibility and lower assembling cost when compared with metals [49-50]. Moreover, nanocomposites find very important applications in aircrafts and even aerospace field when used in laminates and sandwich structures, while they are also commonly used at anti-lightning and anti-radar protectors, and paints [51]. More specific, the A380, which has the lowest percentage of aluminum by weight of all flying Airbus models, has twenty different alloys and tempers compared to the A320/330 aircraft. The A380 also saw the application of a new composite material for fuselage skins which show improved fatigue and impact properties at a lower density than conventional materials [52]. Significant increases in the amount of composite parts has occurred with the Boeing 787 Dreamliner, which mostly consists of carbon fiber reinforced polymers; in the area of 80% [53-54].

Automotive and aerospace industries and engineering was just the beginning for the research concerning polymer nanocomposite materials. Since then, extensive research in the field of their properties has been carried out, with high industrial importance, while many different polymer nanocomposite materials have been produced for a great variety of applications and commercial products.

2.3 Existing methods for preparation of the polymer nanocomposites and the challenges for new technically advanced methods

As a general observation it can be stated that the PNCs are mainly built by "step by step" procedures, while some of them are produced by similar methods that are used for the synthesis of conventional polymer composites. The existing methods for synthesizing PNCs mainly includes blending processes i.e. solution and melt blending, and sol–gel methods (in-situ preparation) [55-63]. Furthermore, there are various other methods for producing PNCs such as emulsion polymerization, photopolymerization, metallo-supramolecular polymerization and coordination approaches, intercalation, microwave irradiation, surface grafting, self-assembly and block copolymer-mediated synthetic processes [60].

As the needs for producing PNCs are growing day by day, the synthesis methods of

such materials are also developed. The employed synthesis method mainly depends on the polymer matrix properties such as its chemical composition, crystallinity and molecular weight, while the nature and the associate properties of the nanoparticles intended to introduce into the polymer matrix are also of considerable importance. The properties and the use of the polymer nanocomposite final product constitute a further important criterion.

The majority of the polymer nanocomposite production with the pre-mentioned methods is limited to the use of nanomaterials in bulk products and foils, at the stage of polymer synthesis. As a result, the nanoparticles are distributed all over the nanocomposite material. Since exfoliation, good orientation, lack of agglomerations, as well as the need for very small, clean nanoparticles with excellent properties and compatibility with the polymeric matrix are important for the final product, the materials prepared are synthesized in limited quantities and their cost is high. Actually it is a technical challenge to achieve the perfect structure with the lowest cost and the right quantities. Low and local use of nanoparticles according to the real and specific needs of the final product is another nowadays' challenge.

2.4 Existing methods for joining polymers and polymer composites - Process selection

Polymeric parts can be joined successfully together in a number of different ways, including mechanical fastenings, solvent and adhesive bonding, and fusion bonding with different welding techniques [26, 64-67]. Each technique has limits on the sizes and types of polymers that can be joined, advantages and disadvantages, which are briefly analyzed below.

Mechanical fastening methods include screws, bolts and rivets and offer one of the simplest, least expensive, most reliable and commonly used joining method for assembling polymeric parts [68]. Only stronger plastics are suitable for this method since the joint must endure the strain of the assembly, the load, and possible repeated use. This method is suitable only for lightly loaded, non-rigid assemblies where precision is not critical.

Solvent and adhesive bonding are probably the most inexpensive joining methods for preparing permanent bonds [68]. The main principle of solvent bonding is that it joins polymers that are dissolvable with the same solvent. This process usually involves treating of the bonding area with the minimum amount of solvent needed to soften the surfaces, then the parts are clamped together under pressure until the bond is completed. However, this is a slow process and not suitable for large scale manufacturing. Adhesive bonding uses commercially available materials that are specifically formulated to bond polymeric parts to themselves or other substrates. Adhesive bonding is easy to carry out in the laboratory, but the disadvantage of this method is that foreign materials are introduced into the polymer microstructures, resulting in inhomogeneous surfaces. This method is particularly used to join thermosets.

Fusion bonding's main principle is that the interfaces of the polymers are heated with different mechanisms to their viscous state under pressure, in order for the polymer chains to inter diffuse physically to each other [66]. When the polymer cools down to room temperature, the bond is generated and the various parts are joint together. Fusion bonding techniques can be classified based on the type of the heat generation mechanism, to (a) thermal welding; such as hot gas welding and laser welding, (b) electromagnetic welding; such as induction welding and dielectric welding, and (c) friction welding; such as vibration welding and ultrasonic welding [66]. Thermal welding methods need an external source of heating the polymer in order to melt the surfaces of the joining parts so that they can be jointed together. This makes the microstructure easy to collapse or deform during the bonding, causing polymer degradation. This is the main reason for not being suitable for sensitive polymeric foils, embedded with nanostructures. In electromagnetic welding, different high-frequency electromagnetic fields are used directly to the interfaces, in order to produce heat to melt and fuse the polymer parts together to create the joint. The main disadvantage of these methods is that they are expensive with high equipment cost and welding procedure; moreover, the presence of different welding additives that remain within the joint can affect its strength.

Finally in friction welding, the last category for fusion bonding, there is no need for external heat generation to joint polymeric parts together, while the required heat is generated by mechanical friction of the surfaces to be joint together [66]. It is a quick

process, in the order of a few seconds, and easy joining, combined with direct heat input into the weld interface, leads to relatively good joints. Dissimilar materials can also be joined together, while it produces joints without extra weight.

Good assemblies are mostly affected by the selection of the proper joining method which substantially is depended on the use of the final product; as well as its geometry, the environment where it will be used (ambient or chemical), the mechanical loading and stress that the final product will front. The selection of the proper polymer combined with a fundamental knowledge of joint design is the key.

According to all the above mentioned, as well as the need for high-performance materials and the need for the introduction of nanoparticles into polymeric matrices for producing polymer nanocomposite materials suitable for various uses; such as for aerospace and automotive industry, made this thesis to focus on fusion bonding techniques, and specifically to ultrasonic welding. As a result, it is expected to synthesize an ideal structure for those purposes without joints, since joints are potentially sources of weakness and additional weight. Since ultrasonic welding is the most widely used joining technique for thermoplastics that produces permanent and aesthetically pleasing joints, as well as it has short bonding duration and local heating, these were the main reasons for the purpose of this research. Comprehensive information about ultrasonic welding follows.

2.5 Ultrasonic welding process and equipment

Ultrasonic welding is a very effective technology, both technically and economically, to join polymer parts. It is the most commonly used welding process for thermoplastics because it is very fast with short cycle times in the range of just a few seconds, is easily automated, it repeatedly produces high quality joints, and consists of comparative cost effective machines. It can be characterized as the joining technique with no additional or foreign substances, such as adhesives and solvents. It introduces well defined local heating only at the joint area. It finds plentiful applications in industry, including consumer products, automotive and aerospace engineering, appliances,

12

electrical products, toys, packaging and biomedical substances [26-27], in a huge variety of shapes and sizes matrices, starting from blister packs up to car fuel tanks, dashboards and aircraft shafts.

Technically ultrasonic welding is a solid state process in which materials are welded by locally applying high-frequency vibratory energy to a joint held together under pressure [69]. It is a versatile technique which, with the appropriate design of the fixtures and parts, can be used in mass production. It eliminates the costs associated with the conventional sewing methods and it allows making different patterns without reducing the productivity or the quality of the joint. Both, frequent use in different production lines and the fact that is easy to use, make ultrasonic welding an excellent choice as a process to study for producing PNCs, with an entirely new method, in order to fabricate new materials for many different applications.

In order to meet requirements for industry, ultrasonic welder machines are manufactured into a range of sizes and styles to suit various applications. They are available from small handheld units, into stand-alone semi-automatic assembly stations, or fully automated assembly lines, and can occur different types of welding, such as continues and spot welding modes [69]. The main difference in the spot welding mode is that the parts are placed under the horn until a welding cycle is finished, while in the seam welding mode the polymer passes under the horn on a continue basis. An ultrasonic welding machine usually consist of a high frequency power supply, a converter, a booster, a welding horn, pneumatic pressure system, anvil, weld and hold time controllers and a fixture for holding the parts [27, 70-71]. Typical components of an ultrasonic welding system are presented in Figure 2.1 [72].
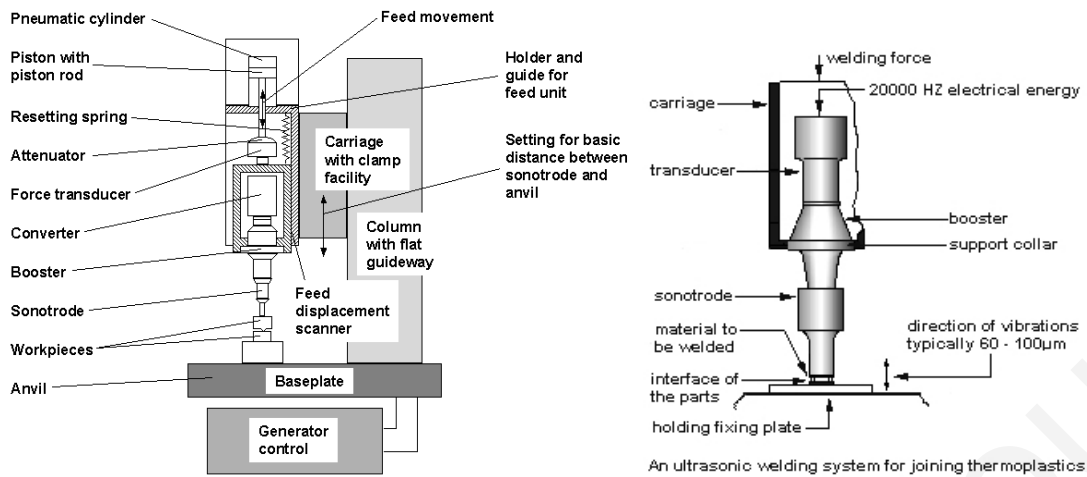
Figure 2.1 Schematic drawing of an ultrasonic welding machine [72-73]

The operation method of an ultrasonic welder is quite simple and is illustrated in Figure 2.2. The power supply or the generator, transforms the simple 50 or 60 Hz electrical power to the desired high frequency electrical energy usually 20 or 40 kHz, while for bonding foils and plates, the frequency most commonly used is 20 kHz [74-75]. Higher frequencies tend to be used with small, delicate parts because of the low-amplitude characteristics of high frequency systems. The high frequency electrical energy is then conducted to an electro mechanical converter, the piezoelectric transducer, where high frequency electrical oscillations are transformed into mechanical vibrations with amplitude of 20 to 60 μm. These mechanical vibrations are then transferred to the polymer part via a waveguide assembly. The horn is pressed against the polymer parts to be joined together by a pneumatic pressure system so that vibrations are introduced to the matrices under the action of force. The vibrations are transmitted through the polymer parts, and travel uninterrupted until the interface of the joining polymers, where friction heat is generated from the complex shear and compressional waves, that causes the contacting surfaces to melt and fuse to each other. At that moment ultrasonic energy is stopped, the applied pressure is holding the parts together for some more fractions of second in order to give time to polymer to re-solidify. The direction of these horn vibrations is usually perpendicular to the polymer.
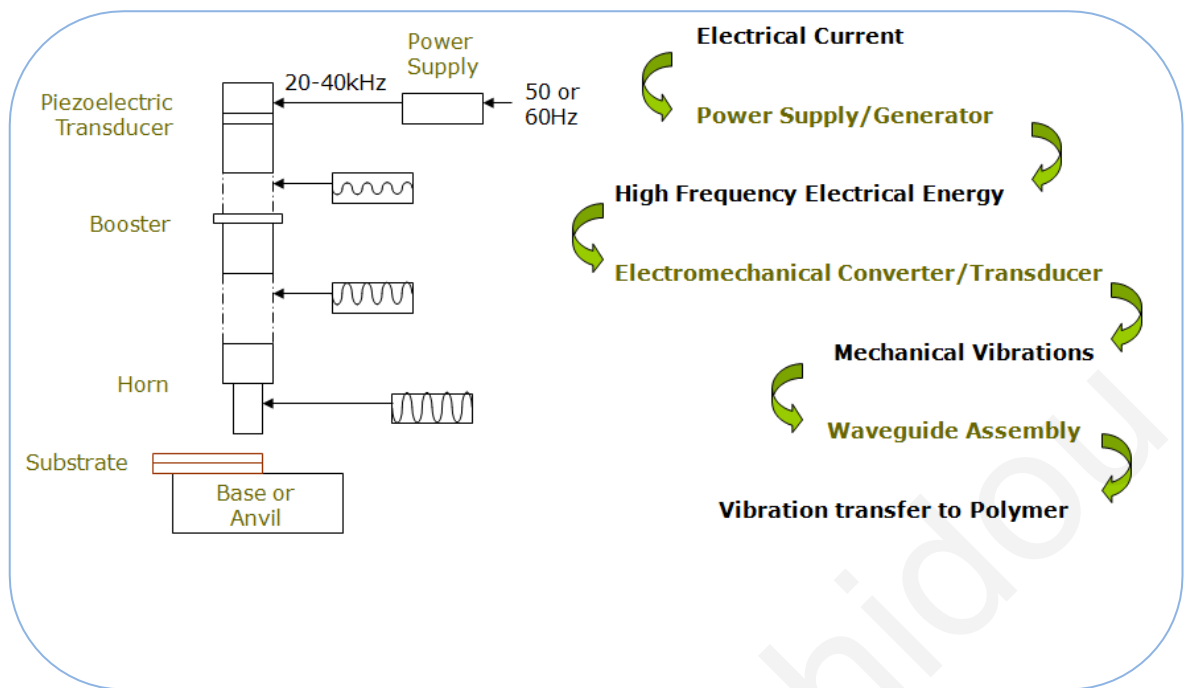
Figure 2.2 Schematic diagram of the conversion of the electrical energy to mechanical motion during ultrasonic welding procedure [76]

There is a strong correlation between bond quality and ultrasonic welding parameters, including welding time, welding pressure, vibration frequency, horn amplitude and holding time [77-80]. Welding time and horn time controllers are available in different types depending of the polymer parts to be joined; welding time is the amount of time for which the actual welding process or ultrasonic vibration is active. In general, by increasing the welding time, the energy dissipation also increases, as well as the weld strength, until an optimum time is reached. Moreover, the welding pressure provides better energy transfer and melt-flow at the interfaces and improves the weld strength until an optimum value [77].

Converter and booster are designed at a specified frequency and are kept unchanged for most applications. Since the output surface of the horn should match the welded polymer for efficient energy transfer, the lateral dimensions and profile of the horn are determined by the size and its shape [81]. Because of the complexity of horn structure, most of the work on horn design has been conducted with finite element methods and in order to calculate its resonant frequency and vibration mode, and to predict its dynamic performance [82]. Moreover, the anvils are made to have various patterns to produce fabrics with different bond designs and dimensions.

In many ultrasonic welding procedures, energy directors are used. The energy directors are polymeric materials molded on one of the joint surfaces and their primary function is to concentrate the energy to rapidly initiate the softening and melting of the joining surface [26, 34, 77, 83]. The energy director, which has the smallest cross section and therefore the highest strain, heats, melts and flows to both fill the interface with molten polymer and fusion joint parts. It usually has a triangular shape, is mainly used in big structures and its use results in lower welding times. A typical process diagram of the mechanism of melting of an energy director, while ultrasonic welding procedure, is illustrated in Figure 2.3.
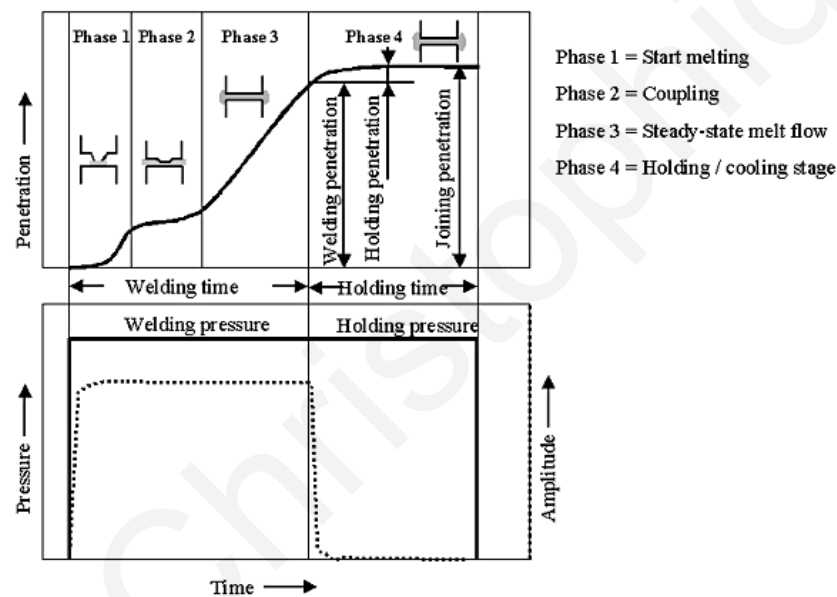
Figure 2.3 Process diagram of the ultrasonic welding procedure using energy director [74]

2.6 Energy transformation and polymer chains redistribution while ultrasonic welding

When two similar pieces of polymers are brought together under ultrasonic welding, the temperature on their surfaces must be higher than a critical; this is their glass transition temperature (Tg), in order to make the polymers soften, flow and weld. The main principle of ultrasonic welding is based on the fact that vibrations are transmitted through the work piece to the joint area, where vibratory energy is converted to heat through friction of polymer chains and meld. After this, the molecules near the surfaces become mobile, and the weld strength develops by a combination of surface

16

rearrangement, wetting and diffusion [84]. In fact, the polymer chains can then migrate and entangle each other, while the matrices continues to be pressed together until they re-solidify, and the bond is made (Figure 2.4). No external heat source is required, and also no glues or softeners are used, since adhesives are potentially sources of weakness and additional weight. The heat generated by internal damping, which is highest at the surface due to its roughness, while is sufficiently high to melt the polymers and bond the parts together. Energy dissipation is concentrated in the weld zone by providing a line contact between the joining parts; this is the weld affected zone. The ultrasonic vibrations cause the largest deformation at points where the supporting structure is the weakest.
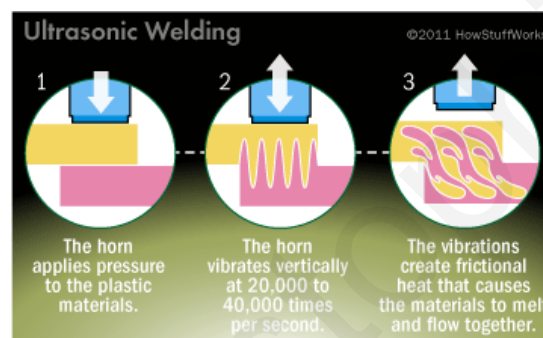
Figure 2.4 Diagram of ultrasonic welding of polymer foils [85]

Much work has been done by researchers in order to explain the mechanism of polymer joining under ultrasonic welding [80]. According to Land [86], the welding process, in a typical ultrasonic welding procedure of thermoplastic matrices, occurs in stages, rather than continuously.

2.7 Polymers suitable for ultrasonic welding

Among the three main polymer families namely thermoplastics, thermosets and elastomers, the thermoplastics also known as "thermo-softening" or "engineering" or "technical" plastics, are generally able to go through many repeatable cycles of melt when heated, to solid state when cooled, with no considerable dimensional or chemical change over a wide range of operational temperatures and pressures [87]. This is the main difference to thermosets and elastomers, and the most significant reason that makes

them suitable to be used in various manufacturing techniques, including ultrasonic welding [88-89]. In contrast, thermosets are materials that once formed undergo an irreversible chemical change, cannot be reformed with the reintroduction of heat and pressure, and therefore cannot be ultrasonically assembled in the traditional sense. Elastomers are also poor candidates for ultrasonic welding procedures because their rubber structure reduces their ability to transmit ultrasonic vibrations, resulting in the need for higher amplitudes in order to generate melting. Moreover, thermoplastics are chosen for the purposes of the experiments in this thesis because they can be characterized as polymers that meet higher and improved performances such as heat resistance and impact strength.

PVC as well as CA foils are thermoplastic polymers which can be joined together under ultrasonic welding, with a medium difficulty according to manufacturers [90]. Both have many potentials since they are suitable and already used in a wide variety of industrial applications, due to their interesting properties, as analysed in Chapter 1. Moreover, they are versatile thermoplastics that can be easily functionalized and reinforced with various nanoparticles in order to produce nanocomposites with desired properties. PVC nanocomposites embedded with CNTs, carbon black, calcium carbonate and iron oxides; mainly by in-situ polymerization, with improved properties, have been the aim of research in the recent years [91]. Furthermore, a comprehensive review regarding the method of preparation, the properties and the applications on "smart" materials based on cellulose was published by Xiaoyun and Shuwen [92]. Detailed information about PVC and CA are summarized in a variety of literatures and books [93-95].

2.8 Nanoparticles and microfibers suitable for manufacturing nano and micro-composites by means of ultrasonic welding

Recently, substantial progress has been made in developing technologies in the field of magnetic nanoparticles aiming to be included into various polymer matrices. Ferromagnetic fluids, also called ferrofluids, are a special category of nanomaterials which exhibit magnetic properties, comprised of very stable colloidal suspensions of magnetic

nanoparticles such as iron oxide particles in various liquid carriers. The very fine magnetic nanoparticles with diameters usually equal to 5 to 7 nm are stable colloidal structures dispersed in various liquid carriers.

Fe_3O_4 nanoparticles are chosen to be enclosed as additives into the PVC polymeric foils in order to increase/control the magnetic properties of the polymer matrix, and therefore to investigate the creation of composite materials for many different applications such as data storage, magnetically actuated diaphragms in biomedical devices (e.g. stents), sensors and magnetic shielding for electronic and armament industry. Not all nanoparticles are suitable for such use; however, magnetic fluids (MF) provide the ability for ultra stabilized and well-dispersed nanoparticles, ready for use in specimens produced in this thesis [96-100]. Magnetic fluids have been prepared in polar carriers, such as short-chain-length alcohols and water, so one can avoid particle agglomerates because of Van der Waals attraction, as well as to be compatible with PVC.

CNTs are graphene-based structures which consist of graphene cylinders enclosed to each other, and can be considered as single molecules or micro-crystals regarding their small size; their diameter is equal to ≈nm up to ≈μm its length. They can occur in two different forms, the single-wall and the multi-wall CNTs. They are also employed in the experiments in this thesis because of their remarkable mechanical, conductive and other physical properties [3, 101]. These properties, in combination with the need of very low content of CNTs in the final product, makes them ideal candidates for high-performance PNCs [102-103]. Adding CNTs to conventional polymeric matrices can undoubtedly provide significant improvements in various properties, such as electrical conductivity, mechanical strength, thermal stability and many other [104-105]. Uniform and homogeneous dispersion of CNTs in the polymer matrix is required in order to achieve the best possible results, while the availability of high quality (high crystallinity) of them in sufficient quantities is also of critical importance [106-107]. Without proper dispersion, carbon nanotube aggregates tend to act as imperfections into the polymer matrix, resulting in limitations in their mechanical performance, which negatively influence the physical properties of the nanocomposites. Other factors that affect the properties of the final nanocomposites include orientation and distribution of CNTs into the polymer matrix, the manufacturing method, the surface behavior and adhesion between the

polymer matrix and the carbon nanotube [108].

Different processing methods have been used so far in order to synthesize CNT-PNCs, as these have been described in Chapter 2.3 [109-113], while there are quite limited references in the literature related to synthesis of PVC reinforced with CNTs nanocomposites [108, 114-117]. Again, there are no references available regarding the manufacture of CNT-PNCs by means of ultrasonic welding.

A great deal of attention has been paid over the last years to CA micro/nano-fibers as components in composite materials, because of their wide abundance, their renewable, biodegradable, biocompatible and environmentally being nature, and their good mechanical properties with high levels of strength and stiffness per unit of weight. Concerning that, many studies have been carried out on existing cellulose microfibers from various sources with a view on using them as reinforcement in composite manufacturing [22-24, 118-119]. A CA as well as CA/PAni micro fibril structure is the material employed in this study in order to be introduced as reinforcement in CA foils, by means of the ultrasonic welding.

2.9 The evolution of computational analysis for ultrasonic welding

The ultrasonic welding process, as described in detail above, has been developed for almost five decades and is widely used in the polymer industry with many different applications. Different studies for the ultrasonic welding process have been carried out, resulting in different theoretical and mathematical models that focus on different localized solutions, mainly raised from industry. Most of the analytical solutions (models) that have been designed so far, focus mainly on the heating and bonding mechanisms of thermoplastics and their effect on bond strength, by analyzing the joint quality during the ultrasonic welding procedure. The effects of welding parameters such as the energy that is transferred into the welding area (energy input) as a function of static pressure, welding time, boosters amplitude of vibration, frequency etc. have been studied. Extensive work has been done by researchers in order to clarify the role and model the geometry and the proper design of the energy directors in order to produce the proper

welds [80, 83, 120-125]. Moreover, there is only a limited number of publications available that model the ultrasonic welding procedure of composite thermoplastics [28, 126-127]. As the demand for polymers increases, the requirements for joining by means of ultrasonic welding increases also and therefore the need for more comprehensive simulations.

It is important to mention that there are no references available on the dispersion of nanoparticles into a polymeric matrix due to ultrasonic welding, since this is the first time ultrasonic welding has been used in order to manufacture nanocomposite materials. The ability to predict the behavior of a material is of fundamental importance for all engineering and design applications as its role is important with regard to optimizing the processes and the final products and save sources, money and time.

2.10 Molecular dynamics - Carbon nanotubes

Molecular dynamics is a form of investigation where virtual atoms and molecules, which interact for a certain period of time under the known laws of physics, are studied. Today, it is automatically assumed that these virtual representations are numerical and their evolution is calculated in the microchips of a computer. Early molecular dynamics studies involved physical substitutes of atoms like steel spheres, seeds or gelatin balls. These early attempts gave relatively good results, but were limited by the concrete difficulty of handling a large number of physical objects and also by the fact that gravity can never be eliminated. The natural evolution of this approach was to use mathematical rather than physical objects and calculate their motion through numerical procedures. The first computer code envisaged for this task was made in 1953 by M. Tsingou and, although she does not appear in the list of authors, it was used to carry out the calculations of the Fermi-Pasta-Ulam paper [128]. Since then, the theory and the application of molecular dynamics have developed quickly, driven by advances both in numerical techniques and in computer hardware.

Over the last years many simulations employed molecular dynamics to investigate interactions of polymer systems and carbon nanotubes, since there are many potentials

regarding the inclusion of carbon nanotubes into various polymer matrices. Those simulations at first were simple, but in the very recent years are much more complex and demanding, due to the development in the field of computer science. The interactions between the polymer matrix and the CNTs, the probable chemical reactions that occurs in their interface (the interfacial bonding) and shear strength development, as well as the elastic properties of the interfacial region, are only some of the demands that molecular dynamics should respond [129-133]. Studies in this field are not able to show macroscopic nanocomposite properties, but they are able to develop an obvious view of the interfaces of the composed parts. The proposed simulations in this thesis were carried out in the period from 2007 to 2008.

Chapter 3.   Manufacturing of polymer nanocomposites by means of ultrasonic welding

3.1 Introduction - Outline of experimental procedure

The main objective of this Chapter is to present the experimental procedure for manufacturing several polymer nano/micro-composites from stacked polymer foils with intermediate sandwiched layers of nanoparticles/microfibers respectively, by means of solid-state ultrasonic welding. Moreover, the ability to distribute/disperse the nanoparticles/microfibers homogeneously all over the polymer matrix surface is of prime importance and is also being studied in this Chapter. The importance is based on the fact that in this manner proper conditions are employed to establish the further dispersion of nanoparticles/microfibers within the polymeric matrix and consequently to manufacture ideal nanocomposites.

The experimental procedure that is follows can (in most cases) be divided into two main steps and is quite simple for the proper nanoparticles and foils to be joined together. Succinctly, in the first step the liquid suspensions with included nanoparticles are deposited onto the polymeric foils surface via a spin coating technique; in the case of micro fibers, they are just manually laid out and deposited onto the polymeric foils. After the surfaces dry out, the second step follows, which includes the joining of the polymeric foils with the included nanoparticles/microfibers with the ultrasonic welding machine and thereby the manufacturing of nano/micro-composites. A simplified diagram of the

experimental procedure that was employed is presented in Figure 3.1. The heat affected zone is defined in this thesis as the interface between the two polymer foils which melt and re-solidify due to ultrasound in order for the weld to occur and it is shown in Figure 3.1b as transversal stripes which are starting from the interface and are extended to the outer surface of the two polymeric foils. The width/penetration of the nanoparticles is defined as the depth of the dispersed nanoparticles into the polymer matrix and it is shown in Figure 3.1b as small black continuous dots. Comprehensive information and experimental conditions follow below in this Chapter.
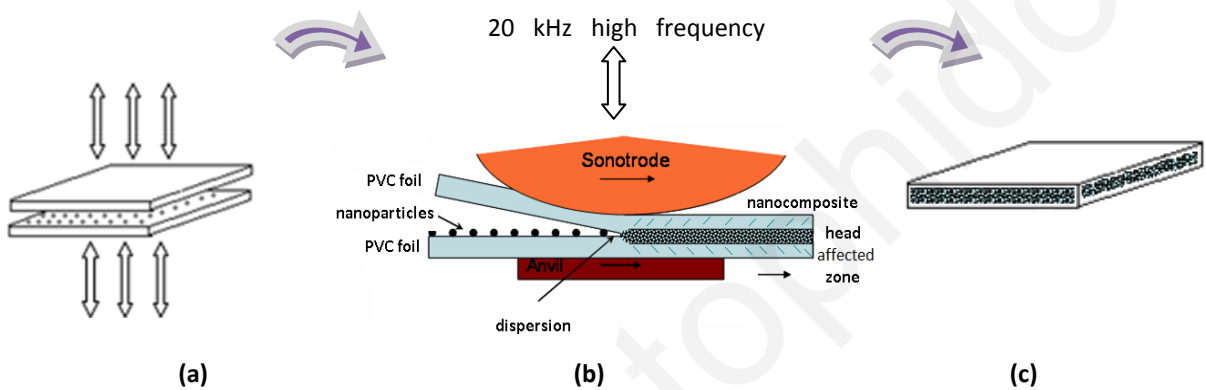
Figure 3.1 Simplified diagram of manufacturing polymer nanocomposites by means of ultrasonic welding, (a) dispersion of nanoparticles/microfibers onto polymer foil surfaces, (b) polymer ultrasonic welding, (c) manufactured nanocomposites

Moreover and prior to the above described procedure, the proper synthesis parameters were investigated, since this is the key to achieve best and optimum properties of the prepared nanocomposites. In fact, the difficulty of this research was in the selection of proper polymeric materials along with achieving best possible nanoparticle dispersion, in response with the determination of the optimum welding parameters, in order to produce appreciable nanocomposites with improved properties. These arise from the fact that polymer nanocomposite properties/quality are affected from various factors, as this explained in detail in Chapter 2. As a consequence, the finding of the appropriate particles as well as the archiving of proper welds to fulfill the thesis main goal was the most challenging part of the research.

The tasks of the manufacturing procedure of polymer nano/micro composites by means of ultrasonic welding are the following:

1. Welding of different polymer foils (matrices) according to their ability to be joined by an ultrasonic welding procedure.

2. Supply and/or composition of different nanoparticles/micro fibers, suitable with the chosen polymer matrices and compatible for ultrasonic welding procedure.

3. Uniform deposition of the nanoparticles/micro fibers onto the polymer foils, confirmed by microscopic analysis.

4. Determination and application of optimum conditions of welding.

5. Development of polymer nano/micro-composites with the best possible dispersion of nanoparticles/microfibers into the polymer matrix.

After many experimental trials, PVC and CA foils were chosen as the substrates, while various magnetic (Fe_3O_4-containing) ferrofluids, palladium and carbon nanotube suspensions, as well as CA microfibers were selected as sources of nano and micro-particles, respectively, resulting in the manufacturing of several nano/micro-composites.

3.2 Selection of polymer matrices after experimental ultrasonic welding of different thermoplastic foils

Several tests for welds have been carried out in the laboratory with different thermoplastic foils under diverse conditions, in order to choose the proper ones that meet the requirements of the scope of this research, that is, the manufacturing of PNCs with advanced properties. PVC, polystyrene (PS), acrylonitrile-butadiene-styrene (ABS), poly(methyl-methacrylate) (PMMA), polyether-ether-ketone (PEEK) and CA are some of the foils that have been tried to bond together with the ultrasonic welding machine. Each polymer behavior was different enough under ultrasonic welding procedure, some resulting in good and some in weak bonds; i.e. melt more than desired or not stable created weld.

The most proper joints were achieved with PVC and CA thin foils, as their response to bonding was satisfactory enough. Some of the problems faced with the other polymeric foils can be summarized as, degradation of the polymer matrix, very difficult conditions in order to get a joint together, thick films for the scope of the preparation of

the final nanocomposites, very expensive specimens, low quantities available etc.

3.2.1 PVC foils

PVC apart from the fact that it can be easily welded under the experimental ultrasonic welding procedure used in this work, is a polymer with high potentials, as it has good mechanical properties, thermal stability and flame resistance, it is dimensionally stable with high density and it has light weight [12]. Furthermore, PVC is a widely used polymer which finds plentiful applications, such as in construction and building materials (i.e. windows, pipes, for protection of cables and wires), in the toys industry, in many parts in the automotive and aviation industry, for packaging and medical applications (blood storage containers), while it has low cost which is an important criterion for its widespread use.

Moreover, PVC is suitable for use in the experiments here for the reasons described above in this paragraph. It is a chemically stable polymer with quite good resistance to different environments such as acidic, alkalic, inorganic chemicals and it is hard to be dissolved in organic solvents, except in aromatic hydrocarbons, ketones, and cyclic ethers where it swells or dissolves [134-137]. This gives PVC an advantage, regarding the cabability of nanoparticles to be dispersed in various solvents, in order to easily spread onto its surface. Furthermore, a good indicator that PVC is a proper host matrix for nanoparticles is it chemical structure and the fact that it has polar chlorine groups and mixes well with various other substances such as plasticizers, stabilizers, fillers and coloring agents in order to fabricate different structures for several uses [134]. In addition, its amorphous structure along with its viscoelastic behavior make PVC ideally suitable for ultrasonic welding.

Amorphous PVC foils from Renolit-Hispania, S.A. were employed as substrates in the experiments. The foils, according to the manufacturer's data sheets, have the following technical characteristics: 0.2 mm ± 5% thickness and $1.37 ± 0.03\%$ g/cm^3 (at 23 ^{o}C) density. Its structure is illustrated in Figure 3.2 (a), while some of its main properties are summarized in Table 3.1.

3.2.2 CA foils

CA foils were also easily joined together under the experimental procedure of ultrasonic welding. Furthermore, CA has many beneficial characteristics and high potentials to be used as host matrices in the experiments; i.e. they are low cost, inert, biocompatible, biodegradable, amorphous polymers that contain biochemically active macromolecules resulting in high selectivity [134]. Furthermore, it has good mechanical properties, is stable, with high flexibility and lacks toxicity. CA membranes are widely used as separators in many chemical, food and biochemical industries, in applications such as highly selective separation membranes in reversed osmosis for desalination of seawater and brackish water, and in blood dialysis [138]. Other applications include clothes fabrication, medical products and toys manufacturing. CA structure and main properties are also presented in Figure 3.2 (b) and Table 3.1, respectively.

Amorphous CA foils with thickness of 0.2 mm and density of 1.3 g/cm^3, were also selected in the experiments and were purchased from Goodfellow Cambridge Ltd [139].

(a)   (b)
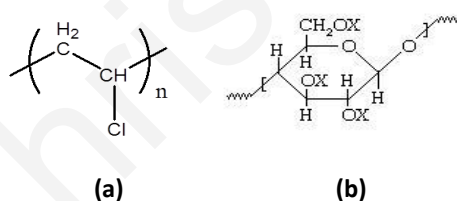
Figure 3.2 Molecular structure of (a) PVC, (b) CA (where X = H or CH$_3$CO)

Table 3.1 PVC and CA properties [134, 139-141]

Material/ Properties	Glass transition temp. (^{o}C)	Decomposition temp. (^{o}C)	Density (g/cm^3)	Specific heat (kJ/Kg K)	Thermal conductivity @23°C (W/m/K)	Temp. rate for use (^{o}C)
PVC (rigid)	85	250	1.40	1.05	0.16	-15 - 60
CA	105	300	1.3	1.5	0.2	-20 - 60

3.3 Selection of nanoparticles and microfibers

Extensive research was done in order to find the best possible reinforcing nanoparticles and microfibers to establish useful nano/micro-composite polymers with

improved properties. For achieving the above mentioned aim, the nanoparticles/ microfibers must satisfy basic requirements, such as to be compatible with the chosen polymer matrices, to have improved properties compared with the pristine polymer matrix, to have such a structure so they can be dispersed uniformly onto the polymer matrix (this is the first stage of the procedure, before ultrasonic welding occurs), as well as to be able to be ultrasonically welded. For fulfilling these purposes, a wide range of individual nanoparticles and groups of nanoparticles, after their selection with regard to their properties, have been tested. The majority of them included Fe_3O_4 and Pd nanoparticles, as well as CNTs dispersed in different solvents; these are water, different organic solvents (e.g. ethanol (EtOH), cyclohexanol (($CH_2)_5CHOH$)) and different oils. CA microfibers were used as received. The difficulty of this stage was to disperse the nanoparticles homogeneously onto the polymeric matrices irrespective of their nature, their structure and their compatibility with the polymeric foils. Based on that, experimental deposition of various nanoparticles/microfibers onto the polymer matrices was initially investigated.

3.3.1 Ferromagnetic and ferrimagnetic nanoparticles

Different types of magnetic fluids have been used before converging to those with the optimal properties that best suit the experiments. In attempts to select the appropriate magnetic nanomaterials, problems encountered included disadvantageous aggregates, non-uniform dispersions, low quantities and carrier fluids with inadequate concentration of ferromagnetic and ferrimagnetic nanoparticles, resulting in low magnetization. In addition, non-stabilized solutions were experimented with, before identifying stabilized water-, hexanol- and oil- magnetite Fe_3O_4-based nanoparticle suspensions as the best materials for use in the experimental procedure. These were produced and provided by the Laboratory of Magnetic Fluids of the Center of Fundamental and Advanced Technical Research, Timisoara Branch of Romanian Academy of Science University [96-99].

Details of the magnetic fluids that are successfully used in the manufacture of nanocomposites by means of ultrasonic welding are presented in Table 3.2; where MF is magnetic fluid, $C_6H_{13}OH$ is hexanol-1, and TR-30 is transformer oil. Among other, provided again by the Laboratory of Magnetic Fluids of Timisoara, those presented in Table 3.2

exhibit the required properties (structural, magnetic, etc.) and were modified with proper stabilizing layers, in order to prevent agglomeration and increase the compatibility with the PVC matrix. It should be noted that Sample No 1 was prepared after request to be consistent with experiments.

Table 3.2 Ferrimagnetic fluids on hexanol-1, water and transformer oil carrier liquids

Sample number	Liquid carrier	Stabilizing layers	Density (ρ_{mf}) (g/cm^3 at 20°C)	Saturation magnetization (Ms) (M at Hmax) (Gs)
1	MF/$C_6H_{13}OH$, Fe_3O_4	Oleic acid - double (OA)	0.061	261
2	MF/H_2O, Fe_3O_4	Lauric acid - double (LA)	0.024	100
3	MF/TR-30, Fe_3O_4	Oleic acid - double (OA)	0.057	244
4	MF/H_2O, Fe_3O_4	Dodecylbenzenesulphonic acid - double (DBS)	1.268	248

The magnetic fluids presented in Table 3.2 exhibit long-term colloidal stability and are synthesized by chemical co-precipitation method which consists of two main steps and is described in references [37, 97-98, 142]. Briefly, it involves the chemical co-precipitation of magnetite (Fe_3O_4) from aqueous solution of $FeSO_4$ and $FeCl_3$ salts with NH_4OH in excess; this is the stage of the preparation of the magnetic nanoparticles, followed by dispersion/stabilization of magnetite nanoparticles in various polar (i.e. water) or non-polar (i.e. hexanol-1, transformer oil) carrier liquids, using double-layer surfactants with different chain lengths for covering the magnetite nanoparticles.

Nanoparticles in general exhibit strong tendency to aggregate so as to reduce their high surface energy. In the case of magnetic nanoparticles, in order to achieve stabilization in carrier liquids and avoid particle agglomeration resulting from magnetic and Van der Waals attractions as well as gravitational settling, these are functionalized with different chain length molecules; these are the surfactants or the stabilizing agents [143-144]. Surfactants are actually long-chain hydrocarbons with polar heads that have the ability to anchor onto the surface of the magnetite particle and prevent the close approach of nearby magnetite particles [145]. For the purpose of the experiments in this

work, the used stabilizing agents consist of double layers of oleic acid, lauric acid and dodecylbenzenesulphonic acid. A typical schematic drawing of double layer oleic acid molecules adsorbed on the surface of magnetic nanoparticles is illustrated in Figure 3.3 while, the double layers are introduced in order for the resulting nanohybrid to be compatible with the liquid carrier. The molecular formulas of the stabilizing layers have either 12 or 18 carbon atoms and some of them have also double bonds, while their further properties are presented analytically in Table 3.3. The chain length of surfactant as well as the presence or not of the double bond, influence the properties of magnetic fluids by means of stabilization/dispersion of magnetic nanoparticles [146]. In general, the absence of a double bond as well as the shorter chain length, as in the case of lauric acid, reduces its efficiency to disperse particles. Lauric acid becomes size selective and it stably disperses only the smallest size magnetite particles, resulting in medium magnetization (Table 3.2) [146]. On the other hand, oleic acid has 18 carbon atoms and a double bond which makes it highly efficient in the stable dispersion.
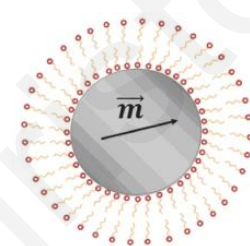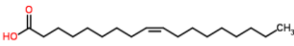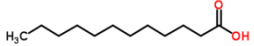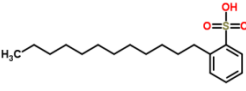
Figure 3.3: Schematic drawing of double layer oleic acid molecules adsorbed on the surface of magnetic nanoparticles [147]

Table 3.3 Properties of stabilizing layers of ferrimagnetic fluids [148]

Stabilizing layer	Molecular formula	Density (ρ_{mf}) (g.cm^3 at 20°C)	Molecular weight (g/mol)	Melting point (T_m) (^{o}C)	Boiling point (T_b) (^{o}C)
Oleic acid (OA)	$C_{18}H_{34}O_2$	0.895	282.46	13	360
Lauric acid (LA)	$C_{12}H_{24}O_2$	0.9	200.32	45	296.1
Dodecylbenzenesulphonic acid (DBS)	$C_{18}H_{30}O_3S$	1.1	326.49	10	315

According to TEM analysis provided by the Laboratory of Magnetic Fluids of Timisoara, the mean diameter of nanoparticles of Sample 4; this is $Fe_3O_4/H_2O/DBS$-double, was 7.04 ± 0.16 nm, with reduced standard deviation of 2.24 ± 0.14 nm (Figure 3.4a) and magnetization equal to 248 Gs (Figure 3.4b), while for Sample 2; this is $Fe_3O_4/H_2O/LA$-double, mean diameter of nanoparticles is equal to 6.1 ± 0.15 nm and with reduced standard deviation of 2.4 ± 0.13 nm [99].

(a)   (b)
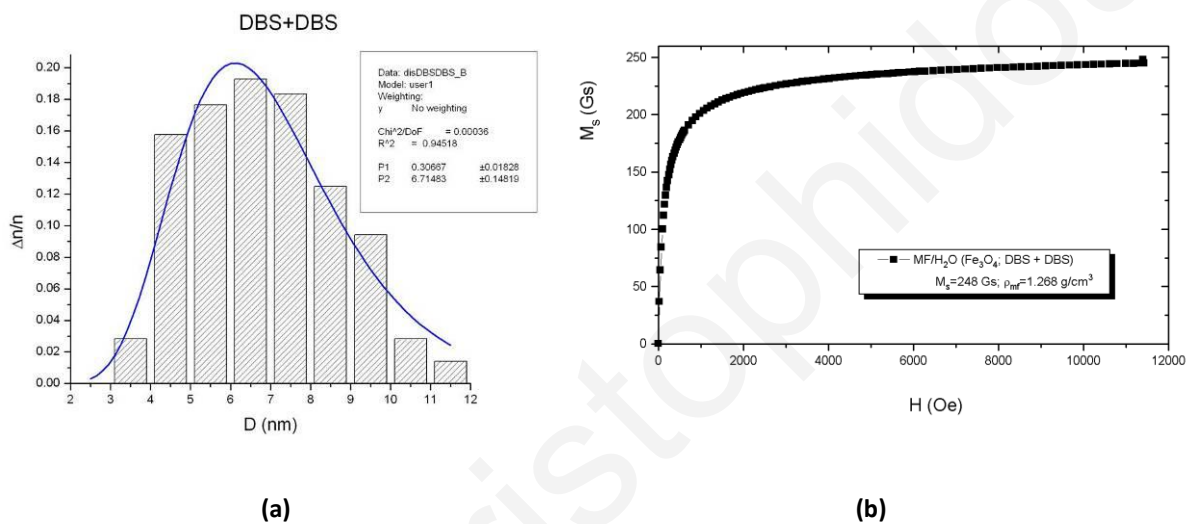
Figure 3.4 MF/H_2O (Fe_3O_4; DBS+DBS), (a) size distribution measured by TEM and (b) magnetization curve, provided by the Laboratory of Magnetic Fluids of Timisoara

In general, the used magnetic fluids have high saturation magnetization, good stabilization and their structures as well as their chemistry are compatible with the PVC matrix.

3.3.2 Pd nanoparticles

Palladium (Pd^0) nanoparticles were also chosen in order to be introduced into the PVC matrix by means of ultrasonic welding because of their ferromagnetic behavior [149-150]. The Pd nanoparticle suspensions were provided by the Polymer Synthesis and Polymer Processing Laboratory of the Department of Mechanical and Manufacturing Engineering, University of Cyprus and were formed in n-hexane and covered by poly(LauMA)b-poly(2-(acetoacetoxy)ethyl methacrylate) (LauMAx-b-AEMAy-Pd) [151-152]. The resulting hybrid micelles have an average size 30 - 50 nm, whereas the

concentration of Pd in the solution is quite small; this is around 4 mg Pd in 1 mL of solution. Available properties of the palladium suspension are presented at Table 3.4.

Table 3.4 Properties of Pd suspension [151-152]

Material/ Properties	Average particle size (nm)	Liquid carrier	Stabilizing layers
Pd/LauMA	30-50	n-hexane	(LauMAx-b-AEMAy)

3.3.3 CNTs

Two different types of CNT, these are short multi-walled CNTs and long multi-walled CNTs, have been used in this thesis. Since the main aim was to develop mass production PVC nanocomposites with a fast and economic process (through ultrasonic welding), with improved mechanical properties, consideration should be given to the fact that the used CNTs are economic and derived from mass production. Relevant information about their solutions is presented in Table 3.5, while details are given below in this paragraph. Multi-walled CNTs have different properties and are dissolved in different liquid carriers.

Table 3.5 CNTs in dimethylformamide, cyclohexane and de-ionized water carrier liquids

Sample number	CNTs / Company	Synthesized method	Liquid carrier	Stabilizing layers
1	Ros1 / Rosseter	LSA (Liquid-phase Self-regulated Arc)	Cyclohexane	-
2	AQ0101 / Nanocyl	CCVD (Catalytic Carbon Vapor Deposition)	D. I. Water	Anionic Surfactant
3	Ros1 / Rosseter	LSA (Liquid-phase Self-regulated Arc)	Dimethylformamide	Poly(2-(dimethylamino) ethyl methacrylate

The Ros1/sh-MWCNTs were provided by the Rosseter Holdings Limited and were produced in their main process; this is the Liquid-phase Self-regulated Arc (LSA), with no use of catalysts [153]. As described from the producer, most parts of Ros1 (sh-MWCNTs)

batches contain 50-80 wt.% of MWNTs and 15-35 wt.% of carbon polyhedral nanoparticles, while the rest are different forms of disordered graphite (including single graphite sheets, graphite platelets) [154]. Inorganic impurities are not higher than 0.5 wt.% and can be easily removed by successful washing in inorganic acids, such as HCl, HNO_3 and H_2SO_4. The TEM pictures of the samples are provided by Rosseter and are presented in Figure 3.5a-b. Ros1/sh-MWCNTs series have average outside diameter equal to 8.4 nm, average inside diameter equal to 2.5 nm, average length equal to 280 nm and density 2.510 kg/m^3. Their distributions (provided by Rosseter) are presented in Figure 3.5c. Moreover, their analytical properties are presented in Table 3.6. Interlayer distances of the sh-MWCNTs are in the order of 0.341 and 0.345 nm, measured by typical X-Ray Diffraction patterns and Micro-Raman spectra, respectively [154].
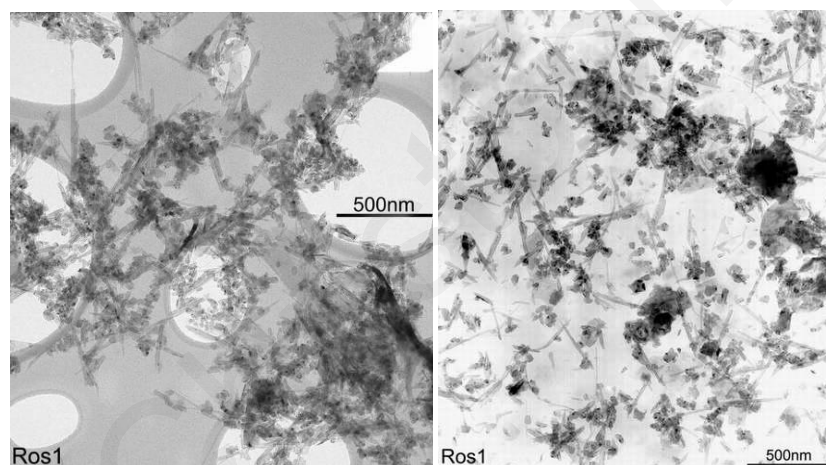
(a)   (b)
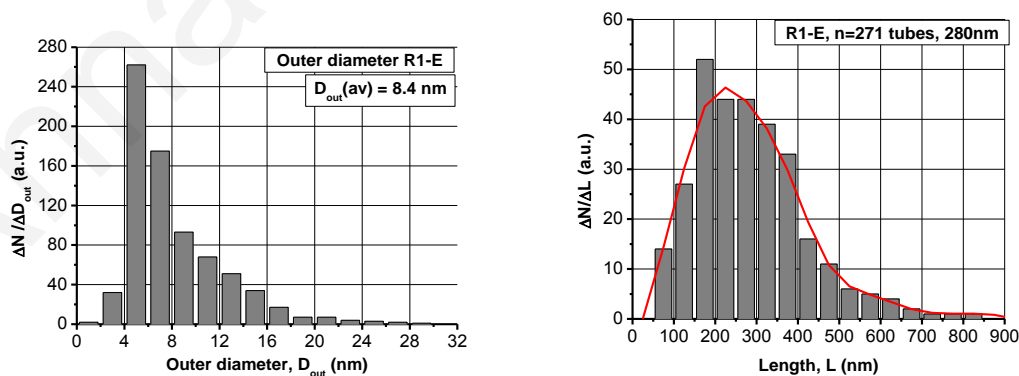
(c)

Figure 3.5 (a) and (b) TEM pictures of Ros1/sh-MWCNTs deposited onto a lacy carbon grid [154], (c) size distributions of Ros1/sh-MWCNTs, where N is the CNTs number [154]

Table 3.6 Properties of sh-MWCNTs [154]

Material/ Properties	Average outside diameter (Dout) (nm)	Average inside diameter (Din) (nm)	Average length (L) (nm)	Interlayer distances (d) (nm)	Average number of carbon layers (n)	Density (kg/m³)
Ros1/sh-MWCNTs	8.4	2.5	280	0.341 - 0.345	9*	2.510

* $n = 1 + (D_{out} - D_{in}) / 2 \cdot d = 1 + (8.4 \text{ nm} - 2.5 \text{ nm})/2 \cdot 0.34 \approx 9$

The solution of the first sample (Sample 1 - Table 3.5), which this illustrated in Figure 3.6, was prepared in the laboratory, since short multi wall CNTs (sh-MWCNTs), which have average lengths within the range of 200-350 nm, are easily dispersed in most organic solvents, such as alcohols (e.g. ethanol) and aromatics (e.g. benzene, toluene). In order to overcome the problem of quality/purity of the CNTs and their ability to disperse uniformly onto the polymer matrix surface, the CNTs were first kiln-dried. The preparation method, as this provided by Rosseter, included the following steps:

i. The Ros1/sh-MWCNTs were first dis-agglomerated by a mill (Figure 3.5b)

ii. The Ros1/sh-MWCNTs were then kiln-dried at 530 °C for 3 hours in order to help oxidation and burn out sub-layers of amorphous carbon (Figure 3-5c). The analytical conditions of kiln increase temperature was as follows:

- step 1: 150 °C for 2 min
- step 2: 250 °C for 2 min
- step 3: 400 °C for 2 min
- step 4: 530 °C for 3 hr

From the samples weight before and after the kiln a weight loss of ≈1 wt.% was realized, and also smaller particles were formed, in order to achieve easier dispersion in cyclohexanol.

iii. Finally, after the Ros1/sh-MWCNTs reach temperatures lower than 100 °C, they were then dispersed in cyclohexanol with ultrasonication (applying ultrasound energy to mix particles with liquid carrier) for 30 minutes. Each suspension consists of 1.5 mg of Ros1/sh-MWCNTs in 5 ml of cyclohexanol.

The limitation with the Ros1/sh-MWCNTs suspensions was the lack of stabilizing layers to cover the CNTs. Concerning that, the suspensions had to be used immediately

after their preparation.

(a)   **(b)**   **(c)**
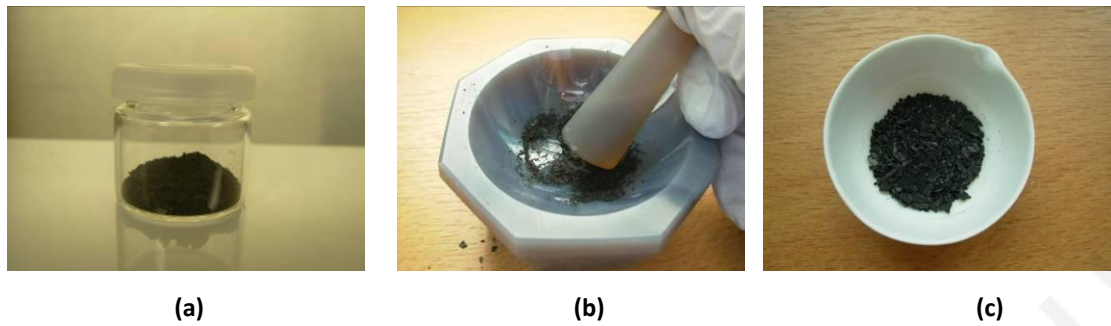
Figure 3.6 (a) Ros1/sh-MWCNTs as they received, (b) and (c) preparation of Ros1/sh-MWCNTs

The second sample (Sample 2) is a water dispersion of MWCNTs, named "Aquacyl 0101", and supplied by the Nanocyl Inc, Belgium, and was used as received. The Aquacyl 0101/long-MWCNT consists of very thin multi-wall carbon nanotubes in concentration of 1 wt.% of MWCNTs of the Nanocyl 7000 series, which are characterized by average outside diameter of nanotubes 9.5 nm, average length 1.5 μm, carbon purity 95 wt.%, and surface area 250-300 m^2/g dispersed in de-ionized water (Table 3.7). They are also characterized by surface tension of about 57 N/m, viscosity equal to 36 cP and pH equal to 7 [155-156]. They are stabilized suspensions with anionic surfactants.

Table 3.7 Properties of long-MWCNTs [155-156]

Material/ Properties	Average outside diameter (Dout) (nm)	Average length (L) (nm)	Surface area (m^2/g)	Carbon purity (%)	CNT content (%)	pH
Aquacyl 0101/ long-MWNTs	9.5	1.500	250-300	90	1	7.0

Finally, the third sample (Sample 3) was again provided by the Polymer Synthesis and Polymer Processing Laboratory of the Department of Mechanical and Manufacturing Engineering, University of Cyprus. The stabilizing layer of the Ros1/sh-MWCNTs (Table 3.6) was the poly(2-(dimethylamino) ethyl methacrylate, and the liquid carrier was the dimethylformamide. Although this sample seems to be very promising for the experiments, due to its good dispersion and its further properties, there were not enough quantities in order to prepare several nanocomposites for further examining of their properties.

35

3.3.4 CA microfibers

CA and CA/PAni microfibers were fabricated in the Micro- and Nano-Systems Laboratory of the Department of Mechanical and Manufacturing Engineering, University of Cyprus by Mrs. T. Christoforou with the electrospinning method [157] in order to be introduced as reinforcements in CA foils, by means of the ultrasonic welding. Electrospinning is the method that uses electrostatic forces to create a wide range of fine micro and/or nanofibers from a liquid state of molten polymer or polymer solutions for a great variety of applications [158]. Furthermore, the presence of PAni in CA microfibers results in beneficial effects on materials properties, i.e. mechanical properties and electrical conductivity [159-160]. The electrospinning parameters, as well as the size and the shape of the produced fibers, of the four different electrospun membranes are presented at Table 3.8.

Table 3.8 Properties of CA microfibers

Sample number	Material / Solution concentration	Solution flow rate	Electric voltage	Tip-to-collector distance	Internal needle diameter	Outside diameter*	Morphology
1	90 wt.% CA - 10 wt.% PAni 12.5 w/v.% CA/acetone solution	0.1 ml/min	15 kV	10 cm	20-gauge	165 nm (43 nm - 443 nm)	Beads-on-string, quite uniform fibers, membrane thickness ≈0.19 mm
2	12.5 w/v.% CA/acetone solution	1 ml/min	10 kV	10 cm	16-gauge	320 nm (69 nm - 1.03 µm)	Rare beads-on-string, cylindrical fibers, membrane thickness ≈0.13 mm
3	12.5 w/v.% CA/acetone solution	1 ml/min	15 kV	10 cm	16-gauge	383 nm (157 nm - 866 nm)	Cylindrical uniform fibers, membrane thickness ≈0.15 mm
4	15 w/v.% CA/acetone solution	1 ml/min	20 kV	15 cm	16-gauge	751 nm (188 nm - 1.72 µm)	Non-uniform flat fibers, wrinkle in beads, membrane thickness ≈0.19 mm

* the numbers in parenthesis denote the smallest and the largest fiber diameters respectively, while the number outside provide the average outside diameter of the microfibers

3.4 Multilayer preparation - Deposition of nanoparticles/microfibers onto the polymer matrix

The deposition of all nanoparticles was achieved by spin-coating of various quantities of different fluids, as described above, onto PVC foils (Figure 3.7), whereas the microfibers were just deposited manually onto the CA foils. A Delta6RC TT spin coater was used in order to apply a uniform thin foil of the fluids onto the polymer substrate. To be precise, the quantities of the different fluids were calculated based on the concentration of the nanoparticles of each fluid that was applied each time, in association with the desired concentration of nanoparticles of the prepared nanocomposites. The coatings were performed with spinning velocities from 300 rpm to 1.000 rpm, at room temperature, and spinning times commensurate to the radius of the polymer matrix since they were circle shaped in order to match the spin coater base as this is illustrated in Figure 3.7. The spinning time was in the order of fraction of seconds and it was not possible to be measured each time since the spin coater was stopped manually when the fluid completely covered the desired surface of the polymer matrix. The significant properties that influence the spinning velocity and the time to complete the spin coating are the kind of the fluid, its properties such as density and viscosity, and its compatibility with the PVC substrate. All applied liquid carriers, such as hexanol, cyclohexanol and water, correspondingly evaporate and leave the nanoparticles finely dispersed onto the PVC substrate. In practice, organic solvents evaporate immediately, followed by water which evaporates after 2 to 5 minutes depending on the amount of the deposited fluid (as a result of the vent of the spin coater cabin); however, the oil carrier of ferrimagnetic samples needed about a day (24 to 48 h) under a laboratory hood, depending on its quantity, to dry on the surface. The oil does not evaporate immediately under the conditions used. In general, some magnetic fluids disperse easier than others, such as alcohol-carrier magnetic fluids which are easier to disperse than water-based ones and certainly easier than oil fluid suspensions. All depositions of nanoparticles were performed in class 1000 clean room conditions at room temperature.

Figure 3.7 Dispersion of different nanofluids onto the PVC foils using a Delta6RC TT spin coater device

Once the nanoparticles are deposited onto the first PVC foil, a second foil is stacked on the top, to create a bilayer "sandwich" containing foils of either Fe_3O_4 and Pd nanoparticles or CNTs. The same procedure was used after the deposition of CA microfibers at the interfaces of the cellulose foils.

However, regarding the Ros1/sh-MWCNTs samples in cyclohexanol, an additional step is required, which occurs after the deposition of CNTs onto the PVC and before the two PVC foils been joined together under ultrasonic welding. The additional step presupposes the specimens; these are the two PVC foils with the included CNTs, to be pressed together under 10 tons with a manual screw press at room temperature, in order to ensure the CNTs are stabilized onto the surface. This extra step is necessary and critical because of the lack of stabilizers of the CNTs and their tendency to move away during the stage of ultrasonic welding, because of the ultrasonic oscillation. That step is critical when the nanotubes are not included in colloid liquids and are just dispersed onto the polymer surfaces with the help of an organic solvent.

3.5 Microscopic analysis of the deposed nanoparticles onto the polymer matrix

It should be mentioned again that whatever the type of nano-fluids are used, it is important to ensure good nanoparticle dispersion all over the polymer surfaces, in order to establish the best possible perspectives for further penetration of nanoparticles into the polymer matrix. Moreover, the distribution of the nanoparticles onto the polymer matrix depended essentially on the ability of the fluids (that include nanoparticles) to

cover the PVC surface uniformly. For that purpose, Scanning Electron Microscopy (SEM) and Atomic Force Microscopy (AFM) were employed, after deposition of ferrimagnetic Fe_3O_4 and Pd nanoparticles onto the PVC matrices and before ultrasonic welding occurs, in order to reflect the assessment of nanoparticle dispersion onto the polymer surfaces. All the pictures are taken in class 1000 clean room facilities, in order to minimize dust deposition onto the prepared specimens.

Figure 3.8 illustrates SEM (Tescan Vega SEM) pictures of the uniform dispersion of Pd nanoparticles onto the PVC foil in different magnifications. The specimens were first coated with a 10 nm thin gold layer in order to avoid surface charging, while this is the reason that the Pd-containing micelles were illustrated with bigger size.

| (a) | (b) | (c) |
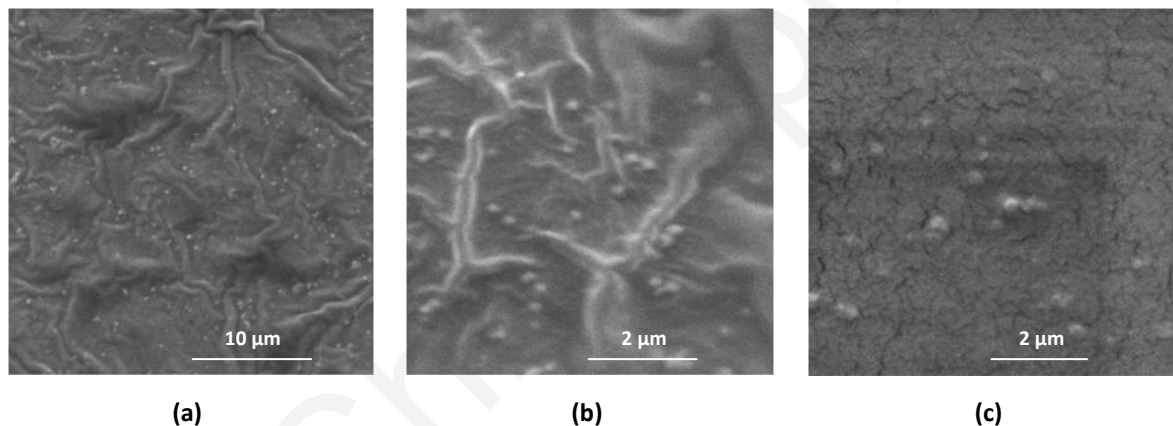
Figure 3.8 SEM micrograph of the surface of the PVC foil after deposition of Pd nanoparticles onto the surface (uniform Pd dispersion)

AFM (model Q-Scope/350 CL) was employed in order to study the dispersion of ferrimagnetic nanoparticles (Fe_3O_4) onto the PVC foil, after the deposition of a spin coating (stage 1) and before ultrasonic welding was performed Figure 3.9. The Fe_3O_4 nanoparticles in water dispersion were used, stabilized with double layer of dodecylbenzensulphonic acid (H_2O/DBS+DBS). The resulting AFM 3D topography images show a nano-layer of the order of 60 nm onto the PVC foil. This is an expected result, because of the generated surrounding of the stabilizing agent outside the approximately 7 nm nanoparticles diameter, as well as the grain growth during the scanning with the AFM tip.
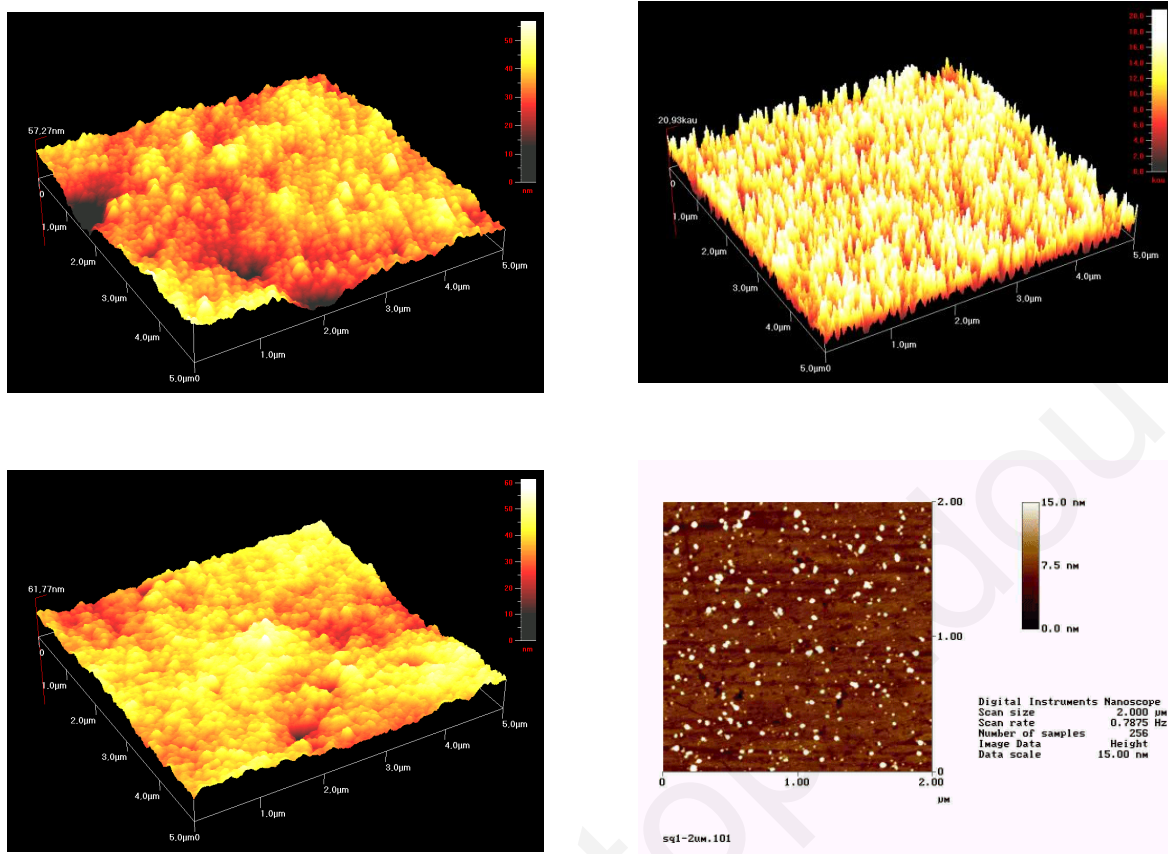
Figure 3.9 AFM 3D topography image of spin-coated with magnetic Fe$_3$O$_4$ nanoparticles PVC foil

3.6 Ultrasonic welding process

The next step (2nd step) in the procedure is the ultrasonic welding of the foils which contains layers of the nanoparticles and microfibers prepared as described above onto their surfaces, in order to join them together and prepare the nano/micro-composites (Figure 3.10). For the manufacturing of all of the nano/micro-composite polymers, a polymer ultrasonic welder was involved, from 'Ultrasonic Fabric Sealing System', model FS-90. This is a stand-alone system equipped with an ultrasonic power supply (model 2000bcd) that works at 20 kHz and 1100 watt, an ultrasonic horn configuration (model 611*001*109, BUC, 373**RR), along with the appropriate seam sealing stitching wheel, model blank stitch SSM300 (medium male knurled pattern) and booster configuration (silver 101-149-094), made by Branson Ultrasonic Corporation. This configuration is chosen in order to match the polymers kind and their geometry; i.e. foils.

41

Figure 3.10 Schematic drawing of PVC nanocomposites fabrication with Branson ultrasonic welder

The welding pressure was adjusted by controllers at 138 kPa and the welding time assessed after repeated welds to be equal to 619 ms, in order to obtain good results with regard to the welding. On the other hand, the welding amplitude was calculated according to the above combination of the equipment, that produces vibrations with an amplitude of 0.033 mm and kept constant. The experiment configuration stages are illustrated in Figure 3.11, while the calculations of welding amplitude follows:

Welding Amplitude = Total Amplitude * Percentage Amplitude   **Eq. 3-1**

Total Amplitude = Converter Amplitude * Gain Booster * Gain Horn   **Eq. 3-2**

where, percentage amplitude adjustment was set at 25%, converter amplitude equals to 0.02 mm according to booster configuration, booster gain is 2x and horn gain equal to 3.3. Total Amplitude is calculated to be 132 μm, defined as the peak-to-peak longitudinal displacement at the face of the horn.
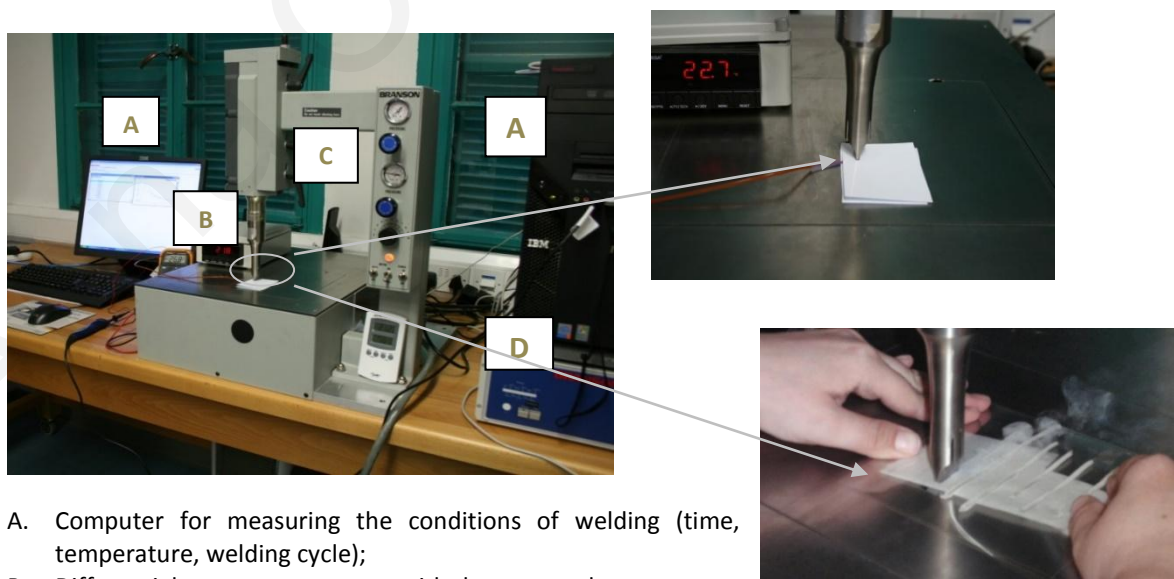
A. Computer for measuring the conditions of welding (time, temperature, welding cycle);
B. Differential temperature meter with thermocouple;
C. Ultrasonic welding device;
D. Ultrasonic power supply

Welding area

Figure 3.11 Ultrasonic welding setup picture: A. computer for measuring the conditions of welding (time, temperature, welding cycle); B. differential temperature meter with thermocouple; C. ultrasonic welding device; D. ultrasonic power supply

42

In the experiments a near-field welding was performed in order to accomplish the joining of polymer foils, whereas far-field mode is when the distance between the horn surface and the joint is within 6.35 mm, and far-field mode welding is the term used when the joint is farther away [28, 80, 83].

A differential temperature meter with an r-type thermocouple (DP26-TC) from Omega.com was employed, combined with a PicoScope PC Oscilloscope (data aquisition system) pico technology, in order to measure the welding temperature of the PVC with the nanoparticles. The welding temperature (T_w) was measured at $T_w = 86^oC$ and demonstated the theoretical hypothesis that ultrasonic welding of amorphous thermoplastics occurs at/above glass transition temperature (Tg). Figure 3.12 illustrates the welding curve.
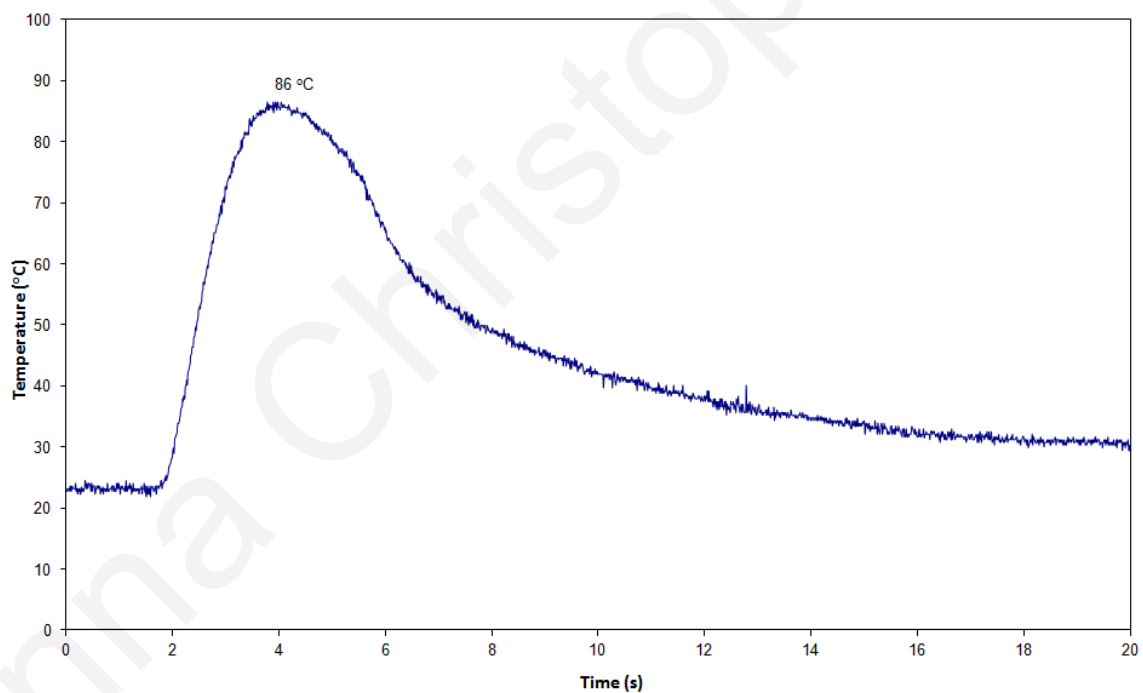
Figure 3.12 Welding curve of the temperature of PVC samples, under ultrasonic welding

3.7 Fabrication of polymer nanocomposites

3.7.1 PVC with embedded ferrimagnetic nanoparticles

Several synthesis experiments were carried out in order to obtain a wide range of

ferrimagnetic nanoparticle concentrations in PVC composites as these are analyzed in Table 3.9, by using each one of the four different ferrofluids described in Table 3.2. The concentration of the iron oxide (Fe_3O_4) of the produced Fe_3O_4-nanocomposites is depended essentially on the properties of the ferrofluids that cover the PVC surface uniformly; i.e. their density, liquid carries, stabilizing layers, viscosity etc. Sample 4, this is the $Fe_3O_4/H_2O/BDS+DBS$-PVC, is the nanocomposite (Sample 4e) with the higher concentration; this can be justified because of the high density of the nano-fluid, where ρ = 1.268 g/cm^3.

Table 3.9 PVC with embedded ferrimagnetic nanoparticles, by means of ultrasonic welding

Sample number	Sample 1 PVC+MF/$C_6H_{13}OH$, Fe_3O_4	Sample 2 PVC+MF/H_2O, Fe_3O_4	Sample 3 PVC+MF/TR-30, Fe_3O_4	Sample 4 PVC + MF/H_2O, Fe_3O_4
a	PVC/Fe_3O_4 0.1 wt.%	PVC/Fe_3O_4 0.04 wt.%	PVC/Fe_3O_4 0.1 wt.%	PVC/Fe_3O_4 0.5 wt.%
b	PVC/Fe_3O_4 0.3 wt.%	PVC/Fe_3O_4 0.1 wt.%	PVC/Fe_3O_4 0.3 wt.%	PVC/Fe_3O_4 1 wt.%
c	PVC/Fe_3O_4 0.5 wt.%	PVC/Fe_3O_4 0.3 wt.%	PVC/Fe_3O_4 0.5 wt.%	PVC/Fe_3O_4 2 wt.%
d	PVC/Fe_3O_4 1 wt.%	PVC/Fe_3O_4 0.5 wt.%		PVC/Fe_3O_4 3 wt.%
e	PVC/Fe_3O_4 2 wt.%			PVC/Fe_3O_4 5 wt.%

3.7.2 PVC with embedded Pd nanoparticles

A Pd-PVC nanocomposite was prepared with 0.012 wt.% concentration of Pd (Table 3.10). Concerning this series of nanocomposites, only one sample was prepared due to limited supply of this solution; this is poly(LauMA)-b-poly(AEMA) - Palladium (Pd^0) in n-hexane, Table 3.4 of paragraph 3.3.2. Moreover, the concentration of Pd in this sample is very small because of the very low concentration of Pd particles in the carrier liquid.

Table 3.10 PVC with embedded Pd nanoparticles, by means of ultrasonic welding

Sample number	Sample 5 PVC+Pd/C_6H_{14}
a	PVC/Pd 0.012 wt.%

3.7.3 PVC with embedded MWCNTs

Different varieties of multi-wall CNTs were embedded into the PVC matrix again by virtue of the ultrasonic energy that was infused to the joint, in order to obtain a wide range of multi-wall CNT-PVC nanocomposites. All the prepared nanocomposites are listed in Table 3.11; these are PVC embedded with short and long multi-wall CNTs (PVC+sh-MWCNTs/C_6H_{13}Cl) - Series 6 and PVC+long-MWCNTs/H_2O - Series 7 samples, respectively, which are prepared from the suspensions of Table 3.5. Again, the concentration of the CNTs of the produced MWCNTs-nanocomposites is depended essentially on the properties of the liquid suspensions that cover the PVC surface uniformly; i.e. their density, liquid carrier, stabilizing layers, viscosity etc. The sample 6f of the sh-MWCNTs/C_6H_{13}Cl-PVC has the higher concentration.

Table 3.11 PVC with embedded MWCNTs, by means of ultrasonic welding

Sample number	Sample 6 PVC+sh-MWCNTs/C_6H_{13}Cl	Sample 7 PVC+long-MWCNTs/H_2O
a	PVC/CNTs 0.1 wt.%	PVC/CNTs 0.01 wt.%
b	PVC/CNTs 0.2 wt.%	PVC/CNTs 0.05 wt.%
c	PVC/CNTs 0.3 wt.%	PVC/CNTs 0.1 wt.%
d	PVC/CNTs 0.5 wt.%	PVC/CNTs 0.2 wt.%
e	PVC/CNTs 1 wt.%	PVC/CNTs 0.3 wt.%
f	PVC/CNTs 2 wt.%	

3.7.4 CA with embedded CA and CA/PAni electrospun fibers

The electrospun fibers, described in Table 3.8 of the paragraph 3.3.4, were deposited inside the two CA foils (as membranes), as this illustrated in Figure 3.13 and then the specimens were ultrasonically welded. Four different samples were prepared with this method and are listed in Table 3.12.

| (a) | (b) | (c) |
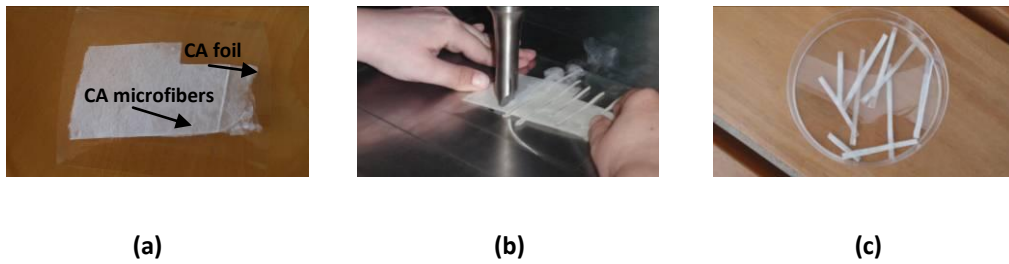
Figure 3.13 (a) CA with CA microfibers "sandwich" ready for ultrasonic welding, (b) ultrasonic welding of the sample, (c) CA composites with CA microfibers after ultrasonic welding with different lengths (welding time)

Table 3.12 CA with embedded CA and CA/PAni microfibers, by means of ultrasonic welding

Sample number	Sample 8 CA/PAni	Sample 9 CA
a	CA & 90 wt.% CA + 10 wt.% PAni & 12.5 w/v.% in CA/acetone solution	CA: CA & 12.5 w/v.% in CA/acetone solution (with rare beads)
b		CA: CA & 12.5 w/v.% in CA/acetone solution (with uniform fibers)
c		CA: CA & 15 w/v.% in CA/acetone solution

3.8 Conclusions of experimental procedure

The main aim of the thesis was accomplished, this is the manufacturing of various polymer nano/micro-composites from stacked polymer foils with intermediate sandwiched layers of nanoparticles/microfibers by means of solid-state ultrasonic welding. For that purpose, a multi-step procedure was introduced with success and is analytically described in this Chapter. Moreover, and before ultrasonic welding occurs, homogenous and proper distribution of the nanoparticles all over the polymer matrix surfaces was achieved. The prepared polymer nano/micro-composites are presented in Tables 3.9 to 3.12, while their properties are analyzed in Chapters 4 and 5.

Chapter 4. Characterization of particle based polymer nanocomposites, results and discussion

Part A. Experimental

4.1 Introduction - Characterization techniques

The experimental part of Chapter 4 deals with the characterization of the properties of the particle based PNCs produced in Chapter 3; these are the Fe_3O_4 and Pd/PVC nanocomposites. For this purpose, various characterization techniques were used. Since distribution of nanoparticles into a polymer matrix is of critical importance regarding their potential properties, all the nanocomposites were investigated microscopically. The microscopic investigation was obtained using SEM and TEM in order to visualize the structure of the ultrasonic joint, as well as the distribution of nanoparticles into the polymer matrix. Energy Dispersive X-ray Analysis (EDX) was also performed, at the cross-section of the nanocomposites, in order to analyze their composition. The magnetic properties of the Fe_3O_4 and Pd/PVC nanocomposites were measured with a Physical Property Measurement System (PPMS). Furthermore, their viscoelastic behavior was studied using Dynamic Mechanical Analysis (DMA) and their relevant mechanical behavior was analyzed with a Universal Testing Machine (UTM). Thermo-gravimetric analysis (TGA) was finally employed to construe the palladium-PVC nanocomposites thermal stability. The discussion of the resulting properties of the nano-composites is also presented in this Chapter.

4.2 Scanning electron microscopy and field emission scanning microscopy coupled with energy dispersive X-ray analysis

SEM pictures were carried out using a Tescan Vega SEM in class 1000 clean room facilities. All the samples illustrated in Figure 4.1 to Figure 4.5 were cut in liquid nitrogen and were coated with a 5 to 10 nm gold thin films (except the one illustrated in Figure 4.3) by an "Anatech Hummer Cold Deposition Sputter Coater", a magnetron sputtering system, in order to avoid charging. Figure 4.1 illustrates cross-sectioned geometries of two un-loaded PVC foils ultrasonically welded together. According to those, one can clearly distinguish the configuration consisting of two PVC foils joined together, with an intermediate heat affected zone, which extents vertically to the interface. Based on theory, the interface is affected by the local generation of heat during ultrasonic welding due to polymer chain friction.
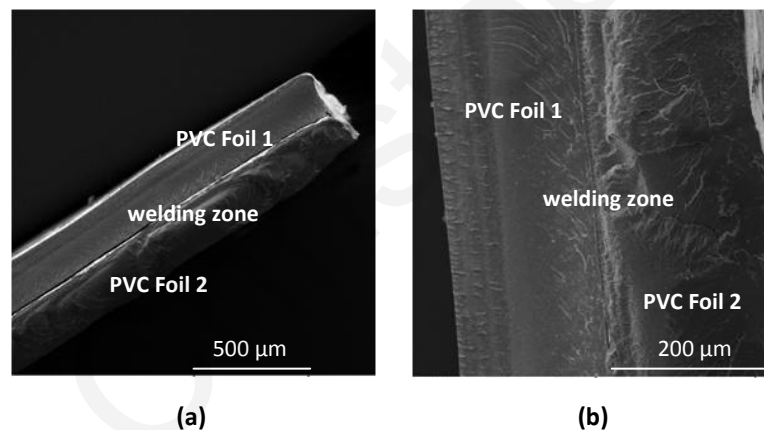
Figure 4.1 SEM micrographs of a cross-section of two PVC foils joint together by means of ultrasonic welding

4.2.1 PVC nanocomposites with embedded ferrimagnetic nanoparticles

Figure 4.2 and Figure 4.3 illustrate the cross-sectioned Fe_3O_4-PVC nanocomposites in various magnifications. From these images, the weld is clearly distinguishable; this is the heat affected zone which expands through the entire thickness of the nanocomposite. The Fe_3O_4 nanoparticles are not visible by SEM, probably because of their organic surfactant surface, their nano-size, as well as due to the fact that they are embedded into large quantities of PVC, which causes charging of the SEM beam.
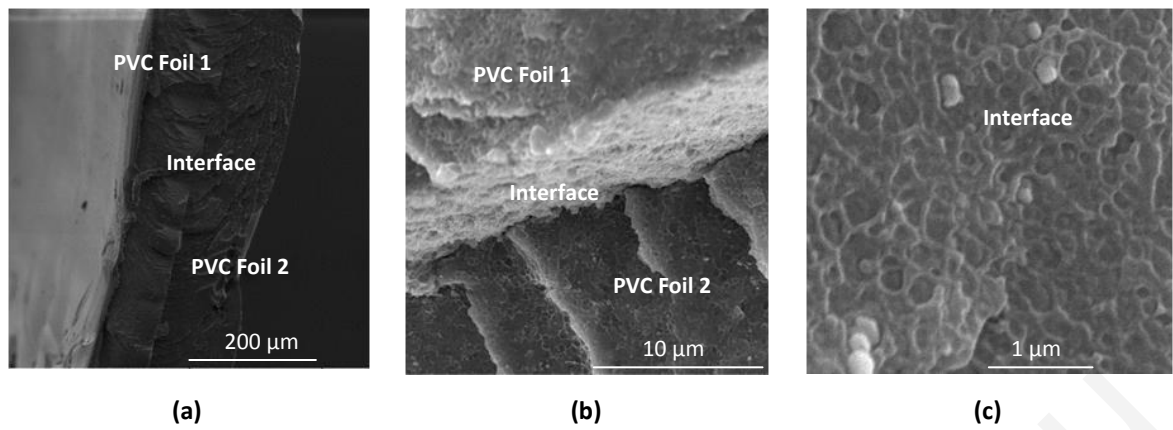
Figure 4.2 SEM micrographs of cross-section of PVC/2 wt.% Fe$_3$O$_4$ (C$_6$H$_{13}$OH/OA+OA) nanocomposites manufactured by means of ultrasonic welding, in different magnifications - Sample 1e
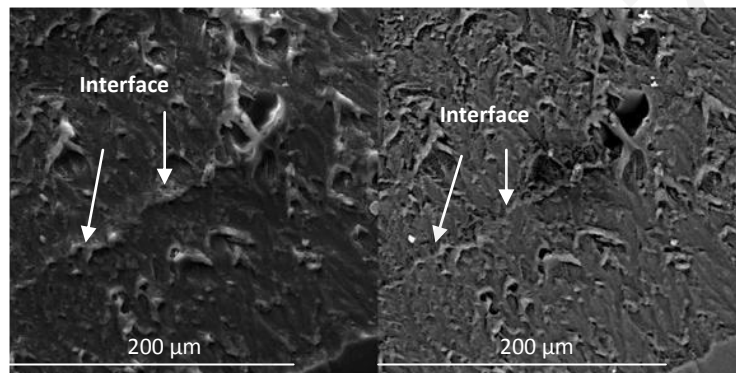
Figure 4.3 SEM micrographs of the heat affected zone of a cross-section of PVC/2 wt.% Fe$_3$O$_4$ (C$_6$H$_{13}$OH/OA+OA) nanocomposites manufactured by means of ultrasonic welding - Sample 1e

In order to "visualize" those Fe$_3$O$_4$ nanoparticles, a Field Emission Scanning Microscopy coupled with Energy Dispersive X-ray Spectroscopy (FE-SEM/EDX JEOL JSM 7401F) was employed at the University of Massachusetts Lowell, to un-coated cross-sectioned Fe$_3$O$_4$-PVC nanocomposites. Sample 4e, PVC embedded with 5 wt.% of Fe$_3$O$_4$ (H$_2$O/DBS+DBS) ferrifluid, is illustrated in Figure 4.4 (a). Signals corresponding to Fe atoms can be seen in Figure 4.4 (b) and confirm the existence of iron (Fe) in the PVC nanocomposite samples.

(a)   **(b)**
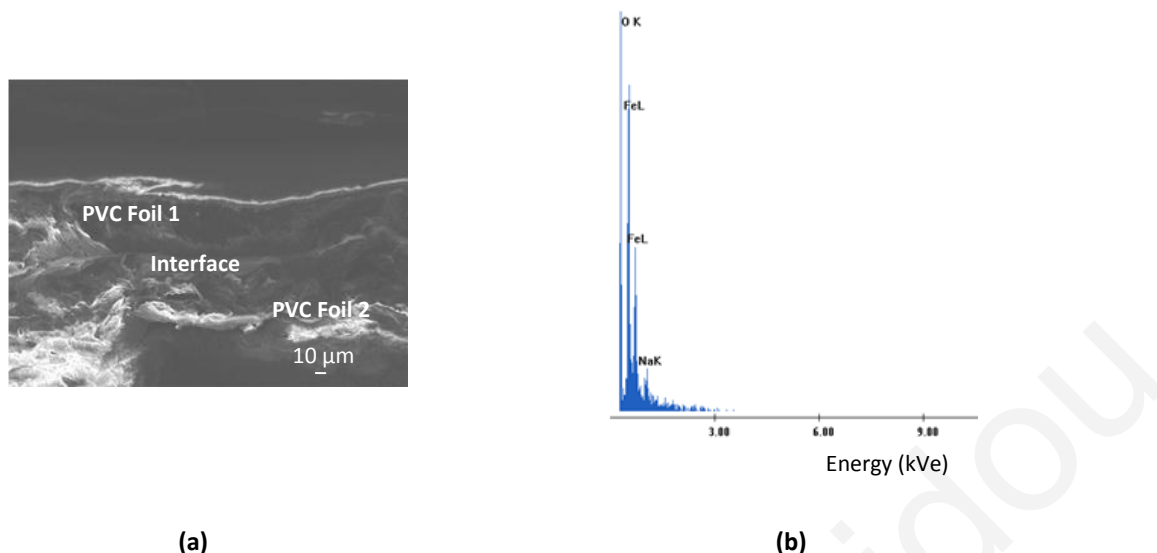
Figure 4.4 (a) FE-SEM micrograph and (b) FE-SEM/EDX of cross-section of the un-coated PVC/5 wt.% Fe$_3$O$_4$ (H$_2$O/DBS+DBS) nanocomposite manufactured with ultrasonic welding - Sample 4e

4.2.2 PVC nanocomposites with embedded Pd nanoparticles

Figure 4.5 illustrates cross-sectioned geometries of Pd-PVC nanocomposite (Sample 5a) in different magnifications. One can also clearly distinguish a configuration consisting of two PVC foils joined together, with an intermediate heat affected zone. The Pd coated nanoparticles can also not be visualized by SEM mainly because of their polymeric coating surface PVC and their very small sizes ($\approx$ 8 $\pm$ 1.7 nm) [151]. Analysis with Field Emission Scanning Microscopy coupled with Energy Dispersive X-ray (FE-SEM/EDX) Spectroscopy did not show any results because of the very small concentration, which was in the order of 0.012 wt.%, of palladium Pd in the PVC nanocomposite, i.e. not detectable by the instrument.

(a)   **(b)**   **(c)**
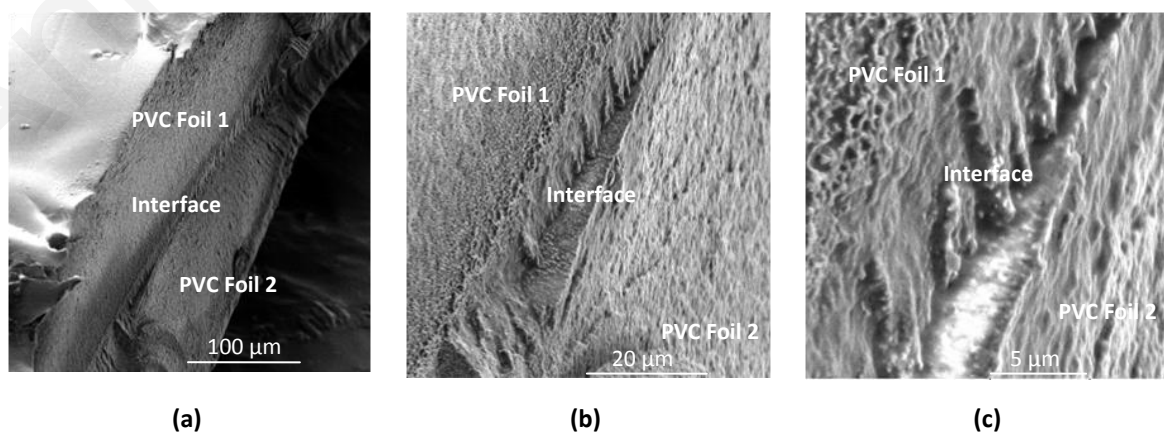
Figure 4.5 SEM micrographs of cross-section of PVC/0.012 wt.% Pd nanocomposites manufactured by means of ultrasonic welding, in different magnifications - Sample 5a

4.3 Transmission electron microscopy and energy dispersive X-ray analysis

TEM analysis was carried out in order to visualize and study the distribution of the ferrimagnetic nanoparticles of the Fe_3O_4-PVC nanocomposite and the Pd particles of the Pd-PVC nanocomposite samples. Ultrathin sections of all the PVC/Fe_3O_4 and PVC/Pd nanocomposite samples were prepared for the TEM, using an ultra 45 degrees and 4.0 mm microtome equipped with a diamond knife. Before cutting the nanocomposites, they were immersed in a polymer resin to get stabilized for the purpose of the characterization technique and to be able to be cut. Following this, the very thin samples were deposited, by simple drop, in ambient conditions onto a TEM copper grid. Micrographs were obtained with two different TEM equipments: a JEM1010 TEM apparatus (JEOL) operating at an acceleration voltage of 80kV of the Institute of Neurology and Genetics Cyprus, and a Philips CM20 TEM with an ultrathin window energy dispersive X-ray analyzer of the National Center for Scientific Research Demokritos.

At first plain PVC, without nanoparticle addition, ultrasonically welded foils were visualized in order to be able to compare those results with the results of the nanocomposites (see Figure 4.6). The smooth black particles illustrated in Figure 4.6 (a) to (d) are titanium dioxide (TiO_2) additives (for the white color in the PVC foil) and were pre-existed in the polymer matrix. Their size is around 100 - 250 nm and their presence is confirmed by Energy Dispersive X-ray Analysis in the cross-section (Figure 4.7i).
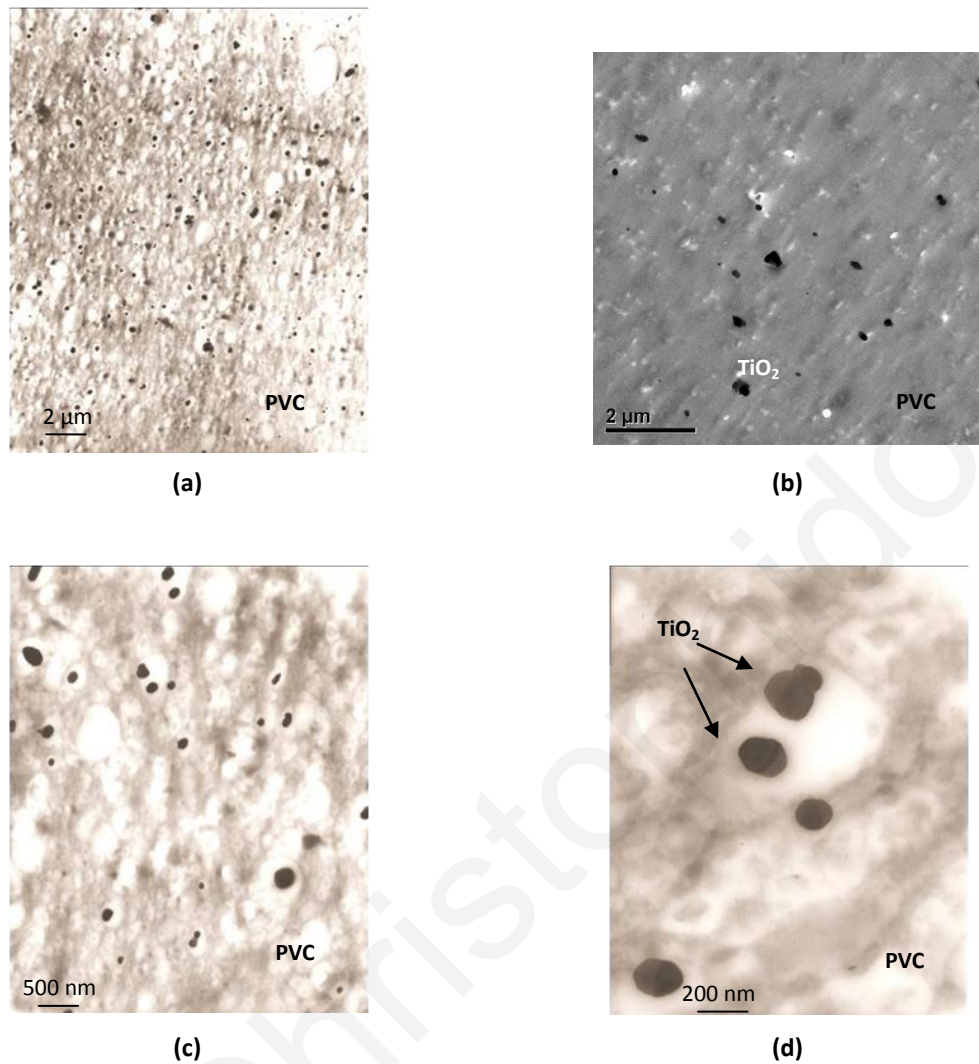
Figure 4.6 TEM micrographs of a cross-section of the two ultrasonically welded PVC foils

The Fe_3O_4-PVC nanocomposites are presented in Figure 4.7 to Figure 4.20. From those, it is obvious that the Fe_3O_4 nanoparticles are dispersed uniformly through the interface of the two PVC foils, in different depths/widths. This is an evidence of the good dispersion of nanoparticles achieved in the stage of nanocomposites preparation, i.e. the matching of nano-fluids with the polymer matrix, the proper dispersion of nanoparticles onto the PVC matrix with the spin coating technique, as well as maintaining of the dispersion during welding. The average size of the Fe_3O_4 nanoparticles is approximately 7 nm and this confirms the manufacturer's mean diameter (University of Timisoara) dimensions. The big ($\approx$ 100 - 250 nm) smooth particles illustrated in the pictures are TiO_2, as mentioned before.

4.3.1 Fe$_3$O$_4$ (C$_6$H$_{13}$OH/OA+OA), magnetic-PVC nanocomposites

Figure 4.7 to Figure Figure 4.10 correspond to nanocomposite samples of PVC foils with embedded Fe$_3$O$_4$ (C$_6$H$_{13}$OH/OA+OA, where the liquid carrier is hexanol/C$_6$H$_{13}$OH and the stabilizing agent is a double-layer covering of OA nanoparticles in different concentrations; this is the Sample 1 series of nanocomposites of Table 3.9. The combination of hexanol, as well as OA surfactant, produces nanocomposites with high concentration of nanoparticles all over the interfaces. Moreover, there is no presence of aggregates/agglomerations, as the nanoparticles retain their nano size.

Figure 4.7 illustrates a Fe$_3$O$_4$/PVC nanocomposite, Sample 1a with 0.1 wt.% Fe$_3$O$_4$ concentration. Analytically, Figure 4.7 (a) is a cross-section overview of two PVC foils joined together by means of ultrasonic welding, where Fe$_3$O$_4$ nanoparticles are discerned as dark shadows ($\approx$ 7 nm), embedded into the polymer matrix, and are uniformly dispersed mainly across all over their interface. The width of the nanoparticles dispersion is approximately equal to 1-2 μm. Figure 4.7 (b) to (h) illustrate the same sample as Figure 4.7 (a) in higher resolutions; however, the weld interface opened up and a hole was formed, because of the TEM beam. It is important to mention that Fe$_3$O$_4$ nanoparticles do not aggregate.

To confirm the presentence of the embedded nanoparticles an EDX Analysis was performed at the cross section, and is illustrated in Figure 4.7 (i). This analysis shows Fe and O peaks that confirm the presence of Fe$_3$O$_4$ nanoparticle in the nanocomposite. The presence of Cl and Ti in the cross-section, which are ingredients of PVC matrix, is also clear. Moreover, Cu is present because of the copper grid the sample was placed in.
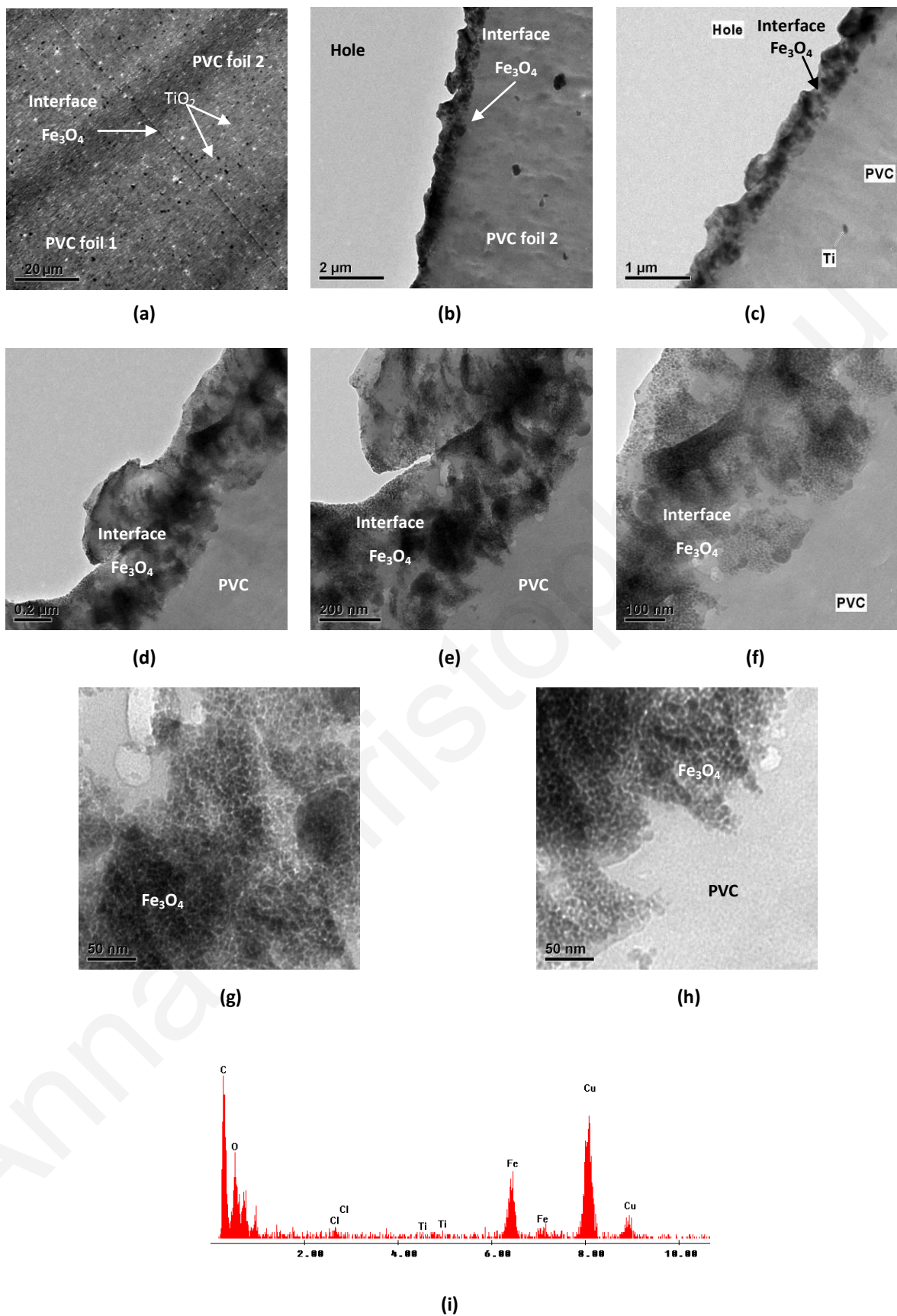
Figure 4.7 (a) to (h) TEM micrographs of a cross-section, and (i) EDX of a cross-section, of the PVC loaded with 0.1 wt.% Fe$_3$O$_4$/C$_6$H$_{13}$OH(OA+OA) nanocomposite foils - Sample 1a

Figure 4.8 (a) to (c) illustrate a Fe_3O_4/PVC nanocomposite, Sample 1c with 0.5 wt.% Fe_3O_4 concentration. The width/penetration of the Fe_3O_4 nanoparticles dispersion is increased to approximately 4-5 µm, while the further dispersion of singularly nanoparticles into the PVC matrix is now visible. The presence of aggregates with size approximately ≈ 200 nm are also shown.

(a) **(b)** **(c)**
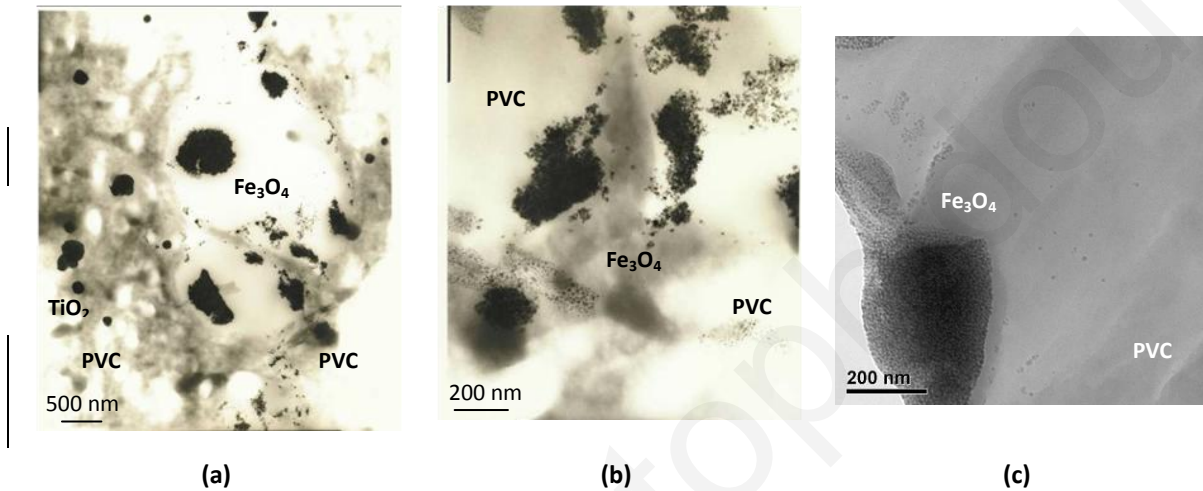
Figure 4.8 TEM micrographs of a cross-section of the PVC loaded with 0.3 wt.% Fe_3O_4/C_6H_{13}OH(OA+OA) nanocomposite foil - Sample 1c

Figure 4.9 (a) to (c) illustrate a Fe_3O_4/PVC nanocomposite, Sample 1d, with 1 wt.% Fe_3O_4 concentration. In this sample, it seems like nanoparticles diffuse within the polymer matrix, while a greater penetration of the Fe_3O_4 nanoparticles into the PVC matrix is evident. Again, TEM beam strain opened up a hole to the very thin weld interface.

(a) **(b)** **(c)**
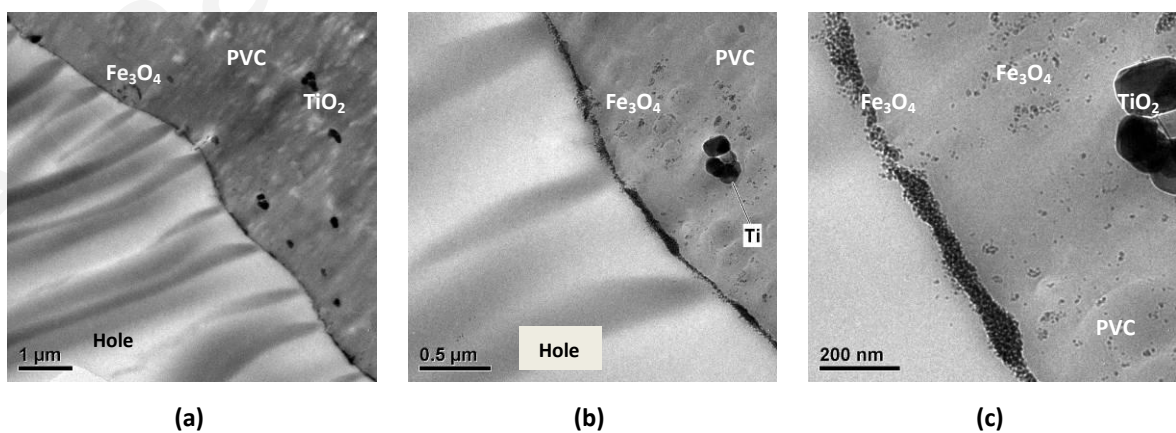
Figure 4.9 TEM micrographs of a cross-section of the PVC loaded with 1 wt.% Fe_3O_4/C_6H_{13}OH(OA+OA) nanocomposite foil - Sample 1d

Figure 4.10 illustrates Sample 1e, a Fe_3O_4/PVC nanocomposite, with 2 wt.% Fe_3O_4 concentration, in different magnifications. The Fe_3O_4 nanoparticle dispersion is visible in wider depth (≈ 10 μm) into the polymer matrix. The interface has also higher particle density, while the distribution of nanoparticles is uniform and continuous all over its range.

(a)   **(b)**   **(c)**

(d)   **(e)**   **(f)**

(g)   **(h)**   **(i)**
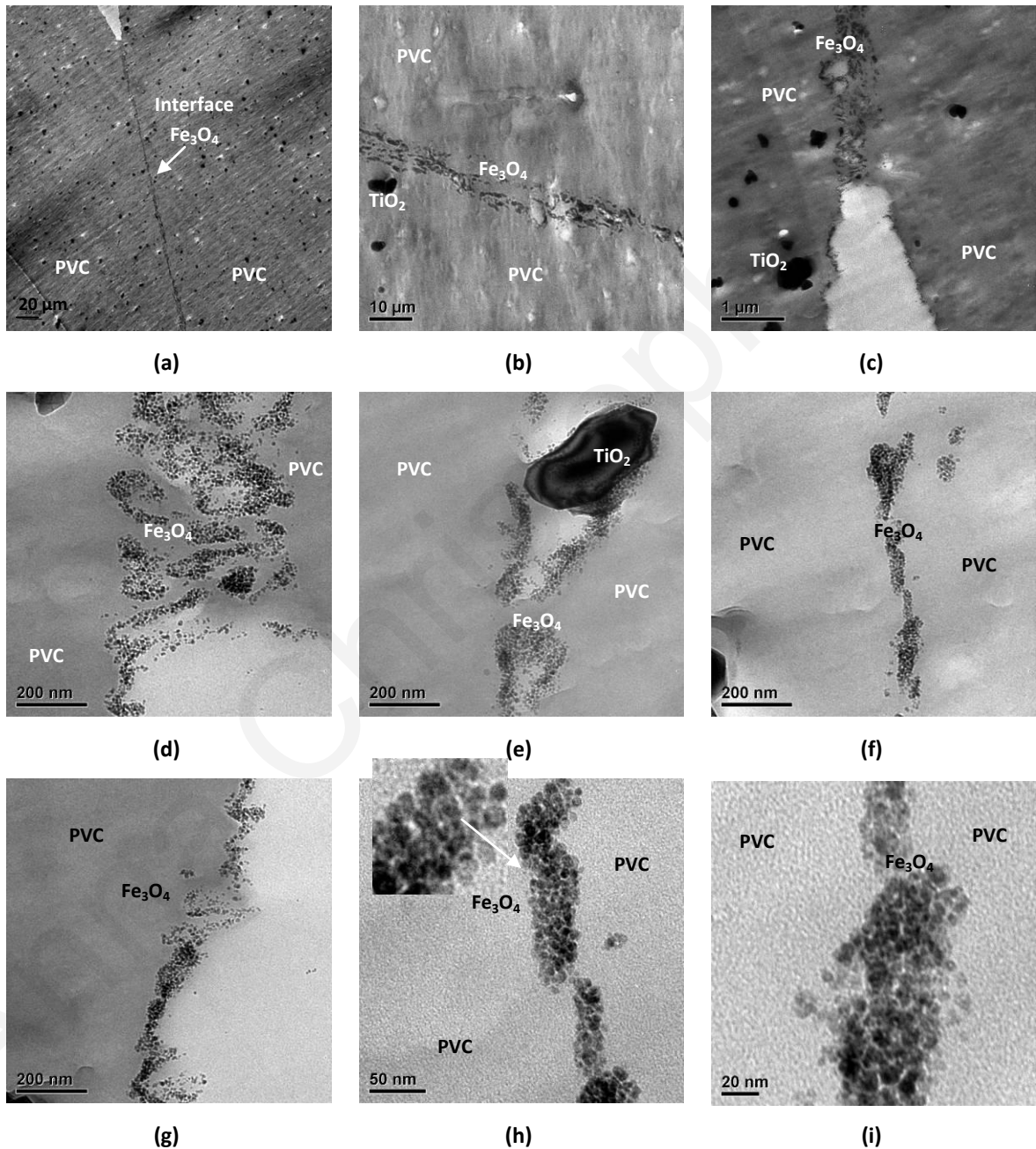
Figure 4.10 TEM micrographs of a cross-section of the PVC loaded with 2 wt.% Fe_3O_4/$C_6H_{13}OH$(OA+OA) nanocomposite foil - Sample 1e

4.3.2 Fe₃O₄ (H₂O/LA+LA), magnetic-PVC nanocomposites

Figure 4.11 to Figure Figure 4.13 correspond to nanocomposite samples of PVC with Fe_3O_4/H₂O/LA+LA, where the liquid carrier is de-ionized water/H_2O and the stabilizing agent is a double-layer covering of LA embedded nanoparticles in different concentrations; this is the Sample 2 series of Table 3.9 in Chapter 3. Regarding those figures, one can observe that the combination of the de-ionized water with LA do not allow Fe_3O_4 nanoparticles to disperse into the PVC matrix, rather than they remain concentrated in the interface; this is an evidence that molecular bonds among nanoparticles prevent their further dispersion into the polymer matrix. The Fe_3O_4 nanoparticles are distinctly visualized, while their texture differs compared to those of Figure 4.7 to Figure 4.10 and could be described as sticky.

Figure 4.11 illustrates cross-sections of the interface of the two PVC foils with 0.1 wt.% Fe_3O_4, Sample 2b, in various magnifications. In this sample, the Fe_3O_4 nanoparticles are forming a discontinuous layer within the interface, with a width approximately equal to 0.1 μm, while no significant dispersion of nanoparticles is observed beyond this width.

(a)   **(b)**   **(c)**
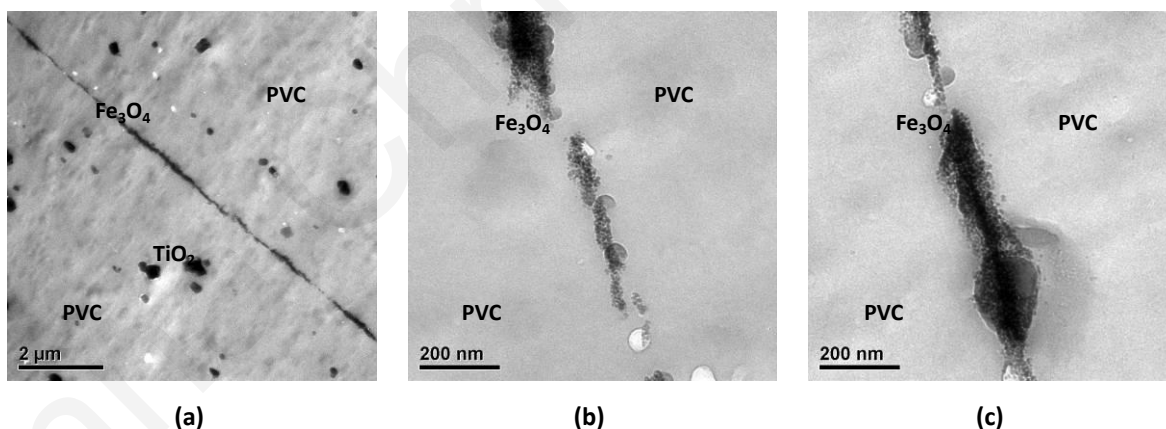
Figure 4.11 TEM micrographs of a cross-section of the of the PVC loaded with 0.1 wt.% Fe₃O₄/H₂O(LA+LA) nanocomposite foil - Sample 2b

Figure 4.12 shows cross-sections of the interface of the nanocomposite Sample 2c, with 0.3 wt.% concentration of Fe_3O_4 nanoparticles, in various magnifications. Similar to Sample 2b, the Fe_3O_4 nanoparticles are forming a discontinuous layer within the interface, with a wider width, which is approximately equal to 0.2 μm. Moreover, there is no significant dispersion of nanoparticles observed beyond this width. Figure 4.12 (e), displays the dark field image of the nanoparticle crystalline structure that illustrated in

Figure 4.12 (d).
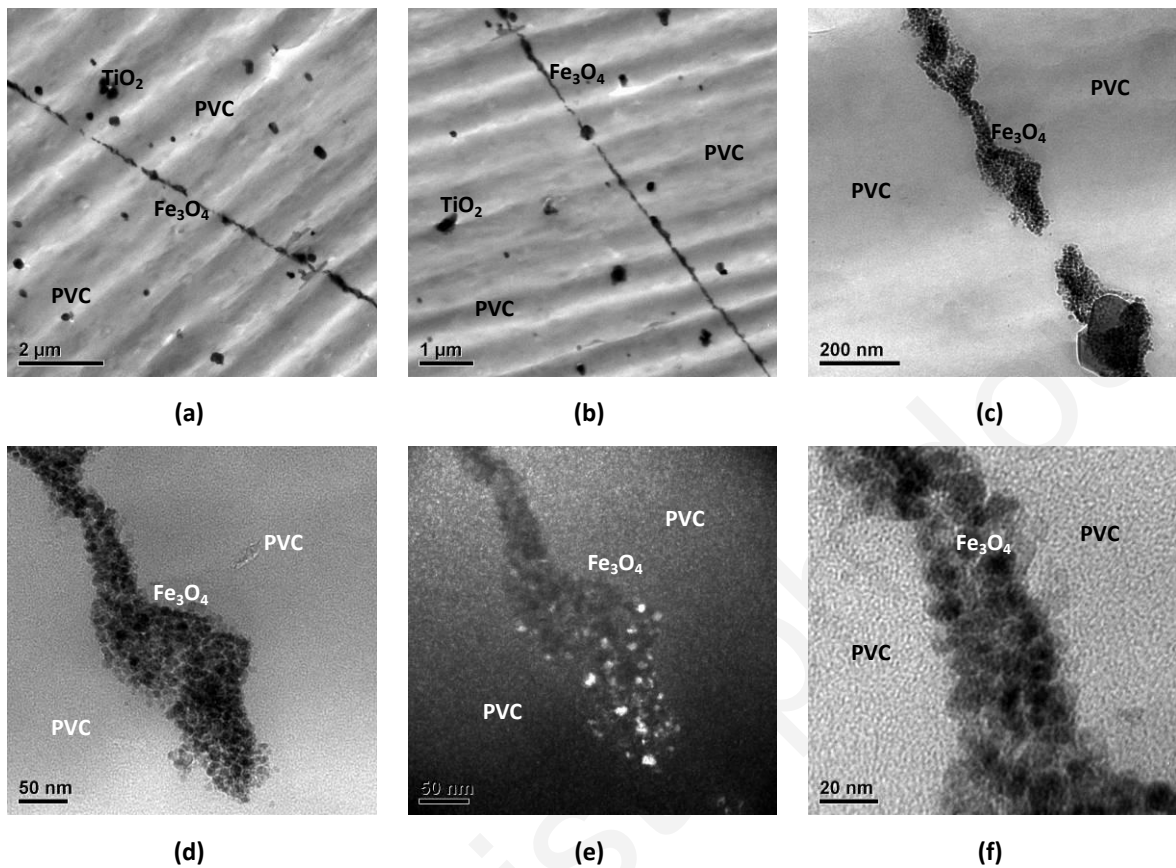
Figure 4.12 TEM micrographs of a cross-section of the of the PVC loaded with 0.3 wt.% Fe$_3$O$_4$/H$_2$O(LA+LA) nanocomposite foil - Sample 2c

Figure 4.13 illustrates Sample 2d, with 0.5 wt.% Fe$_3$O$_4$ concentration, where nanoparticles are again concentrated at the interface; comparing with Samples 2b and 2c, a less discontinuous layer is presented (width approximately 0.2 µm). Small aggregates are clearly present all over the interface.
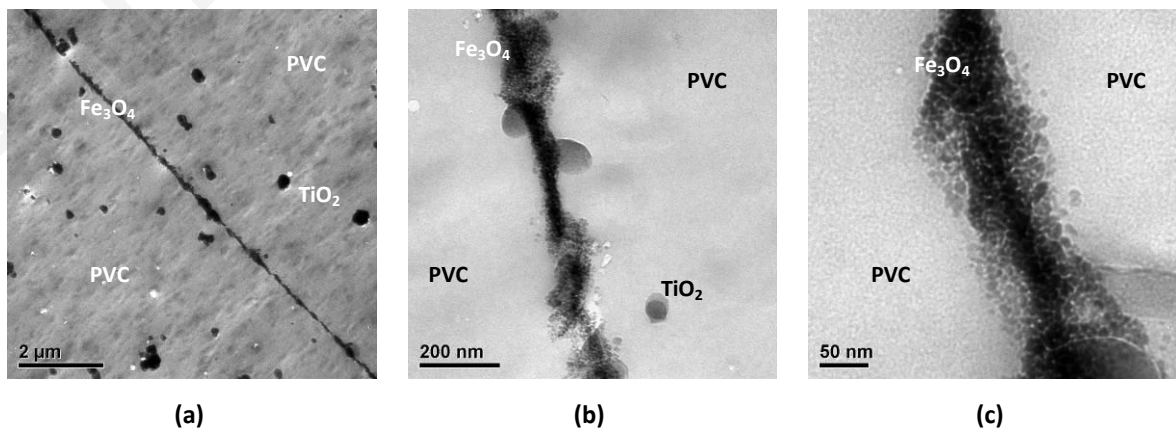
Figure 4.13 TEM micrographs of a cross-section of the of the PVC loaded with 0.5 wt.% Fe$_3$O$_4$/H$_2$O(LA+LA) nanocomposite foil - Sample 2d

4.3.3 Fe_3O_4 (TR-30/OA+OA), magnetic-PVC nanocomposites

Figure 4.14 to Figure 4.16 correspond to nanocomposite samples of PVC with Fe_3O_4/TR-30/OA+OA (Sample 3, Table 3.9), where the liquid carrier is transformer oil/TR-30 and the stabilizing agent is a double-layer covering of OA embedded nanoparticles. In general, good dispersion was achieved all over the interface.

Figure 4.14 illustrates Sample 3a with 0.1 wt.% Fe_3O_4 concentration. According to those images, nanoparticles are well dispersed all over the interface of the nanocomposite. In Figure 4.14 (b) the white color at the interface is created due to the imperfection at the weld interface and the penetration of resin during sample preparation.

Figure 4.14 TEM micrographs of a cross-section of the of the PVC loaded with 0.1 wt.% Fe_3O_4/TR30(OA+OA) nanocomposite foil - Sample 3a

Moreover, in higher nanoparticle concentrations, clusters in the order of 200 nm x 500 nm (Figure 4.15) and 500 nm x 1000 nm (Figure 4.16), were created. Figure 4.15 and Figure 4.16 are illustrating Samples 3b and 3c with 0.3 wt.% and 0.5 wt.% Fe_3O_4 concentration, respectively.

(a)   **(b)**
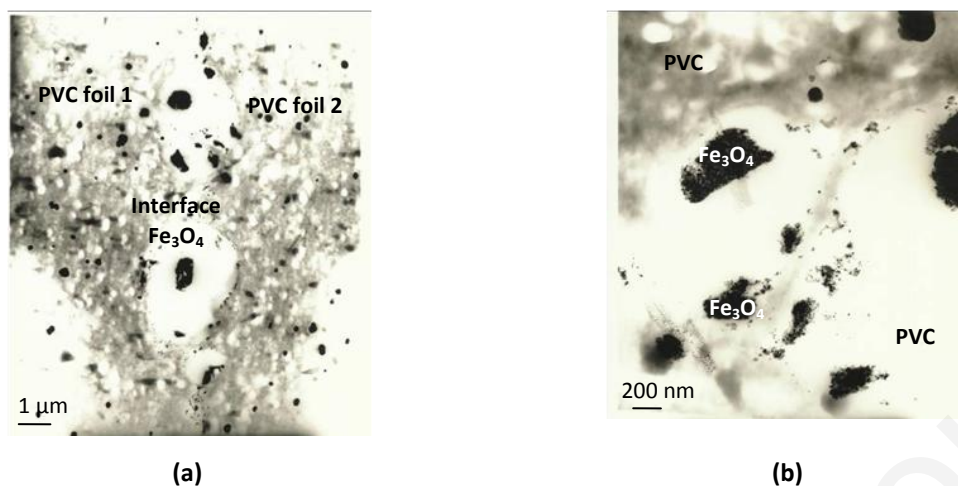
Figure 4.15 TEM micrographs of a cross-section of the of the PVC loaded with 0.3 wt.% Fe$_3$O$_4$/TR30(OA+OA) nanocomposite foil - Sample 3b

(a)   **(b)**   **(c)**
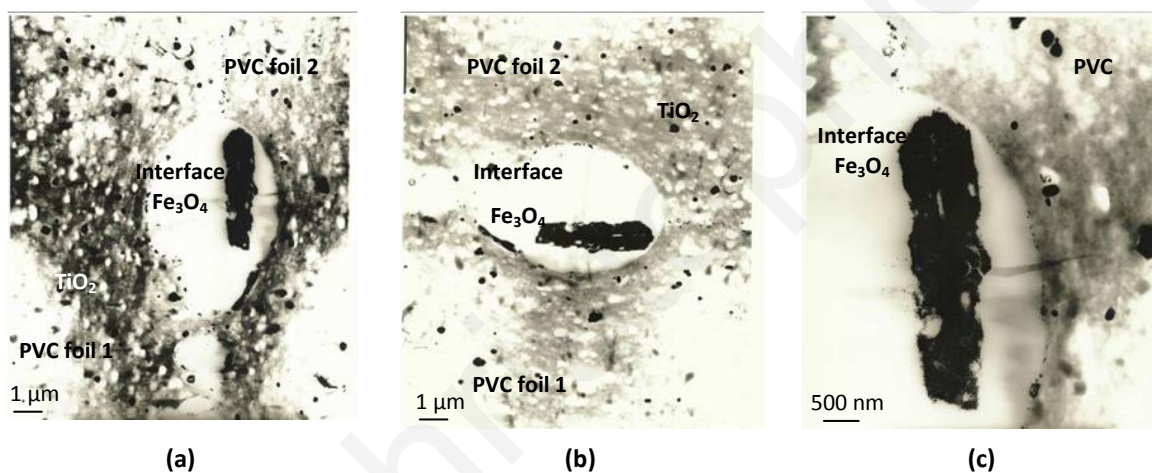
Figure 4.16 TEM micrographs of a cross-section of the of the PVC loaded with 0.5 wt.% Fe$_3$O$_4$/TR30(OA+OA) nanocomposite foil - Sample 3c

4.3.4 Fe$_3$O$_4$ (H$_2$O/DBS+DBS), magnetic-PVC nanocomposites

Figure 4.17 to Figure 4.19 correspond to nanocomposite samples of PVC with Fe$_3$O$_4$/H$_2$O/DBS+DBS, where the liquid carrier is de-ionized H$_2$O and the stabilizing agent is a double-layer covering of DBS embedded nanoparticles in different concentrations (Sample 4 of Table 3.9). As a general observation, one can notice that uniform layers, consisting of nanoparticles, are formed both at the interface, as well as within the polymer matrix, for nanocomposites with higher than 1 wt.% concentrations of nanoparticles. This phenomenon can be explained either by the different mechanism that occurs during penetration of nanoparticles in the polymeric matrix, due to diversity of magnetic fluid, or due to the higher concentrations of nanoparticles that are forced to penetrate into the polymer matrix.

60

A cross-section overview of the two PVC foils with 0.5 wt.% Fe_3O_4 concentration, this is Sample 4a, is illustrated in Figure 4.17, in different magnifications. The Fe_3O_4 nanoparticles are distinctly visualized, while their texture looks the same as of Sample No 2 (Figure 4.11 and Figure 4.13) upon comparison. It should be noted that in both samples, the used nanoparticles were dispersed/stabilized in water. In the present case and contrary to the second sample, the Fe_3O_4 nanoparticles are forming a continuous layer within the interface, with a width approximately equal to 0.2 μm, while again, there is no significant dispersion of nanoparticles observed beyond this width. This phenomenon i.e. the prevention of the further dispersion of the nanoparticles into the polymer matrix, maybe attributed to specific nanoparticle-nanoparticle or nanoparticle-polymer matrix interactions.

(a)   **(b)**   **(c)**
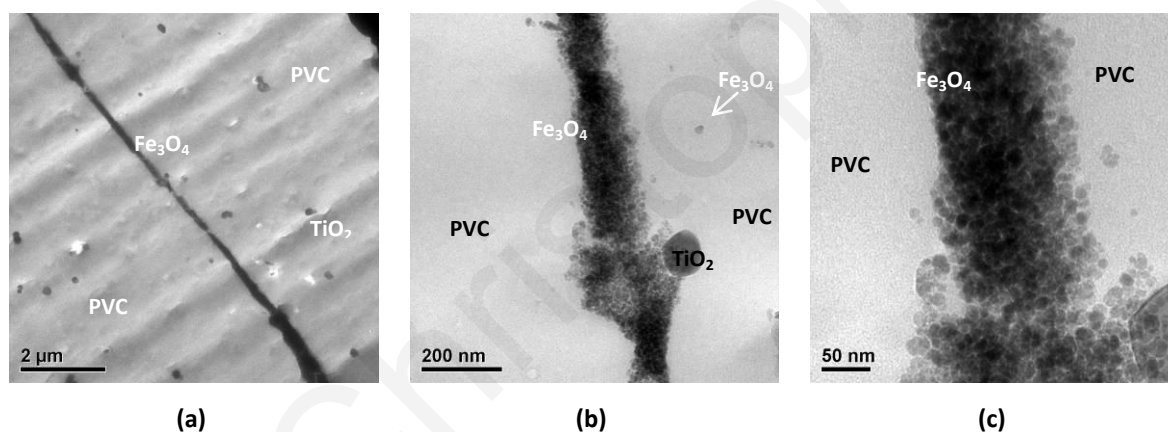
Figure 4.17 TEM micrographs of a cross-section of the of the PVC loaded with 0.5 wt.% Fe_3O_4/H_2O(DBS+DBS) nanocomposite foil - Sample 4a

Figure 4.18 illustrates Sample 4c of Table 3.9, which has 2 wt.% Fe_3O_4 concentration. In this sample, further dispersion of nanoparticles into the PVC matrix is notable, while a layer of nanoparticles has been created and further dispersion has occurred into the polymer matrix. The created layers are containing concentrated amounts of nanoparticles, while agglomerations are evident. The behavior of this nanocomposite to ultrasonic welding seems to be different from those that have been examined so far, maybe due to the higher concentrations of nanoparticles (2 wt.%), that are forced to penetrate into the polymer matrix.

(a)

(b)

(c)

(d)
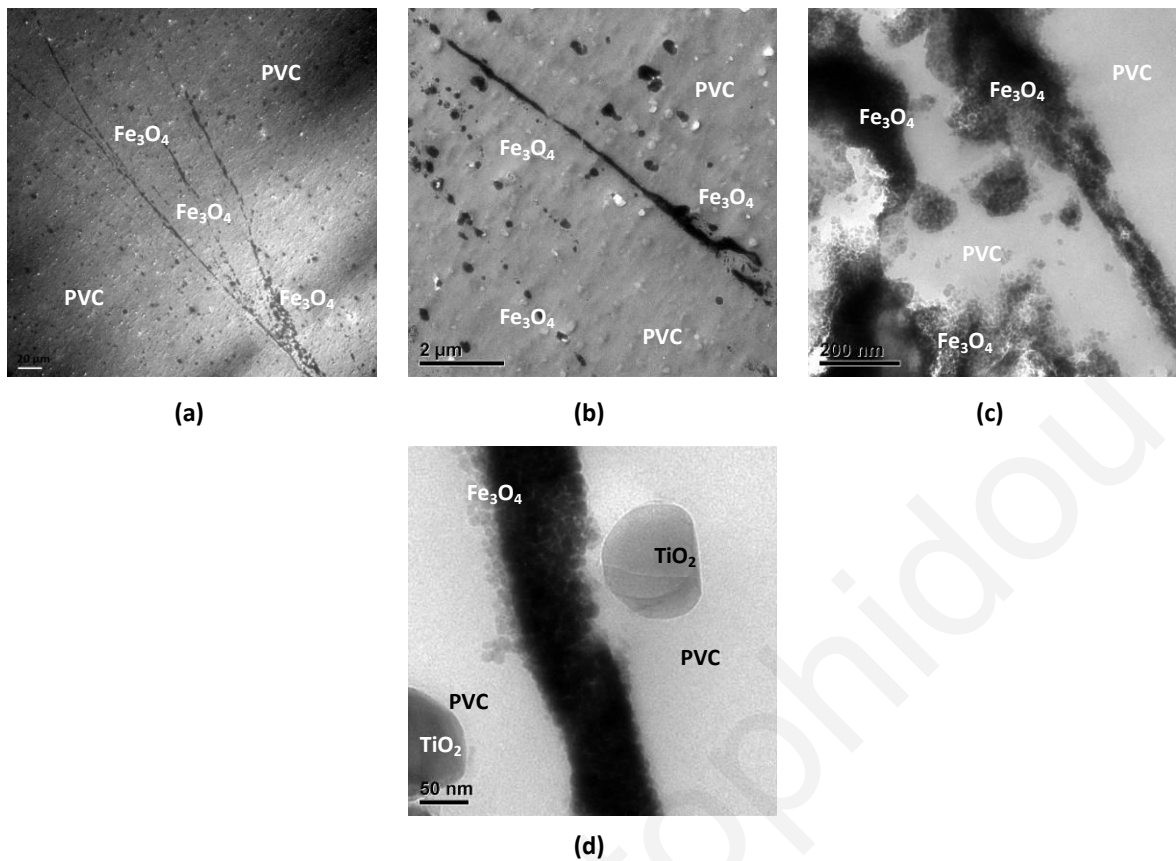
Figure 4.18 TEM micrographs of a cross-section of the of the PVC loaded with 2 wt.% Fe$_3$O$_4$/H$_2$O(DBS+DBS) nanocomposite foil - Sample 4c

Sample 4e, which is illustrated in Figure 4.19, with 5 wt.% Fe$_3$O$_4$ concentration, exhibit relevant to Sample 4c mechanism of further nanoparticle dispersion, possibly until 100 μm. Moreover, many parallel layers of agglomerated nanoparticles have been created as a consequence of the high nanoparticle concentration (5 wt.%) over the surface. Their average width is in the range of 100-200 nm, and dispersed throughout the nanocomposite matrix.
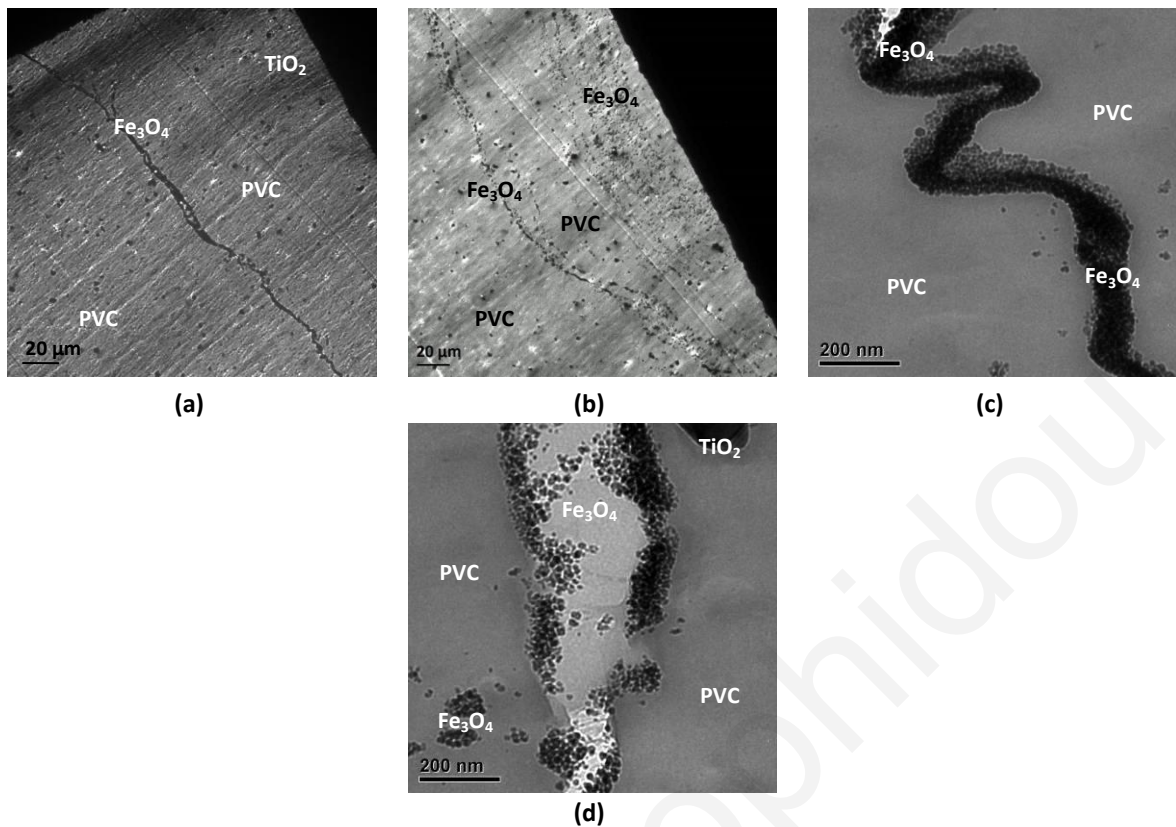
Figure 4.19 TEM micrographs of a cross-section of the of the PVC loaded with 5 wt.% Fe_3O_4/H_2O(DBS+DBS) nanocomposite foil - Sample 4e

4.3.5 Pd-PVC nanocomposites

TEM micrographs were also taken for the Pd/PVC nanocomposite with 0.012 wt.% Pd concentration (Figure 4.20). Pd nanoparticles were also visible in images with magnification x10000 and are very well dispersed into the nanocomposite interface. Compared to iron Fe_3O_4, the Pd particles are smoother and their size is approximately 8 nm. Again, the presence of TiO_2 particles is obvious and creates discontinuities to the nanocomposite.
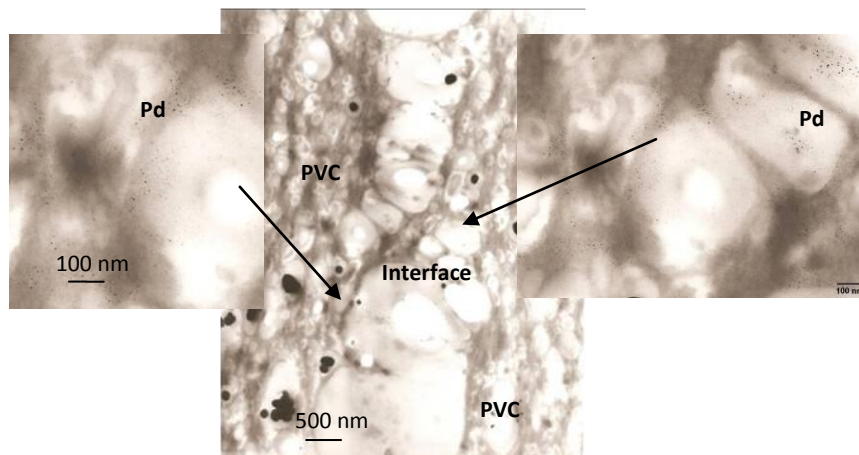
Figure 4.20 TEM micrographs of a cross-section of the sample Pd-PVC nanocomposite foil, with a particle concentration of 0.012 wt.% - Sample 5a

4.4 Optical microscopy

The structure of ultrasonically welded Fe_3O_4/PVC nanocomposite system was also studied by an Ambios white light optical profilometer (Xi 100). Figure 4.21 displays the cross-section of the weld affected zone, which clearly shows the nanoparticle layer at the interface of the two PVC foils. Again, the bigger particles shown in the pictures are TiO_2 particles.

(a)   **(b)**   **(c)**
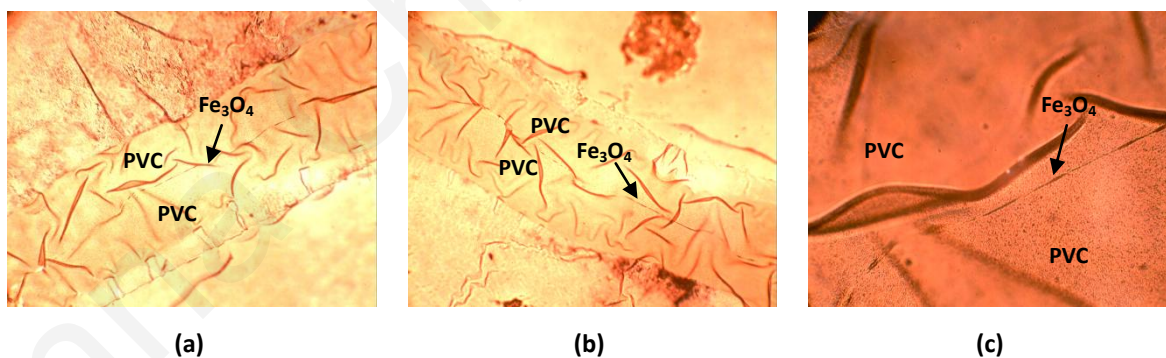
Figure 4.21 White light optical profilometer micrographs of a cross-section of the of PVC loaded with 5 wt.% Fe_3O_4/H_2O(DBS+DBS) nanocomposite foil - Sample 4e

4.5 Magnetic properties of the PVC nanocomposites

The magnetic properties of the nanocomposites are investigated through their magnetic hysteresis loop, illustrating the influence of the magnetic Fe_3O_4 nanoparticles

on the magnetic behavior of the nanocomposites. Magnetization as a function of the applied magnetic field strength plots (M = f(H)), of Fe_3O_4/PVC and Pd/PVC nanocomposites, was studied using a Quantum Design Physical Properties Measurement System (PPMS), at room temperature.

4.5.1 Fe_3O_4-PVC nanocomposites

Figure 4.22 to Figure 4.25 present the magnetization curves for the four series of Fe_3O_4/PVC nanocomposites, each containing a different magnetic fluid and concentration of ferrimagnetic nanoparticles. Almost all samples exhibit superparamagnetic behavior with no observed hysteresis loop, as evidenced by the S-like curve shape, as well as from the fact that the hysteresis loop is perfectly centered around a zero magnetic field. However, some of the samples exhibit ferrimagnetic behavior since in their magnetization curves a small hysteresis loop is present.

According to the literature, superparamagnetism is a kind of magnetism that occurs in small ferromagnetic or ferrimagnetic nanoparticles when their grain sizes are in the order of a few to tenth of nanometers depending on the type of the nanoparticle. Those nanoparticles are actually reacting as single-domain particles, while one can say that the total magnetic moment of the nanoparticle can be regarded as one giant magnetic moment, composed of all the individual magnetic moments of the atoms which form the nanoparticle [161-162].
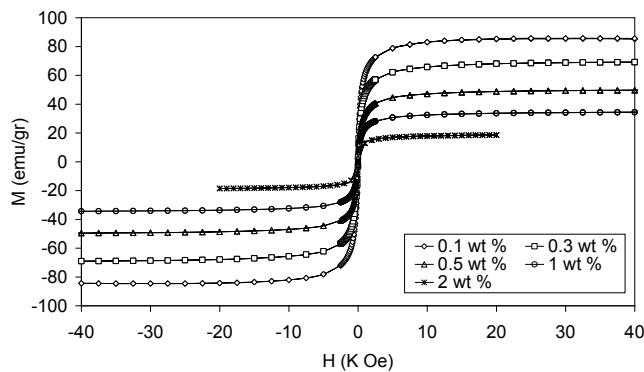
Figure 4.22 Magnetization curves of polymeric PVC foils containing various concentrations of magnetite (Fe_3O_4), PVC/Fe_3O_4 (H_2O/OA+OA) - Sample 1 series
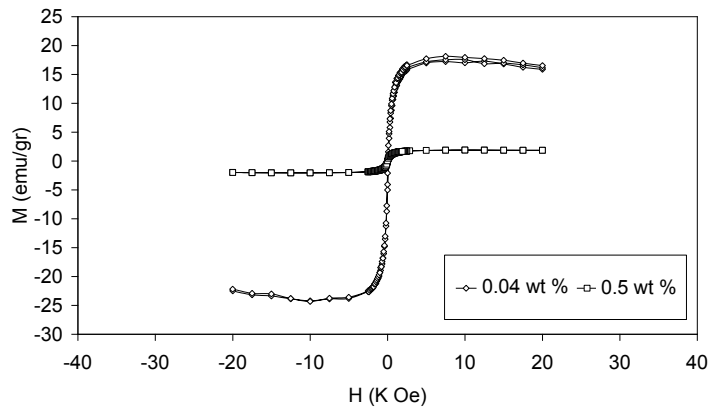
Figure 4.23 Magnetization curves of polymeric PVC foils containing various concentrations of magnetite (Fe₃O₄), PVC/Fe₃O₄ (H₂O/LA+LA) - Sample 2 series
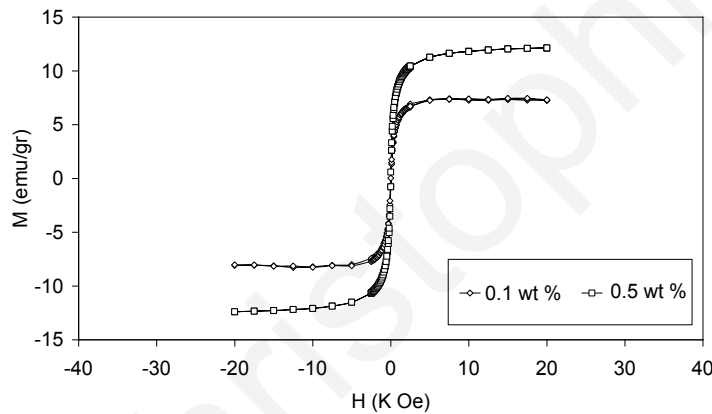
Figure 4.24 Magnetization curves of PVC foils containing various concentrations of magnetite (Fe₃O₄), PVC/Fe₃O₄ (TR-30/OA+OA) - Sample 3 series
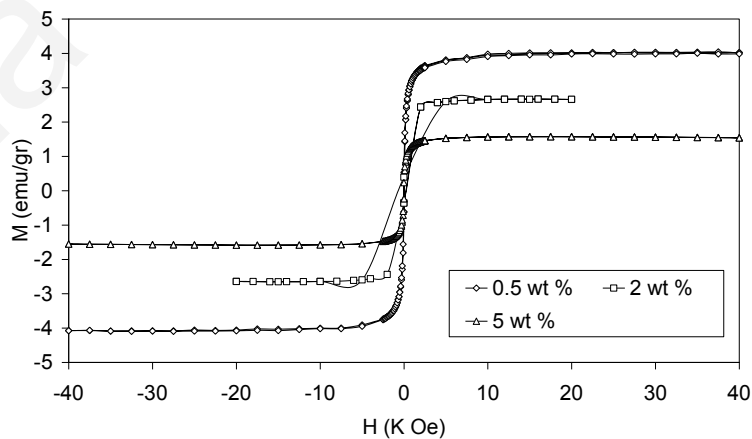
Figure 4.25 Magnetization curves of polymeric PVC foils containing various concentrations of magnetite (Fe₃O₄), PVC/Fe₃O₄ (H₂O/DBS+DBS) - Sample 4 series

By comparing the results of Figure 4.22 to Figure 4.25, measurements of Sample 1

(Figure 4.22) i.e. PVC/Fe$_3$O$_4$ (C$_6$H$_{13}$OH/OA+OA), show superparamagnetic behavior with high saturation magnetization values, compared to samples No 2 (PVC/Fe$_3$O$_4$ (H$_2$O/LA+LA)) (Figure 4.23), No 3 (PVC/Fe$_3$O$_4$ (TR-30/OA+OA)) (Figure 4.24), and No 4 (PVC/Fe$_3$O$_4$ (H$_2$O/DBS+DBS)) (Figure 4.25). The remarkable superparamagnetic behavior of the Sample 1 series is also obvious when compared to other PVC/nanocomposites, with similar concentrations of magnetic nanoparticles, prepared with other synthesis methods [163-166]. The magnetic properties (superparamagnetic and ferrimagnetic) of the Samples 2 to 4 are almost relevant to those found in the above mentioned literature. The probable reason for this remarkable superparamagnetic behavior of the Sample 1 series of nanocomposites is that there was success in keeping the dimensions of the grains to nanoparticle size, that is approximately 7 nm, and single-particle behavior/effects were achieved [167]. A probable explanation for keeping the grains very small thus acting as single-domains, is that the hexanol-1 (Fe$_3$O$_4$(C$_6$H$_{13}$OH/OA+OA) magnetic fluid exhibited excellent stabilization in the carrier fluid, thus preventing nanoparticle agglomeration phenomena to take place. Furthermore a very good dispersion of the Fe$_3$O$_4$ nanoparticles over the surface of PVC was achieved, probably due to the low interfacial tension of PVC and hexanol-1, as well as the immediate hexanol-1 evaporation. Moreover, the stabilizing layer of OA did not allow the Fe$_3$O$_4$ particles to approach each other, while the low melting temperature of oleic OA, which is approximately 13 ^{o}C, should also be considered. In addition, a very good penetration of the Fe$_3$O$_4$ nanoparticles into PVC matrix was also achieved, while the polymer ultrasonic welding process appears to provide the proper mobilization of the nanoparticles to disperse through the interface and no agglomerations were created. A further explanation of this high Ms values is that according to TEM pictures the nanoparticles actually accumulated over the interface with maximum width of 200 nm for concentrations lower that 2 wt.% and as a result the main volume of the nanoparticles are located there, irrelevant to the composition of the final product.

Moreover, it is a fact that in Figure 4.22, Figure 4.23 and Figure 4.25, which correspond to the Sample series No 1 (PVC/Fe$_3$O$_4$ (C$_6$H$_{13}$OH/OA+OA)), No 2 (PVC/Fe$_3$O$_4$ (H$_2$O/LA+LA)) and No 4 (PVC/Fe$_3$O$_4$ (H$_2$O/DBS+DBS)), respectively, when the concentration of iron oxide particles increases, the saturation magnetization decreases. Such a decrease in the magnetization could be attributed to the growth of nanoparticles

67

clusters [162]. Actually, the particle size remains constant but the particle concentration increases. A possible explanation (regarding also the TEM images illustrated above) is that the particles approach each other, the spacing between them is reduced and finally they agglomerate. Therefore, probably antiferrimagnetic correlations between the agglomerations/clusters occur which counteracts superparamagnetic and/or ferrimagnetic properties of the nanocomposites. Another possible explanation is that magnetite phase transition to hematite occurs, probably during ultrasonic welding; however further investigation is required to verify this assumption.

The magnetic parameters, which have been obtained from corresponding magnetization curves of all the nanocomposites, are presented in Table 4.1. Where, coercive field (H_c) is a measure of the ability of a ferrimagnetic nanocomposite to withstand an external magnetic field without becoming demagnetized, and saturation magnetization (M_s) is the maximum possible magnetization, of a ferrimagnetic nanocomposite and represents the magnetization that results when all the magnetic dipoles in a solid piece are mutually aligned with the external field [168].

Table 4.1 Magnetic properties of Fe_3O_4-PVC nanocomposites

Sample number	Liquid carrier/ Stabilizing layer	PVC/Fe_3O_4 (wt.%)	Coercive field H_c (Oe)	Fe_3O_4 Saturation magnetization M_s (emu/g)
1a	$C_6H_{13}OH$/Oleic acid (double)	0.1	44	84.8
1b	$C_6H_{13}OH$/Oleic acid (double)	0.3	42	69.2
1c	$C_6H_{13}OH$/Oleic acid (double)	0.5	43	49.7
1d	$C_6H_{13}OH$/Oleic acid (double)	1	43	34.6
1e	$C_6H_{13}OH$/Oleic acid (double)	2	18	23.3
2a	H_2O/Lauric acid (double)	0.04	35	15.9
2d	H_2O/Lauric acid (double)	0.5	35	2
3a	TR-30/Oleic acid (double)	0.1	35	7.3
3c	TR-30/Oleic acid (double)	0.5	35	12.1
4a	H_2O /Dodecylbenzenesulphonic acid (double)	0,5	40	4
4c	H_2O /Dodecylbenzenesulphonic acid (double)	2	20	2.7
4e	H_2O /Dodecylbenzenesulphonic acid (double)	5	40	1.6

According to Table 4.1, saturation magnetization and coercive field of the nanocomposites are strongly dependent on the nature of the liquid carrier, the nature of surfactant double layer covering of magnetite nanoparticles, as well as the nanoparticle concentration. The maximum magnetization value was achieved in the nanocomposite Sample 1, hexanol-based ferrofluids (PVC/Fe$_3$O$_4$ (C$_6$H$_{13}$OH/OA+OA)), with the content of 0.1 wt.% Fe$_3$O$_4$, and is equal to 84.8 emu/gr. As has been explained above, this indicates that the grain size of the nanoparticles did not increase and this is further verified from the microscopic analysis carried out (Figure 4.7 to Figure 4.10). The decrease of magnetization as magnetic particle concentration increases from 0.1 wt.% to 2 wt.% in Sample 1 is also a fact. On the other hand (Figure 4.26), the coercive field is almost constant and equal to 42-44 Oe from 0.1 wt.% to 1 wt.%, indicating that the particle size was constant up to a concentration of 1 wt.%. When this reaches a value of 2 wt.%, the coercive field value drops to 18 Oe. Since the coercive field is related to the magneto-crystalline anisotropy constant, this means that when interactions between nanoparticles increases, the Fe atoms approach each other and coalesce into larger particles, actually agglomerating into clusters in the order of 200 nm, while the ferrimagnetic advantage of the nanoparticles is suppressed.
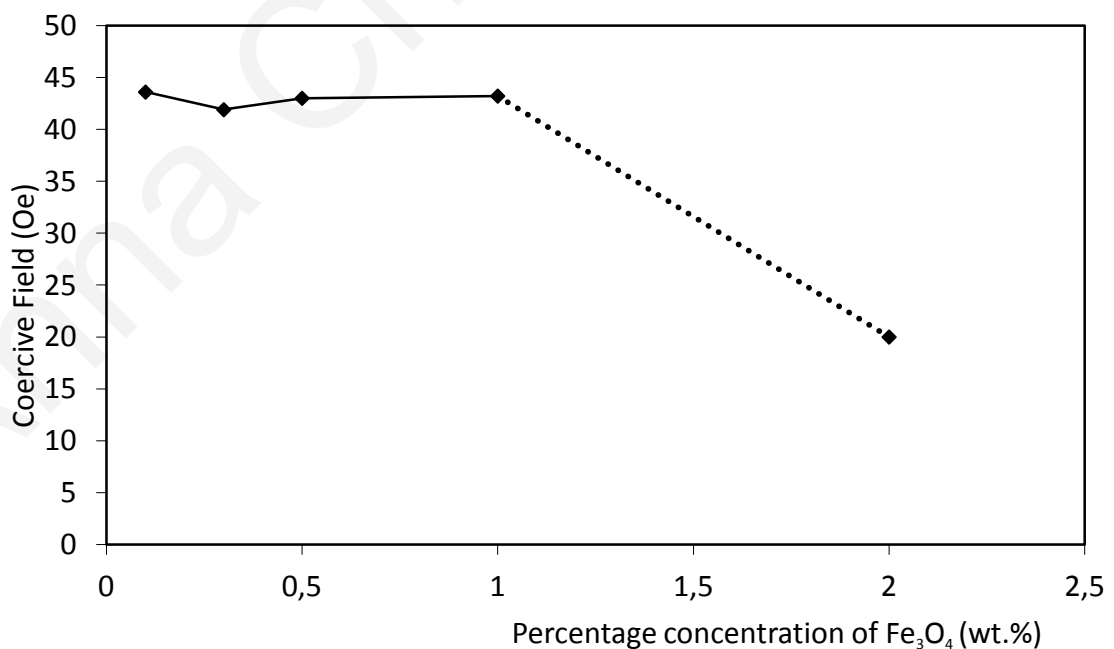
Figure 4.26 Coercive field versus percentage concentrations of magnetite (Fe$_3$O$_4$) in PVC foils, prepared with ferrofluid in hexanol-1, PVC/Fe$_3$O$_4$ (C$_6$H$_{13}$OH/OA+OA) - Sample 1 series

The coercive field of Samples 2 and 3 is constant and equal to 35 Oe for all concentrations, indicating that the particle size was constant, while coercive field of Sample 4 is equal to 40 Oe for 0.5 wt.%, it drops to 20 Oe for 2 wt.% and then reaches to 40 Oe for 5 wt.%. Taking into consideration all the above mentioned, coercive field value is constant to each series of nanocomposites for concentrations of nanoparticles up to 1 wt.%, while its value drops to half when concentration reaches the 2 wt.%. Further increasing the concentration increases also the coercive field.

4.5.2 Pd-PVC nanocomposites

The Pd/PVC nanocomposite sample did not show any magnetic properties, because of the very low concentration (mass lower than 1 mg) of the Pd nanoparticles in the nanocomposite sample (0.012 wt.% Pd concentration, ≈ 0.04 mg of Pd) i.e. at levels not detectable by the instrument. Actually, Pd mass magnetic susceptibility is equal to χ_{Pd} = Magnetization (M) (emu) divided by (Mass (g) x Magnetic field (H) (Oe)) = 5.28 emu/gOe, that is equal to a magnetic signal of 8.85×10^{-6} emu/gOe, which is lower than the resolution of the system, i.e. 10^{-5} emu.

4.6 Viscoelastic properties

A Dynamic Mechanical Analyzer (DMA) was used to characterize the viscoelastic properties of all the PVC/Fe$_3$O$_4$ and PVC/Pd polymer nanocomposite samples. The basic principle of this technique is that a sinusoidal displacement, strain ε, is applied to the polymer sample and the resulting force, stress σ, is measured. In a perfectly elastic polymer, the strain and stress are in phase, while in the case of a purely viscous fluid, there is a 90° phase delay (δ) of strain with respect to stress [169]. The viscoelastic PNCs are characterized by a phase difference/delay (δ) somewhere in between these two values. The extracted information are the storage modulus (E') which represents the stiffness (elastic segment) of the nanocomposites, and is proportional to the energy stored during a loading cycle; The loss modulus (E'') which is proportional to the energy dissipated (converted and not recoverable) during a loading cycle (i.e. the energy lost as heat due to internal friction of polymeric chains) and represents the viscous segment of

the nanocomposite; As well as the tanδ which is the ratio of E′′ to E′, within an investigated temperature range. In other words, the tanδ is a measure of the energy lost, expressed in terms of the recoverable energy (tanδ=E′′/E′), and it represents the mechanical damping (internal friction) in the nanocomposite. Furthermore, the maxima of the tanδ curves were used as the measurements of the glass transition temperatures (Tg), while at Tg the storage modulus (E′) decreases strongly and the loss modulus (E′′) reaches a maximum. The Tg is also a very important thermal property that characterizes the PNCs, as above the Tg, the matrix has rubbery properties and its stiffness drops dramatically, resulting in an increase in viscosity. Actually, the change from the "glass state" into the "rubber-elastic state" is called glass transition, where the polymer chains of the amorphous region begin moving in large-scale [169]. The presence of nanoparticles into the polymer matrix is expected to enhance all the above parameters.

A Triton Technology, Tritec 2000 DMA was employed (Figure 4.27a) to perform tensile mechanical cycling measurements. The samples were measured in the temperature range from −20 to 150 ^{o}C, with a heating rate of 1 ^{o}C.min^{-1}, at 1 Hz frequency and with 10 μm deformation amplitude. The tests were carried out in the tension mode, while all the tested nanocomposite sample dimensions were approximately 50 × 30 × 0.4 mm (Figure 4.27b). Liquid nitrogen was used to achieve the low temperatures of experimental conditions. Figure 4.28 to Figure 4.42 present the results of DMA tests as a function of temperature.

(a) **(b)**
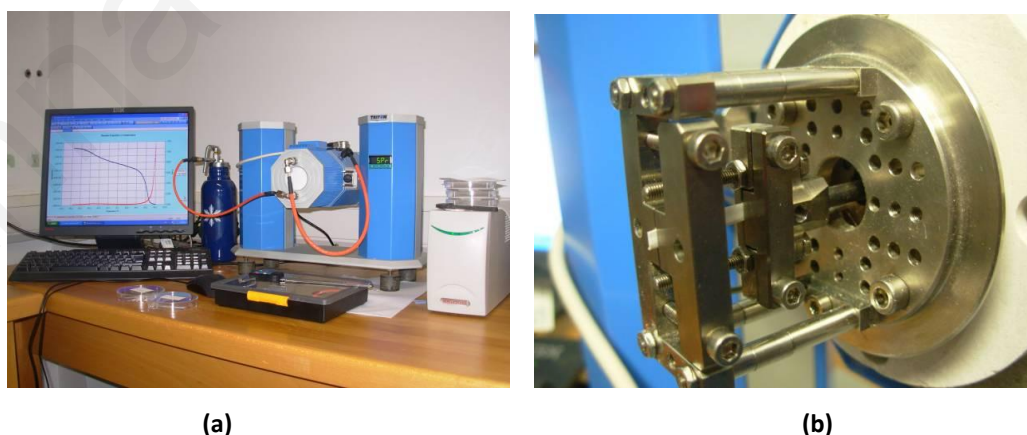
Figure 4.27 (a) Dynamic mechanical analyzer procedure, (b) mounded nanocomposite sample, under DMA tension mode

The curves can be explained by the fact that at low temperatures the polymer

nanocomposite molecules are immobile and unable to resonate with the oscillatory loads of the DMA. This is called glassy stage where samples are stiff, the macromolecular chains do not change shape, and no rotation around carbon-carbon (C–C) bonds is feasible, while the molecular entanglements act as rigid crosslinks. At glassy stage higher friction occurs. As temperature rises to higher values the rubber stage begins, where the molecular chains of the nanocomposites become mobile and more easily resonating with the oscillatory load, the entanglements also try to remain in their place. Furthermore, in higher temperatures the elastic stage occurs, occasionally slip begins and entanglements become disentangled. At glass transition temperature (Tg), molecular motion is initiated and inelastic deformation occurs, and each oscillation yields internal friction. The storage modulus falls to lower values; loss modulus, which is a measure of this dissipated energy, reaches a maximum; while the tanδ (the loss factor), which is the ratio of the loss modulus to the storage modulus, rises initially.

4.6.1 Fe_3O_4-PVC nanocomposites

Figure 4.28 to Figure 4.30 present the information of the storage modulus (E'), the loss modulus (E'') and the tanδ as a function of temperature for the PVC/Fe_3O_4 ($C_6H_{13}OH$/OA+OA) nanocomposites (Sample 1 series, Table 3.9) in comparison the pure ultrasonically welded PVC foil (PVC USW). The addition of with OA coated Fe_3O_4 nanoparticles resulted in a decrease of the storage modulus (E') for all concentrations of nanoparticles (Figure 4.28) in the glassy stage, within the temperature range from -20 to 70 ^{o}C. At higher temperatures, E' does not differ significantly from the pure ultrasonically welded PVC. Moreover, within the series of nanocomposites, the storage modulus (E') decreases with the increase of Fe_3O_4 nanoparticles loading. The decrease of the storage modulus (E') indicates that nanocomposites are less stiff than the pure ultrasonically welded PVC. The (E') of this series of nanocomposites at T = 25 ^{o}C (E'$_{25}$) is presented in Table 4.2 and it can be used as an indication of Young's modulus at the same temperature. The loss modulus (E'') of the nanocomposites (Figure 4.29) within the temperature range from -20 to 70 ^{o}C is practically the same with the pure ultrasonically welded PVC. An exception is for the 1 wt.% nanocomposite (Sample 1d) at temperatures from 0 to 50°C, where its value is higher (higher friction occurs), and the 2 wt.% nanocomposite (Sample 1e) from 50 - 70°C, where it is lower (the composite softens and

the friction is lower, lower E''). Moreover, for temperatures higher than ≈ 70 ^{o}C the loss modulus (E'') of the nanocomposites varies and is higher than the pure ultrasonically welded PVC, except for the 1 wt.% nanocomposite (Sample 1d), where its value is the same. The maximum loss modulus (E''$_{max}$) of the nanocomposites with respect to temperature is presented in Table 4.2. The tanδ parameter (Figure 4.30) marginally increases for all the nanocomposites in temperatures lower than the Tg (peak of tanδ), while at higher than the Tg temperatures it decreases. The maximum tanδ$_{max}$ of all the nanocomposites, as well as the relevant glass transition temperatures (Tg) are presented in Table 4.2.

Figure 4.28 Storage modulus (E') of nanocomposite PVC foils containing various concentrations of magnetite (Fe$_3$O$_4$), PVC/Fe$_3$O$_4$ (C$_6$H$_{13}$OH/OA+OA), as a function of temperature - Sample 1 series

Figure 4.29 Loss modulus (E'') of nanocomposite PVC foils containing various concentrations of magnetite (Fe$_3$O$_4$), PVC/Fe$_3$O$_4$ (C$_6$H$_{13}$OH/OA+OA), as a function of temperature - Sample 1 series
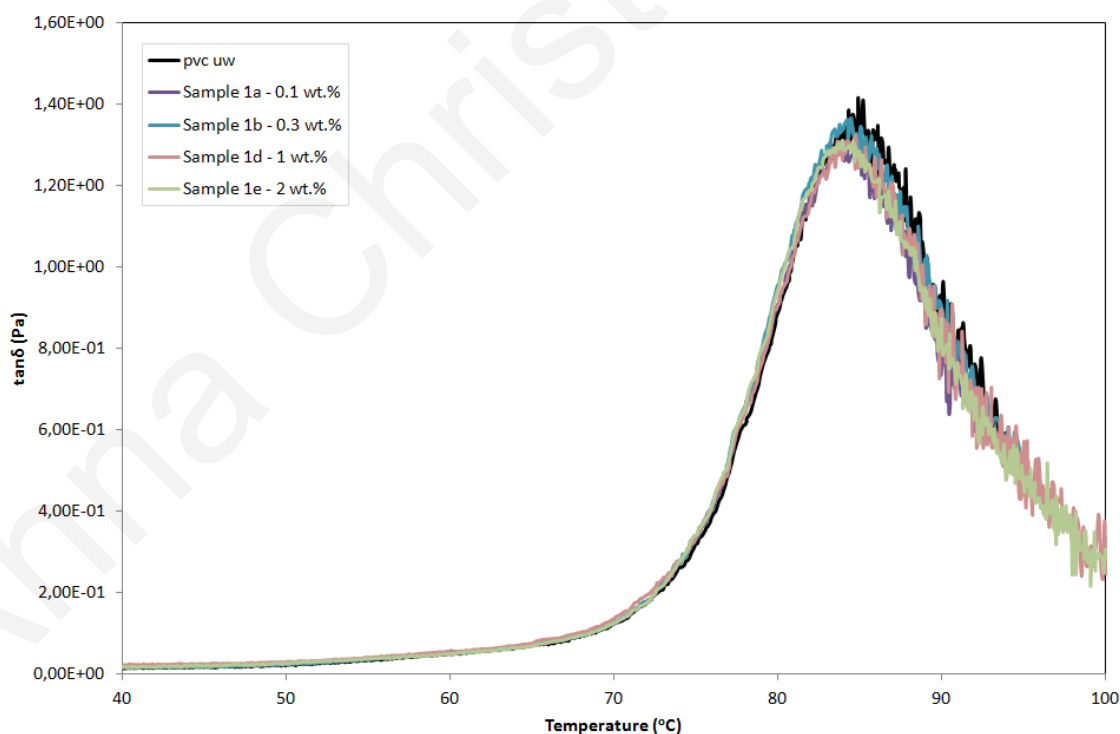
Figure 4.30 tanδ of nanocomposite PVC foils containing various concentrations of magnetite (Fe$_3$O$_4$), PVC/Fe$_3$O$_4$ (C$_6$H$_{13}$OH/OA+OA), as a function of temperature - Sample 1 series

Figure 4.31 to Figure 4.33 present the storage modulus (E'), the loss modulus (E'') and the tanδ as functions of temperature for the PVC/Fe$_3$O$_4$ (H$_2$O/LA+LA) nanocomposites

(Sample 2 series, Table 3.9), in comparison with the pure ultrasonically welded PVC foil. The addition of the coated Fe_3O_4 nanoparticles with LA resulted in a decrease of the storage modulus (E') for all nanoparticles of this series (Figure 4.31) to the same values throughout the temperature range. An exception is Sample 2a with 0.04 wt.% concentration, which has a lower storage modulus (E'), probably because of its very low concentration. Moreover, for the 0.5 wt.% nanocomposite (Sample 2d) in temperatures higher than 70 ^{o}C, E' increases compared with the pure ultrasonically welded PVC. The decrease of the storage modulus (E') indicates that nanocomposites are less stiff than the pure ultrasonically welded PVC. The loss modulus (E'') of the nanocomposites (Figure 4.32) with concentrations of 0.04 wt.% (Sample 2a), 0.1 wt.% (Sample 2b), 0.3 wt.% (Sample 2c) are sufficiently lower than the pure ultrasonically welded PVC. The nanocomposite that has 0.5 wt.% concentration of nanoparticles (Sample 2d) exhibits very high loss modulus (E''), at temperatures from 63 to 78 ^{o}C, when compared with all the other samples. This is an evidence of the constrained friction of the polymer chains. The tanδ parameter stays the same after the addition of Fe_3O_4 nanoparticles for all the samples, except for the nanocomposite with 0.5 wt.% concentration of nanoparticles which has higher values at temperatures below 80 ^{o}C (Figure 4.33). At temperatures approaching Tg (peak of tanδ), the tanδ values differ, while the T_g is about the same for the nanocomposites, except again for the one with 0.5 wt.% concentration of nanoparticles (Sample 2d) which has the lowest Tg. The storage modulus at T = 25 ^{o}C (E'$_{25}$), the maximum loss modulus (E''$_{max}$), the maximum tanδ_{max} as well as the relevant glass transition temperatures (Tg) of all the nanocomposites are presented in Table 4.2.
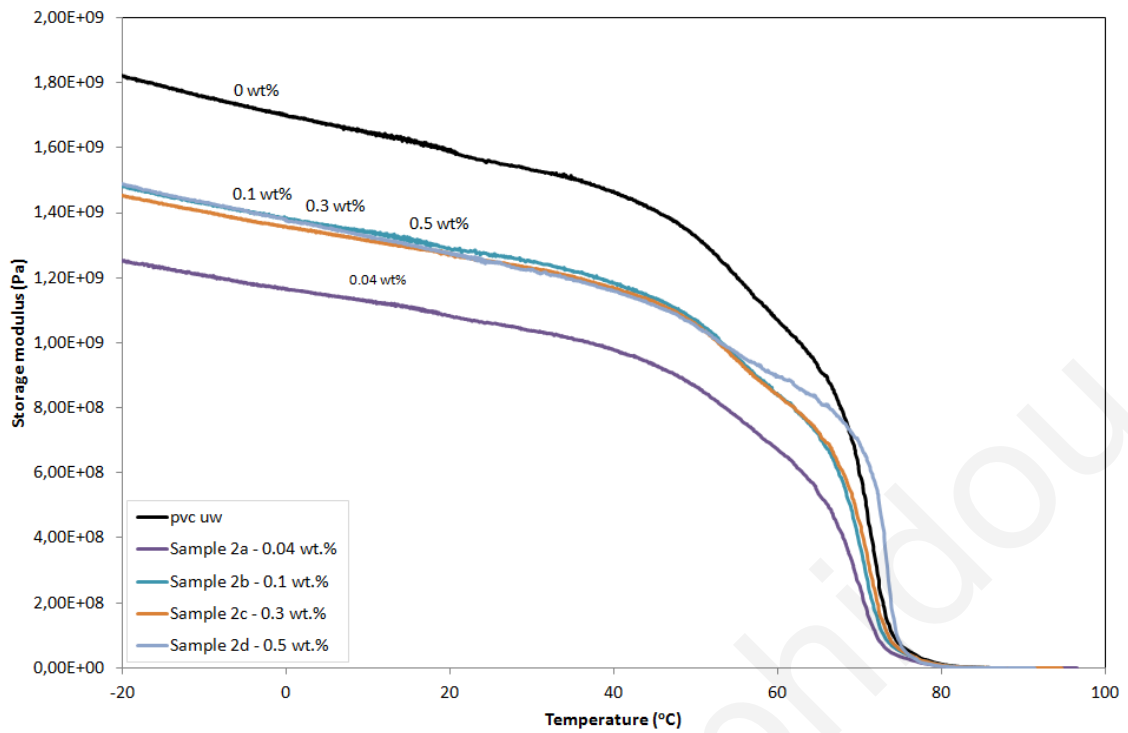
Figure 4.31 Storage modulus (E') of nanocomposite PVC foils containing various concentrations of magnetite (Fe$_3$O$_4$), PVC/Fe$_3$O$_4$ (H$_2$O/LA+LA), as a function of temperature - Sample 2 series
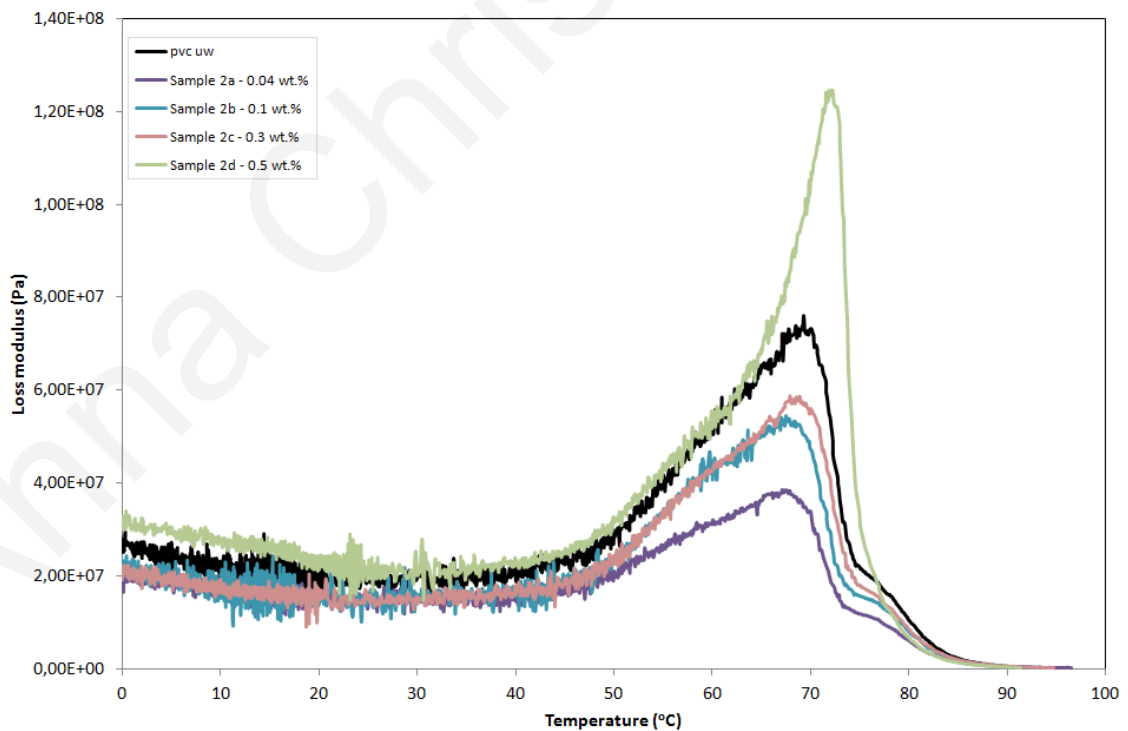
Figure 4.32 Loss modulus (E'') of nanocomposite PVC foils containing various concentrations of magnetite (Fe$_3$O$_4$), PVC/Fe$_3$O$_4$ (H$_2$O/LA+LA), as a function of temperature - Sample 2 series
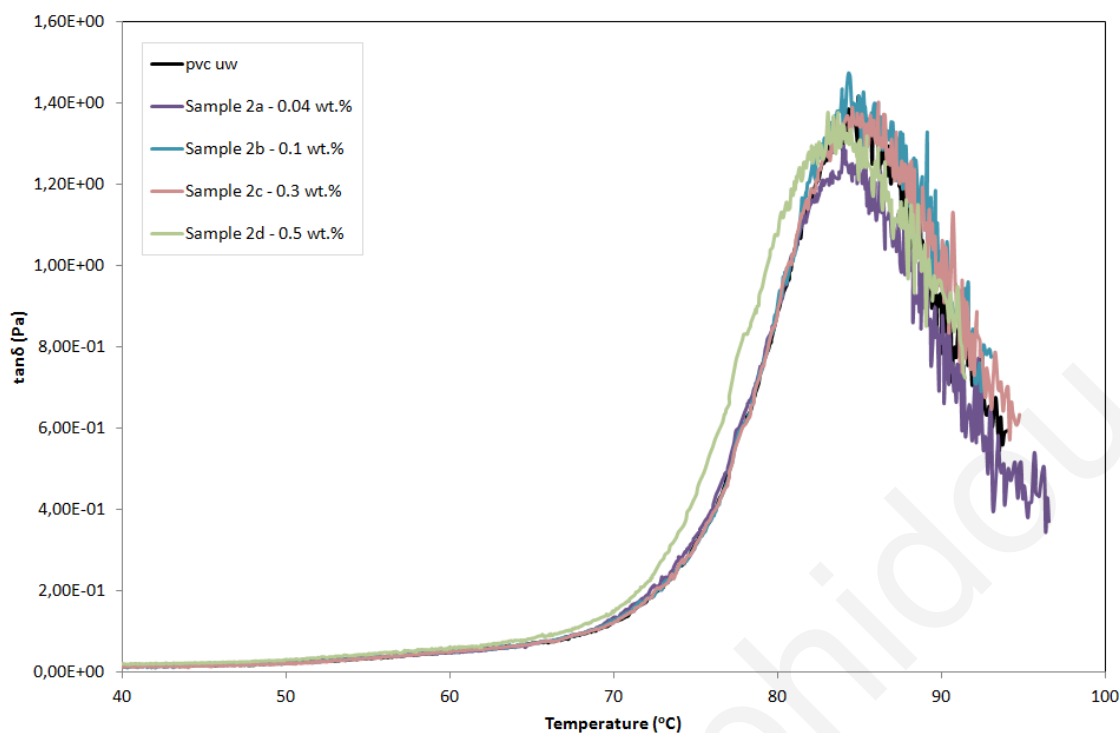
Figure 4.33 tanδ of nanocomposite PVC foils containing various concentrations of magnetite (Fe$_3$O$_4$), PVC/Fe$_3$O$_4$ (H$_2$O/LA+LA), as a function of temperature - Sample 2 series

Figure 4.34 to Figure 4.36 present the storage modulus (E'), the loss modulus (E'') and the tanδ as a function of temperature for the PVC/Fe$_3$O$_4$ (TR30/OA+OA) nanocomposites (Samples 3 series, Table 3.9) in comparison with the pure ultrasonically welded PVC foil. In these series of samples which are illustrated in Figure 4.34, the addition of the coated with OA Fe$_3$O$_4$ nanoparticles, resulted in an increase of the storage modulus (E') for the 0.1 wt.% (Sample 3a). Furthermore with the increase of Fe$_3$O$_4$ loading of nanoparticles, to 0.3 wt.% and 0.5 wt.% (Samples 3b and 3c), the storage modulus (E') decreases to lower values than the pure ultrasonically welded PVC foil, throughout the temperature range. The loss modulus (E'') again increases in the sample with 0.1 wt.% concentration (Figure 4.35). For the sample with 0.3 wt.% concentration, in temperatures lower than 50 ^{o}C, it increases compared to the pure ultrasonically welded PVC; in the temperature range from 50 to 75 ^{o}C it decreases, and at higher temperatures is almost the same. The sample with 0.5 wt.% concentration has a lower loss modulus (E'') comparing this series. The tanδ parameter increases for the samples with 0.1 and 0.3 wt.% concentrations of Fe$_3$O$_4$, while it is almost the same for sample with concentration 0.5 wt.% (Figure 4.36). Tg stays almost the same after addition of the Fe$_3$O$_4$ nanoparticles

77

for all the samples of this series. The storage modulus at T = 25 ^{o}C (E'_{25}), the maximum loss modulus (E''_{max}), the maximum $\tan\delta_{max}$ as well as the relevant glass transition temperatures of all the nanocomposites are presented in Table 4.2.
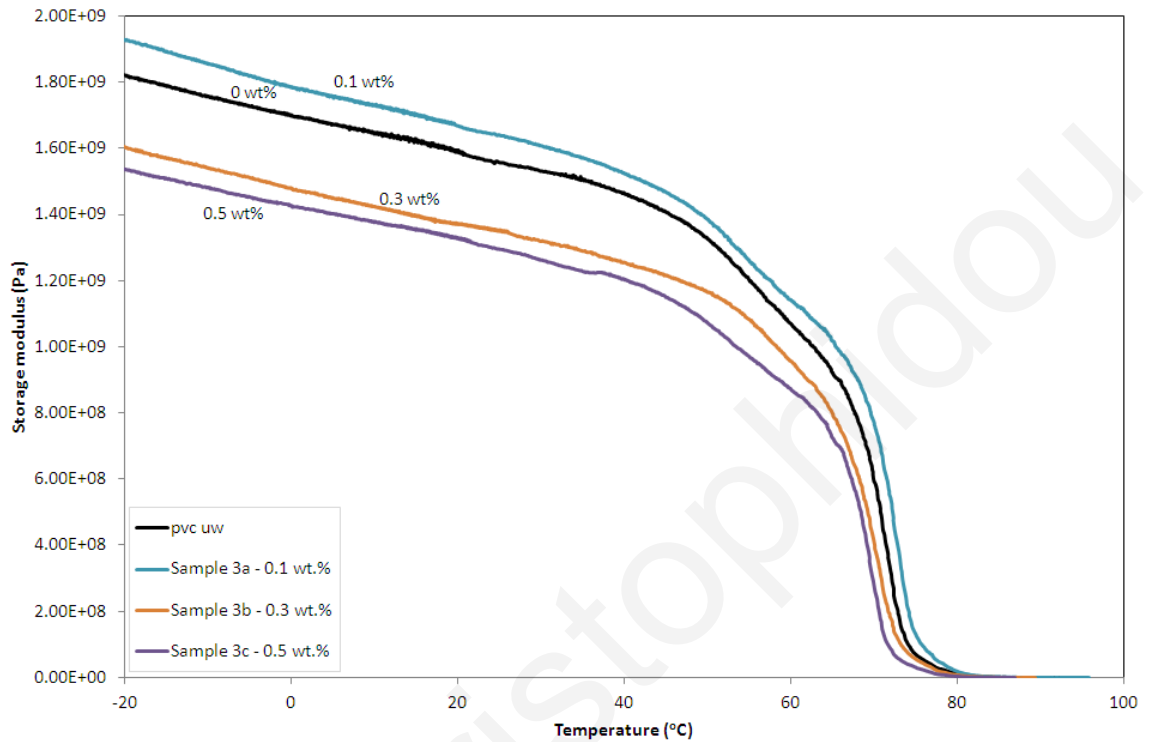
Figure 4.34 Storage modulus (E') of nanocomposite PVC foils containing various concentrations of magnetite (Fe$_3$O$_4$), PVC/Fe$_3$O$_4$ (TR30/OA+OA), as a function of temperature - Sample 3 series
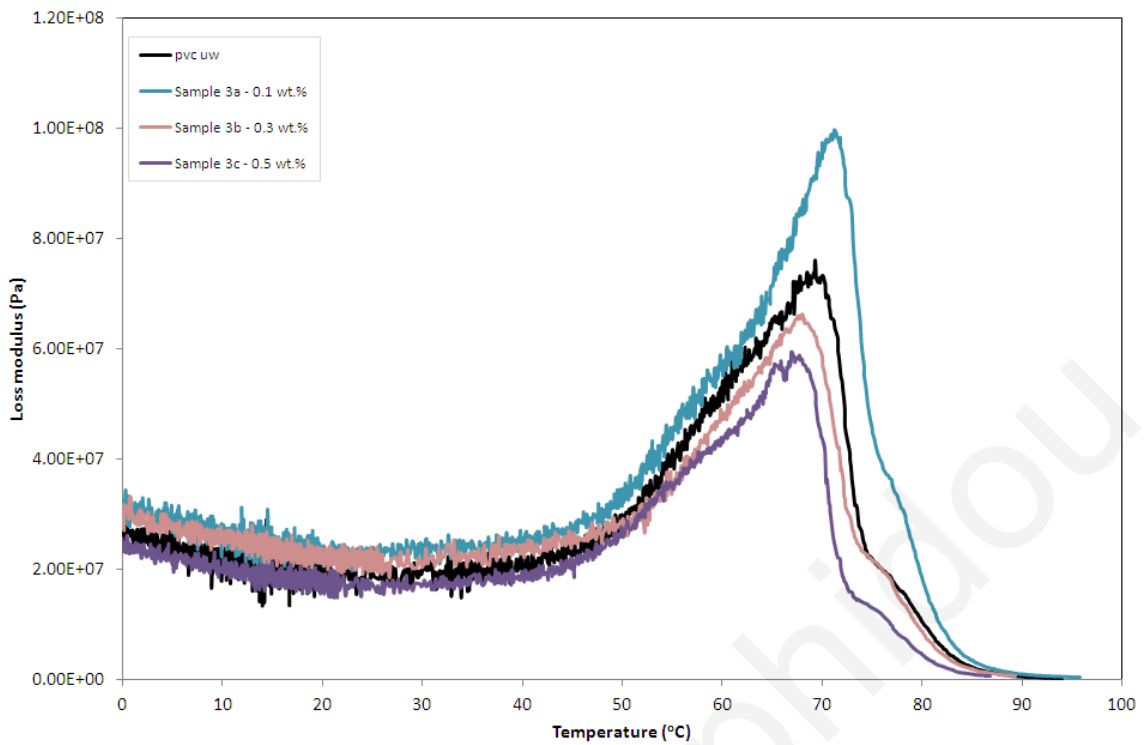
Figure 4.35 Loss modulus (E'') of nanocomposite PVC foils containing various concentrations of magnetite (Fe$_3$O$_4$), PVC/Fe$_3$O$_4$ (TR30/OA+OA), as a function of temperature - Sample 3 series
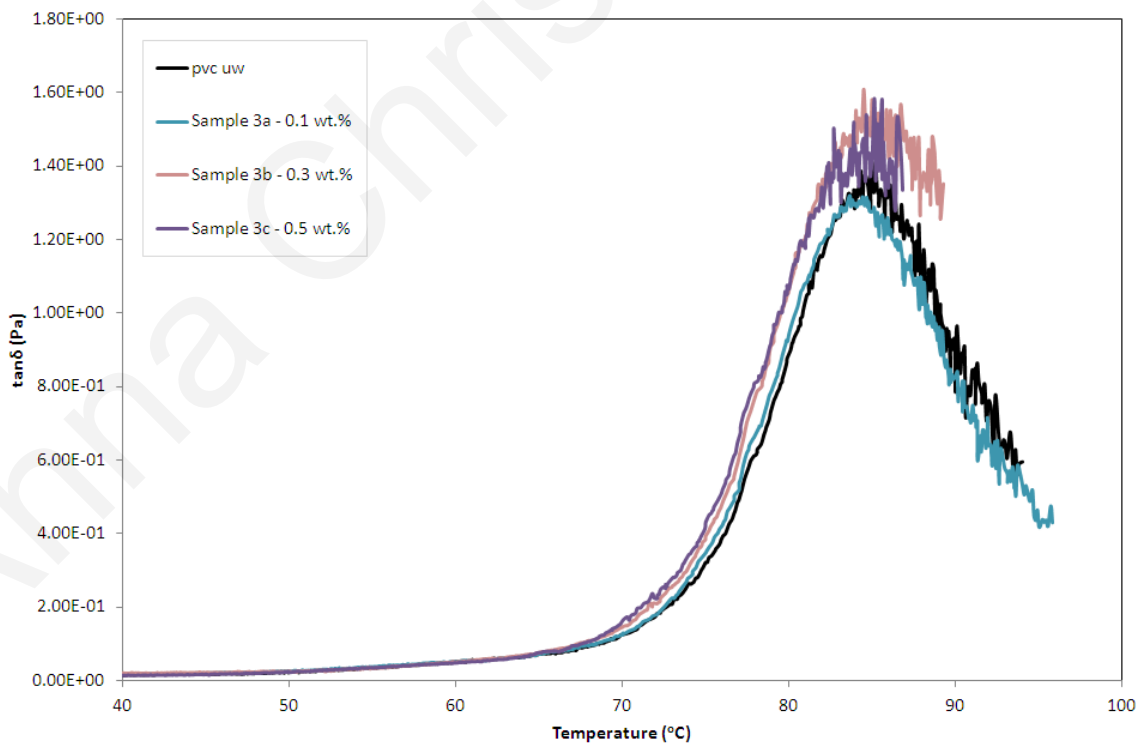
Figure 4.36 tanδ of nanocomposite PVC foils containing various concentrations of magnetite (Fe$_3$O$_4$), PVC/Fe$_3$O$_4$ (TR30/OA+OA), as a function of temperature - Sample 3 series

Figure 4.37 to Figure 4.39 present the storage modulus (E'), the loss modulus (E'')

and the tanδ as functions of temperature for the PVC/Fe$_3$O$_4$ (H$_2$O/DBS+DBS)nanocomposites (Sample 4 series, Table 3.9) in comparison with the pure ultrasonically welded PVC foil. For this series of samples, the addition of coated Fe$_3$O$_4$ with the DBS nanoparticles resulted in an increase of the storage modulus (E') for the 0.5 wt.% (Sample 4a) until the temperature of 70 ^{o}C, while for higher temperatures it follows the curve of welded PVC (Figure 4.37). Furthermore, for temperatures lower than 60 ^{o}C, the storage modulus (E') decreases to lower values than the pure ultrasonically welded PVC foil, with the increase of Fe$_3$O$_4$ loading of nanoparticles. For the Samples 4b, 4c and 4d the storage modulus (E') initially decreases with the increase of Fe$_3$O$_4$ loading, while as temperature rises to higher values the storage modulus converges towards that of the lower or higher concentration samples, respectively. The nanocomposite with concentration of 5 wt.% (Sample 4d) has the lowest storage modulus (E') compared with the other samples. Figure 4.38 illustrates the loss modulus (E'') of the series 4 Samples, for temperatures lower than the peak of E'', varies for the different samples. The loss modulus for temperatures corresponding to the peak of E'', initially increases with the addition of the Fe$_3$O$_4$ nanoparticles, followed by a decrease for concentrations higher than 1 wt.%. Moreover, T$_{E''_{max}}$ decreases to 66.4 ^{o}C for Sample 4e which has Fe$_3$O$_4$ concentration of 5 wt.%, the lowest of all the series of nanocomposites. Concerning the tanδ parameter (Figure 4.39), this again varies for different samples. Tg stays the same after the addition of the Fe$_3$O$_4$ nanoparticles for all the samples, which indicates the absence of strong interactions between the polymer matrix and the embedded nanoparticles. Sample 4b has the higher tanδ parameter and hence the higher damping. The storage modulus at T = 25 ^{o}C (E'$_{25}$), the maximum loss modulus (E''$_{max}$), the maximum tanδ_{max} as well as the relevant glass transition temperatures of all the nanocomposites are presented in Table 4.2.
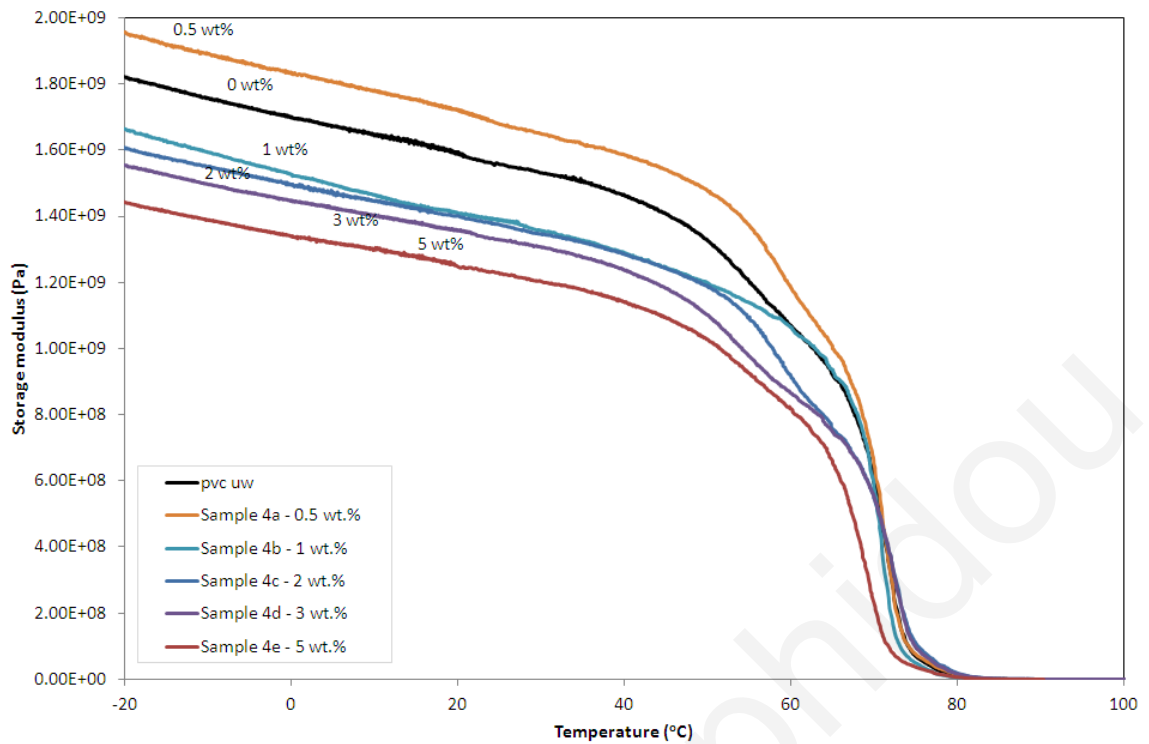
Figure 4.37 Storage modulus (E') of nanocomposite PVC foils containing various concentrations of magnetite (Fe_3O_4), PVC/Fe_3O_4 (H_2O/DBS+DBS), as a function of temperature - Sample 4 series

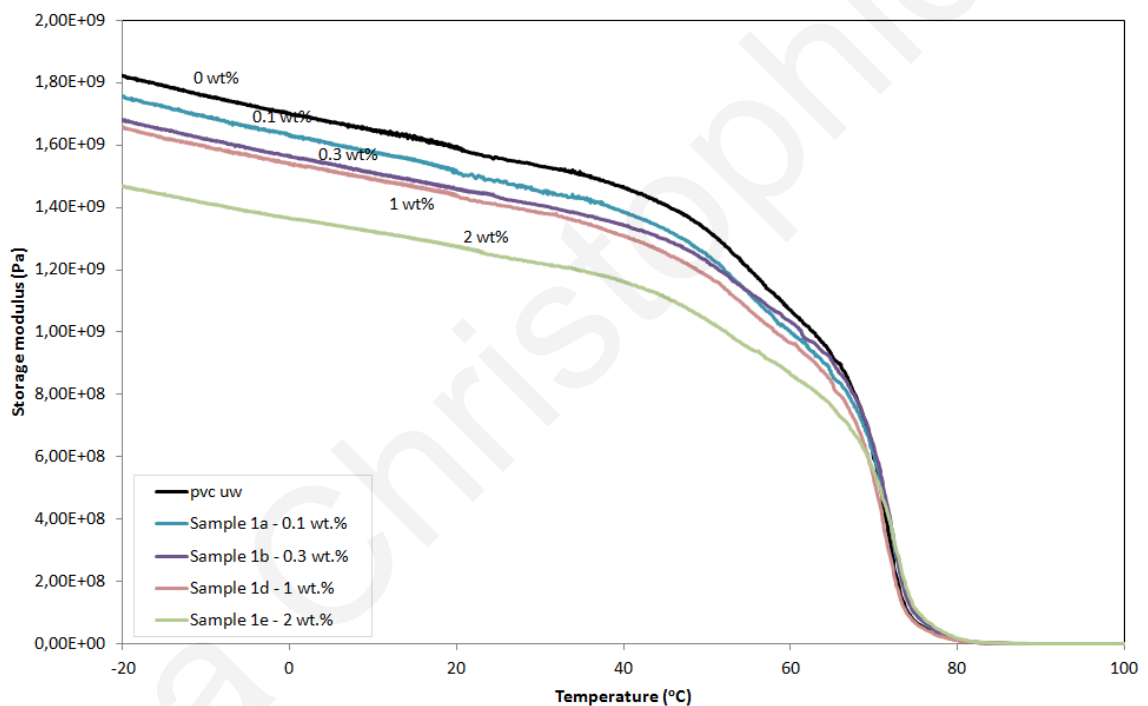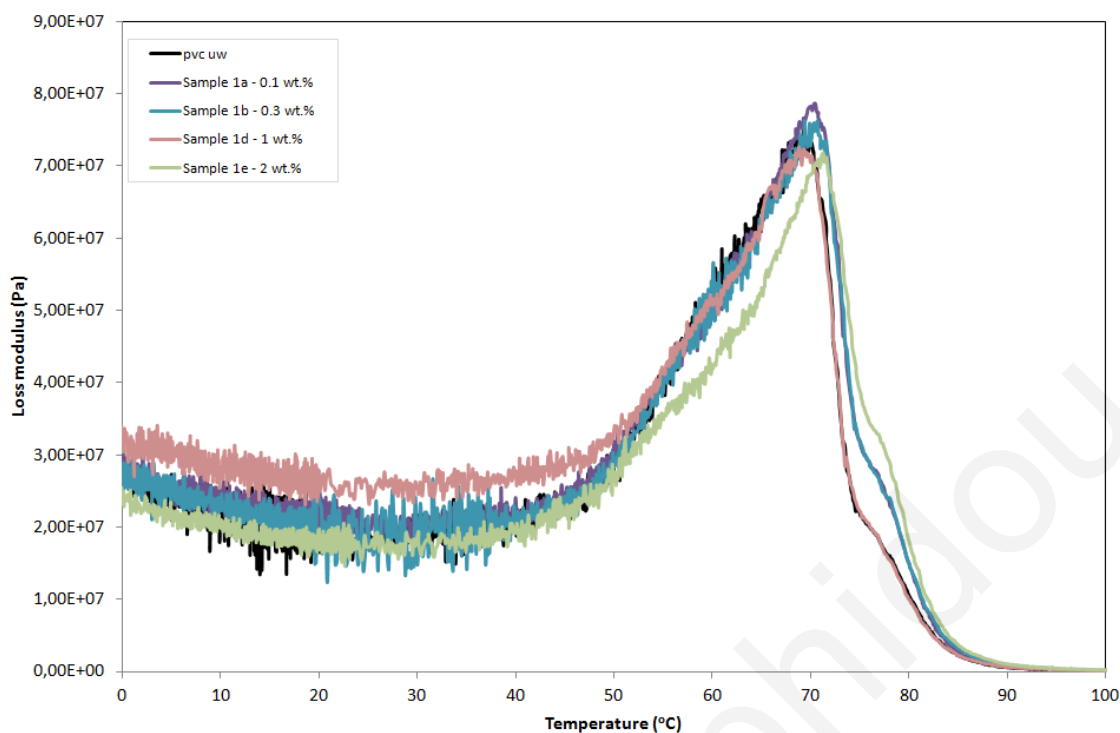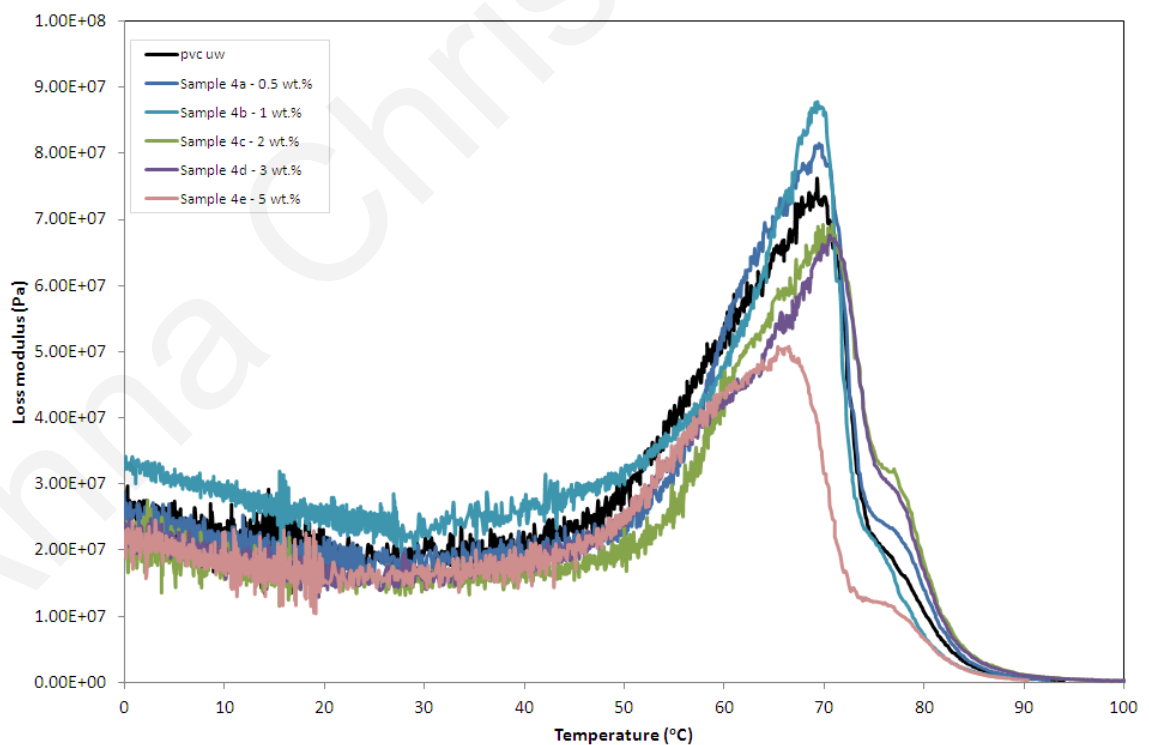**Figure 4.38 Loss modulus (E'') of nanocomposite PVC foils containing various concentrations of magnetite (Fe_3O_4), PVC/Fe_3O_4 (H_2O/DBS+DBS), as a function of temperature - Sample 4 series**
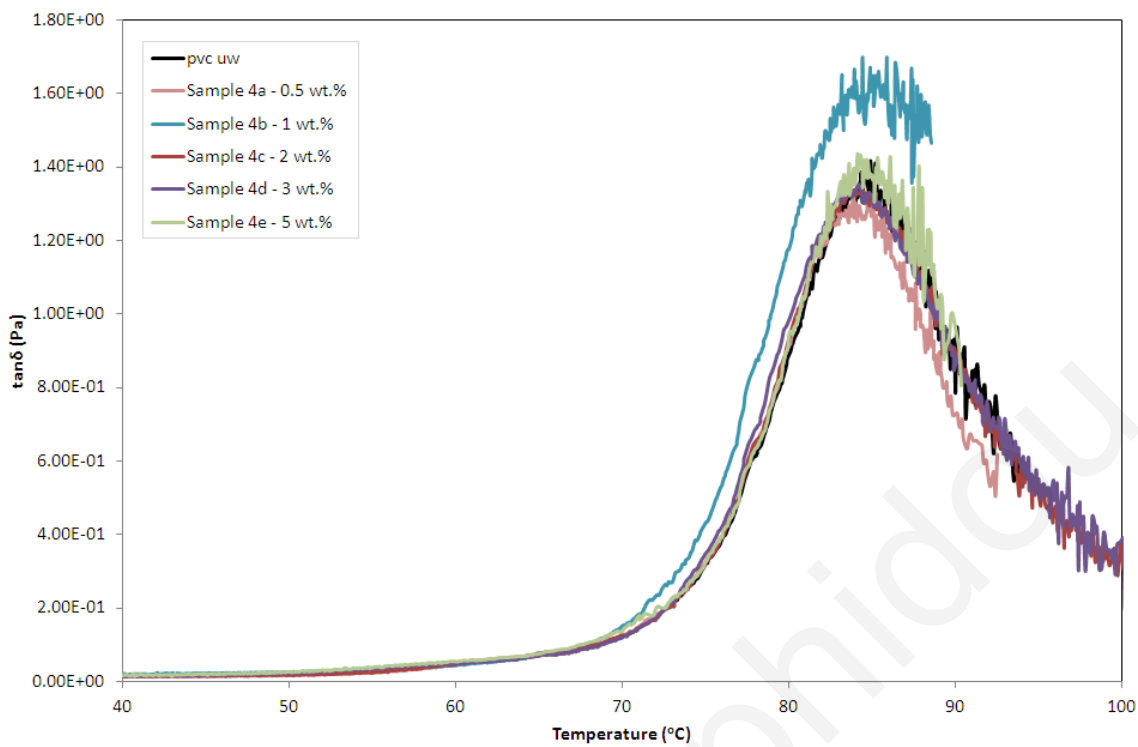
Figure 4.39 tanδ of nanocomposite PVC foils containing various concentrations of magnetite (Fe$_3$O$_4$), PVC/Fe$_3$O$_4$ (H$_2$O/DBS+DBS), as a function of temperature - Sample 4 series

Table 4.2 Viscoelastic properties of Fe_3O_4-PVC nanocomposites*

Sample number	Liquid carrier/ Stabilizing layer	Fe_3O_4 (wt.%)	Storage modulus E'_{25} (GPa)	Loss modulus $T_{E''_{max}}$ (^{o}C)	Loss modulus E''_{max} (GPa)	tanδ T_g (^{o}C)	tanδ tanδ_{max}
PVC UW	-	0	1.56	69.3	0.0761	84.9	1.42
1a	$C_6H_{13}OH$/ Oleic acid (double)	0.1	1.49	70.7	0.0762	84.5	1.37
1b	$C_6H_{13}OH$/ Oleic acid (double)	0.3	1.43	70.5	0.0787	84.7	1.30
1d	$C_6H_{13}OH$/ Oleic acid (double)	1	1.41	69.4	0.0726	84.7	1.32
1e	$C_6H_{13}OH$/ Oleic acid (double)	2	1.24	71.2	0.0718	84.6	1.31
2a	H_2O/ Lauric acid (double)	0.04	1.06	67.1	0.0387	84	1.30
2b	H_2O/ Lauric acid (double)	0.1	1.27	67.5	0.0546	84.3	1.47
2c	H_2O/ Lauric acid (double)	0.3	1.25	67.9	0.0587	84.5	1.39
2d	H_2O/ Lauric acid (double)	0.5	1.25	72.2	0.125	83.7	1.38
3a	TR-30/ Oleic acid (double)	0.1	1.64	71.2	0.0998	84.4	1.32
3b	TR-30/ Oleic acid (double)	0.3	1.35	68	0.0662	84.5	1.61
3c	TR-30/ Oleic acid (double)	0.5	1.30	67.8	0.0588	85.1	1.59
4a	H_2O/ Dodecylbenzenesulphonic acid (double)	0.5	1.68	69.4	0.0815	83.9	1.33
4b	H_2O/ Dodecylbenzenesulphonic acid (double)	1	1.39	69.3	0.0878	84.4	1.7
4c	H_2O/ Dodecylbenzenesulphonic acid (double)	2	1.37	70.8	0.0692	84.4	1.34
4d	H_2O/ Dodecylbenzenesulphonic acid (double)	3	1.33	70.5	0.0676	84.2	1.35
4e	H_2O/ Dodecylbenzenesulphonic acid (double)	5	1.23	66.4	0.0583	84.3	1.44

* Data derived from single measurements

Storage modulus:

By comparing the viscoelastic parameters of Table 4.2, the storage modulus at 25°C (E'_{25}) varies with the addition of Fe_3O_4 nanoparticles into the PVC matrix, in a range of values from 1.06 to 1.68 GPa. For most of the nanocomposites the storage modulus (E'_{25}) decreases, with no great deviations from the parent material, i.e. the pure ultrasonically welded PVC, which is measured to 1.56 GPa. Regarding the fact that the storage modulus (E') can reflect the elastic modulus (stiffness) of the nanocomposites, these lower values of the storage modulus (E'_{25}) is an evidence that nanocomposites are less stiff, i.e. more elastic or less resistant to elastic deformation, than the pure ultrasonically welded PVC. However two samples, i.e. Samples 3a and 4a, exhibit stiffness higher than that of the pure ultrasonically welded PVC storage modulus (E'_{25}) (this will be discussed further to this session). By reviewing each of the series separately, independently of the parent material, the storage modulus (E'_{25}) decreases with the increase of the Fe_3O_4 loading. An exception is the Sample 2a, which has very low concentration of Fe_3O_4 nanocomposites, i.e. 0.04 wt.%, which may act contrary on the desired results. Moreover, by comparing storage modulus (E'_{25}) values for the same concentrations in different series of samples, the values are not equal. However due to the fact that the obtained data derived from single measurements, it is not certain that the observed differences discussed above are statistically significant.

The above mentioned slight decrease of the storage modulus with the increase of coated Fe_3O_4 nanoparticle loading can be explained according to literature because of the decrease of the molar mass of the nanocomposite, as well as by changes of the morphology of the manufactured nanocomposite due to presence of nanoparticles and their stabilizing layers. Moreover, and since all series of nanocomposites include Fe_3O_4 nanoparticles, the fact that nanocomposites from different series do not have the same properties indicates that the presence of different stabilizing agents, covering the Fe_3O_4 nanoparticles, also affects the storage modulus. The distribution of nanoparticles into the nanocomposite matrix, their width into the polymer matrix, as well as the presence of agglomerations or not, the mechanism of nanoparticle penetration into the polymer matrix and possible chemical interactions are the probable explanations of the above described viscoelastic parameters.

The properties of the stabilizing agents are presented analytically in Table 3.3. Moreover, it should be noted that all the stabilizing agents melt in temperatures from 10 to 45 $^{\circ}$C, which are lower than those of the PVC, as well as lower than the Tg of the PVC. This means that they melt at lower temperatures than the welding temperature of the ultrasonic welding procedure, at the stage of manufacturing of the nanocomposites and thus they are contributing to weld as they may act as energy directors during ultrasonic welding. The contribution of energy directors has been discussed in Chapter 2.5. Moreover, their structure has either 12 or 18 carbon atoms and some of them have double bonds. Generally, increasing the number of low molecular weight (soft) chains in polymer composites leads to a decrease in the elastic modulus and decreases its stiffness. Comparing now the Sample 1 series with the Sample 3 series, the corresponding results of properties in Table 4.2 indicate that they are not influenced only by the combinations of surfactants used as stabilizing agents, but also by the carrier liquid of the nanoparticles. In general, hexanol is a non-polar volatile organic solvent and nanoparticles are better distributed into the PVC matrix. It is believed that hexanol evaporates and does not leave any substances to the surfaces to be joined together, as evidenced in optical and magnetic properties measured above. On the other hand, water is a highly polar inorganic solvent that may leave some humidity to the samples, or the created molecular interactions prevent the further dispersion of the nanoparticles into the polymer matrix. Transformer oil is a non-polar and weakly volatile solvent that also may leave some ingredients into the nanocomposite matrix, and/or reveal similar behavior to the water.

By comparing again the different series, the nanocomposites of Sample 2 with the coated with LA Fe_3O_4 nanoparticles, having the lower molecular weight, and thus a smaller thickness of the surface coating, as well as lack of double bonds (except for the acidic), they are measured to have lower storage modulus. Particularly Sample 2a has the lowest storage modulus, probably due to the very low concentration of nanoparticles, affecting negatively the nanocomposite. It is commonly known that lower molecular weight molecules act like plasticizers by embedding themselves between the chains of polymers, spacing them apart and by increasing the free volume between them, and thus making them softer. This is the phenomenon believed to be observed in this case.

The opposite phenomenon, i.e. the increase of the storage modulus with the

presence of nanoparticles, is described in other literature as happening because of the high aspect ratio of the dispersed nanoparticles and their interaction with the polymer matrices [58, 170-171]. The increase of the storage modulus results can be attributed to the decrease in the polymer segment mobility near the polymer/nanoparticle interface and the strong interaction between nanoparticles embedded and polymer segments, which reduces the mobility of macromolecular chains. This should be the obvious explanation for higher than that of the pure ultrasonically welded PVC storage modulus (E'_{25}), as well as stiffness of Samples 3a and 4a. However, the pre-mentioned literature concerns MoS_2 nanotubes, Fe_3O_4 and $CaCO_3$ nanoparticles, respectively. The nanocomposites are prepared with different methods such as the solvent method and in situ polymerization, and at higher concentrations, while none of them has magnetic properties equivalent to the samples.

Loss modulus:

Concerning now the loss modulus maximum (E''_{max}) values, listed in Table 4.2, these vary from 0.0387 to 0.125 GPa at a temperature range ($T_{E''_{max}}$) from 66.4 to 72.2 ^{o}C, while for the parent material $E''_{max}=0.0761 GPa$ at $T_{E''_{max}}=69.3^{o}C$. As a general observation it can be stated that loss modulus maxima (E''_{max}) seem to be influenced more than the storage modulus (E'_{25}) with the addition of coated Fe_3O_4 nanoparticles into the PVC matrix. With the increase of the loading of Fe_3O_4 nanoparticles from 0.04 wt.% to 1 wt.%, E''_{max} of series 1, 2 and 4 initially increases and after this optimum value it decreases; for series 2 actually the E''_{max} increases with a high gap, while for series 3 it decreases. This is further evidence that the mechanism that occurs during penetration of nanoparticles in the polymeric matrix changes after an optimum concentration of nanoparticles (differences were observed during microscopic analysis; reduction of coercive field value to approximately half, as these are listed in Table 4.1). All the above three observations occur when the nanoparticle composition is higher than 1 wt.%.

The $T_{E''_{max}}$ changes independently of the loading concentration and the different series of nanocomposites. The Tg values taken from the maxima of the tanδ, for the PVC and the PVC nanocomposites, show that the nanocomposites did not exhibit significant differences in Tg values, or the range of curves for tanδ did not change, with the presence

as well as the concentration of the coated Fe_3O_4 nanoparticles. Therefore, an average Tg = 84.4 ± 0.7 ^{o}C for the nanocomposites can be defined. Since Tg does not increase with the addition of nanoparticles onto the polymer matrix, this is an evidence that there is no interaction between PVC and Fe_3O_4 nanoparticles.

Tanδ:

Finally, the tanδ describes the damping behavior of the composite, while it is also an indicator of how efficiently the material can lose the energy due to molecular rearrangement and internal friction [168]. In general, the nanocomposites have lower values of tanδ than the parental PVC, while this indicates the lower flexibility of the polymeric matrix. When the loss factor increases, this is evidence that the introduction of coated Fe_3O_4 nanoparticles enhances the rigidity of the nanocomposites. Generally, a high tanδ value is indicative of a material that has a high, non-elastic strain component, while a low value indicates one that is more elastic. Sample 4b correspond to the higher tanδ, i.e. the higher damping. However, the enlargement of the curve of tanδ and reduction of the maximum value may be due to increased density networking and heterogeneity polymer network.

4.6.2 Pd-PVC nanocomposite

Figure 4.40 to Figure 4.42 present the storage modulus (E'), the loss modulus (E'') and the tanδ as functions of temperature, for the Pd/PVC nanocomposite (Sample 5, Table 3.10), in comparison with the pure ultrasonically welded PVC foil. The addition of the coated Pd nanoparticles resulted in decrease of the storage modulus (E') for temperatures lower than 70 ^{o}C (Figure 4.40), while for higher temperatures the opposite phenomenon occurs. This is evidence that nanocomposites at low temperatures are less stiff than the pure ultrasonically welded PVC, while above 70°C they are stiffer, where nanoparticles are acting as cross-links to polymer chain oscillations.

The loss modulus (E'') was about the same for temperatures lower than 70 ^{o}C, resulting in very high loss modulus (E'') for higher temperatures $E''_{max} = 0.145 GPa$, when compared with the pure ultrasonically welded PVC foil $E''_{max} = 0.0761 GPa$ (Figure 4.41, Table 4.3). Moreover, the $T_{E''_{max}}$ increases from 69.3 to 75.5 ^{o}C, which this is also an

evidence of internal friction of the polymer chains occurs. Furthermore Tg and tanδ slightly deceases with the addition of coated palladium nanoparticles into the PVC foil.
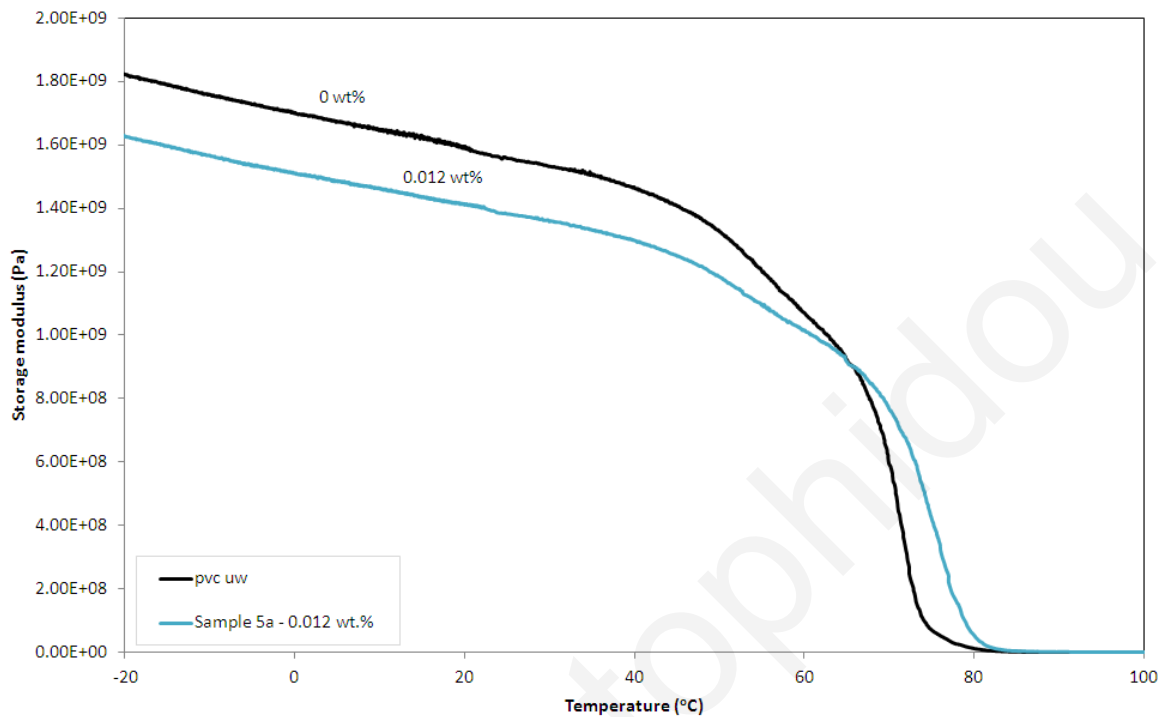
Figure 4.40 Storage modulus (E') of nanocomposite PVC foils containing various concentrations of Pd nanoparticles as a function of temperature - Sample 5 series
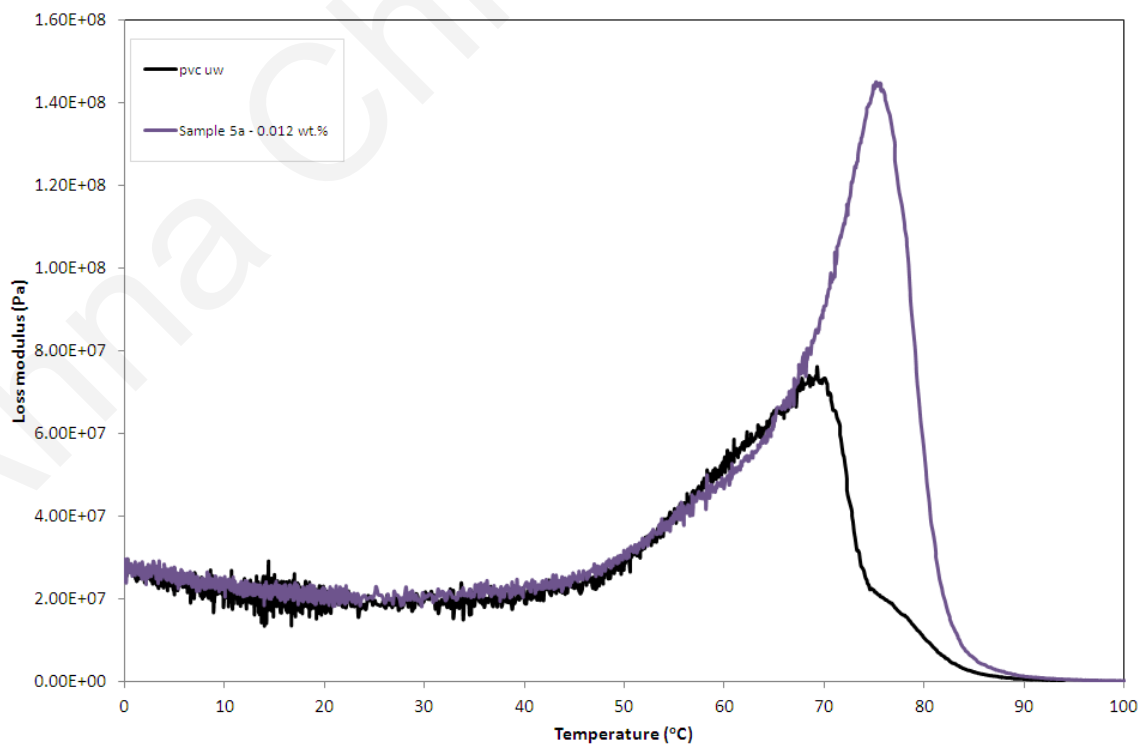
Figure 4.41 Loss modulus (E'') of nanocomposite PVC foils containing various concentrations of Pd nanoparticles as a function of temperature - Sample 5 series
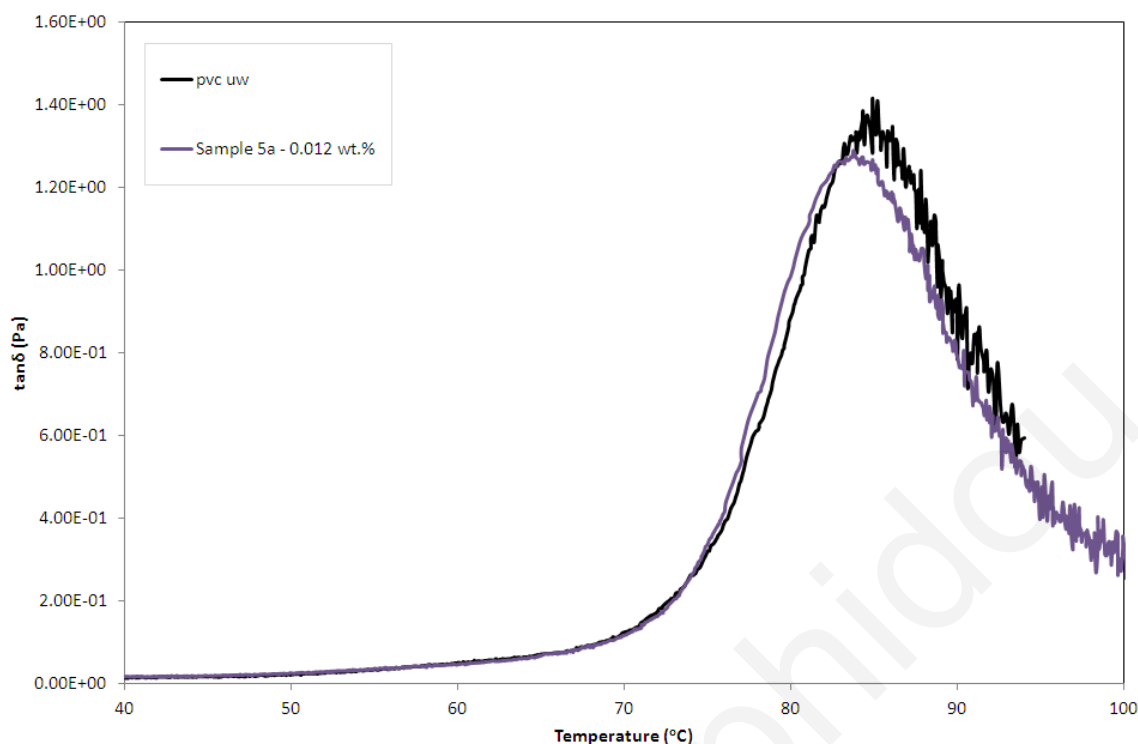
Figure 4.42 tanδ of nanocomposite PVC foils containing various concentrations of Pd nanoparticles as a function of temperature - Sample 5 series

The storage modulus at T = 25 $^{\circ}$C (E'_{25}), the maximum loss modulus (E''_{max}), the maximum $\tan\delta_{max}$ as well as the relevant glass transition temperature of the nanocomposite are presented in Table 4.3. The presence of the Pd coating, this is the poly(LauMA)-b-poly(AEMA), seems to play a more significant role on the viscoelastic properties compared to the surfactant-coated iron oxide nanoparticles, since it is a polymer with long-chains and high molecular weight. However, due to the fact that the obtained data derived from single measurements, it is not certain that the observed differences discussed above are statistically significant.

Table 4.3 Viscoelastic properties of Pd-PVC nanocomposites*

Sample number	Liquid carrier/ Stabilizing layer	Pd (wt.%)	Storage modulus	Loss modulus		$tan\delta$	
			E'_{25} (GPa)	$T_{E''_{max}}$ ($^{\circ}$C)	E''_{max} (GPa)	T_g ($^{\circ}$C)	$tan\delta_{max}$
PVC UW	-	0	1.56	69.3	0.0761	84.9	1.42
5a	n-hexane/LauMA	0.012	1.38	75.5	0.145	83.7	1.29

* Data derived from single measurements

4.7 Tensile test measurements

The mechanical properties of all nanocomposite samples prepared in Chapter 3 were also investigated by tensile testing. More precisely, the resulting tensile strength, Young's modulus, elongation at break and other properties have been examined above. The basic principle of tension tests is that a gradually increasing tensile load is applied uniaxially along the long axis of the nanocomposite sample producing deformation, usually to fracture. Measurements of strength along with elongation are recorded.

4.7.1 Fe_3O_4 and Pd-PVC nanocomposites

The mechanical properties of the Fe_3O_4 and Pd/PVC nanocomposites were carried out by a Universal Testing Machine (UTM), model EZ20 from Lloyds Instruments Ltd (UK), based on EN ISO 6892-1 standards. The measurements were carried out at room temperature conditions of $23 \pm 2\ ^oC$, with humidity 65 ± 5 % and accuracy ≤ 0.5 %. The samples had 20 mm length, around 3 mm width and 0.45 mm thickness; the loading speed was 50 mm/min and preload 1 N. The results are presented in Tables 4.4 and 4.5, respectively.

Table 4.4 Mechanical properties of Fe$_3$O$_4$-PVC nanocomposites*

Sample number	Liquid carrier/ Stabilizing layer	Fe$_3$O$_4$ (wt.%)	Young's modulus (GPa)	Load at max (N)	Tensile strength (MPa)	% Elongation at max load
PVC UW	-	0	1.5	61.9	47.6	8.4
1a	C$_6$H$_{13}$OH/ Oleic acid (double)	0.1	1.38	62.1	47.8	10.2
1b	C$_6$H$_{13}$OH/ Oleic acid (double)	0.3	1.33	64.4	44.1	10.7
1c	C$_6$H$_{13}$OH/ Oleic acid (double)	0.5	1.29	58.3	41.9	10.2
1d	C$_6$H$_{13}$OH/ Oleic acid (double)	1	1.29	59.1	42.4	10.2
1e	C$_6$H$_{13}$OH/ Oleic acid (double)	2	1.25	55.7	40.6	9.8
2a	H$_2$O/ Lauric acid (double)	0.04	1.13	63.2	42.7	10.9
2b	H$_2$O/ Lauric acid (double)	0.1	1.25	66.3	44	11.6
2c	H$_2$O/ Lauric acid (double)	0.3	1.29	67.1	47.2	10.5
2d	H$_2$O/ Lauric acid (double)	0.5	1.35	58.7	43.4	10
3a	TR-30/ Oleic acid (double)	0.1	1.66	66.5	46.5	10.9
3b	TR-30/ Oleic acid (double)	0.3	1.35	54.1	44.8	10
3c	TR-30/ Oleic acid (double)	0.5	1.26	59.5	46.6	11.4
4a	H$_2$O/ Dodecylbenzenesulphonic acid (double)	0.5	1.67	79	51.1	10.1
4b	H$_2$O/ Dodecylbenzenesulphonic acid (double)	1	1.56	61	50.7	11.2
4c	H$_2$O/ Dodecylbenzenesulphonic acid (double)	2	1.31	73.1	47	11.2
4d	H$_2$O/ Dodecylbenzenesulphonic acid (double)	3	1.26	70.1	44.1	11.3
4e	H$_2$O/ Dodecylbenzenesulphonic acid (double)	5	1.2	69.5	43.3	11.4

* Data derived from the average of two measurements

By reviewing the mechanical parameters of Table 4.4, the Young's modulus in the majority of the nanocomposites decreases with the addition of Fe_3O_4 nanoparticles into the PVC matrix. Furthermore, it decreases in each series of nanocomposites with the increase of Fe_3O_4 loading, exception is the Sample 2 series where the opposite phenomenon occurs. The Young's modulus of the parental material, i.e. the un-loaded ultrasonically welded PVC, is measured at 1.5 GPa, while for the nanocomposites is in the range of 1.26 to 1.68 GPa. By comparing the Young's modulus results of Table 4.4 with the storage modulus measured by DMA and are presented in Table 4.2, it appears that despite some variations between the two methods, the results are comparable and evidently a function of the ferrofluid content. The decrease of the Young's Modulus is discussed thoroughly in Paragraph 4.6, while the main probable reason for this decrease is the decrease of the molar mass of the nanocomposite, as well as the changes occurs to its morphology. A corresponding decrease in the Young's Modulus due to the loading of polymers with Fe_3O_4 nanocomposites is mentioned in the literature [172], in polyurethane/Fe_3O_4 nanocomposite films. Finally, Samples 3a, 4a and in addition 4b, exhibit higher Young's modulus than the parental material, evidence that stiffer materials are produced.

The load at max was primarily increased to an optimum value in the series 1, 2 and 3 of nanocomposites, which is higher than the pure ultrasonically welded PVC with a measured load at max equal to 61.9 N; this is when the concentration reaches approximately 0.3 wt.%, while after this value it decreases with the increase of Fe_3O_4 loading. For the Sample 4 series, those nanocomposites have the grater load at max; i.e. Sample 4a is equal to 79 N, while it decreases with the increase of nanoparticle loading to 69.5 N (Sample 4d).

The tensile strength increased for Samples 1a, 4a and 4b when compared to the un-loaded PVC, while for the other samples it marginally increased. The phenomenon of decreasing tensile strength can be observed possibly due to nanoparticles distribution, as well as the decrease of polymer segments' mobility/rigidity that occurred to the interface of the dispersed Fe_3O_4 nanoparticles with respect to the PVC matrix, due to the high surface area of the dispersed nanoparticles and their interaction with the polymer. Moreover, the % elongation at max increases with the loading of Fe_3O_4 nanoparticles. The

mechanical properties achieved with the preparation of Fe_3O_4-nanocomposites with ultrasonic welding resulted in better mechanical properties, i.e. higher tensile strength compared with other relative structures [172]. Moreover, although in literature there are some references [164] on the results of mechanical measurements with higher tensile strength on magnetic PVC nanocomposite foils, these are not comparable because of the higher loadings of nanoparticles; these are 5 - 50 wt.%. While in general, the rigidity of Fe_3O_4/PVC nanocomposites can be boosted because of the concentration of the nanocomposites to the welding zone, this could lead to the phase separation and causes the decrease of tensile strength.

Figure 4.43 summarizes the results of Table 4.4 where "YM" is Young's modulus, "LaM" is load at max, "TS" is tensile strength, "Elong" is % elongation at max load, and "1, 2, 3, 4" are Sample 1, Sample 2, Sample 3 and Sample 4 series, respectively. It actually illustrates the % relative parameters versus the nanoparticles concentration (wt.%), while the 100% parameter is the plain ultrasonically welded PVC (0 wt.%). This figure clearly certifies that best mechanical properties were achieved for lower concentrations of Fe_3O_4 nanoparticles; these are from 0.1 to 0.5 wt.%, since they have the higher values for the most of the mechanical properties. Concentrations higher than 1 wt.% cause negative effects to the mechanical properties of the nanocomposites.
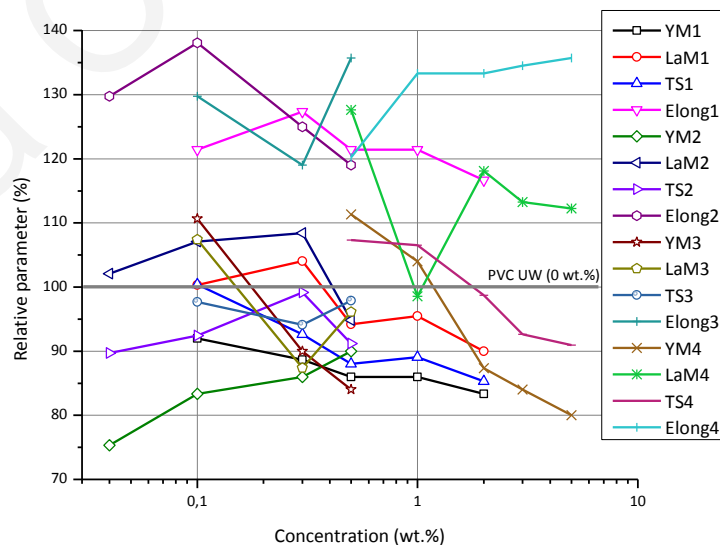
Figure 4.43 Mechanical properties of Fe_3O_4-PVC nanocomposites

The mechanical parameters of the Pd/PVC nanocomposite are listed in Table 4.5,

and match those of Fe_3O_4 nanocomposites.

Table 4.5 Mechanical properties of Pd-PVC nanocomposites*

Sample number	Liquid carrier/ Stabilizing layer	Pd (wt.%)	Young modulus (MPa)	Load at max (N)	Tensile strength (MPa)	% Elongation at max load
PVC UW	-	0	1.5	61.9	47.6	8.4
5a	n-hexane/LauMA	0.012	1.36	65.3	44.1	9.2

* Data derived from the average of two measurements

The distribution of nanoparticles into the nanocomposite matrix, their structure (coating, etc.), their depth into the polymer matrix, as well as the presentence of agglomerations or not, the mechanism of nanoparticle penetration into the polymer matrix and possible chemical bonds all affect the mechanical properties of nanocomposites. However, the inclusion of the coated magnetic nanoparticles in low percentages do not seem significantly affect the mechanical behavior of the nanocomposites.

4.8 Thermogravimetric analysis

To investigate the effect of Pd content on thermal stability of the Pd/PVC nanocomposite, thermogravimetric analysis (TGA) measurements were carried out. A Perkin Elmer TGA thermo-analyzer was used, with nitrogen flow of 20ml/min and temperature was raised from room temperature to 800°C. Figure 4.44 presents the TGA results and provides the comparison of the mass loss curves of the degradation of plain ultrasonically welded PVC foil and PVC/Pd nanocomposite foil. Both samples exhibit two weight loss stages (degraded in two stages), while the decomposition of PVC/Pd nanocomposite took place at higher temperatures ($\approx$ 15 – 20 ^{o}C), with the same weight loss. The first degradation stage occurs in the temperature range of 235 to 350 ^{o}C and 255 to 265 ^{o}C, respectively, for the PVC foil and PVC/Pd nanocomposite foil and is assigned to the progressive dehydrochlorination (loss of HCl) of the PVC foil and the formation of a

conjugated polyene structure. The second degradation stage of the PVC foil and PVC/Pd nanocomposite foil occurs in the temperature ranges of 400 to 490 $^{\circ}$C and 425 to 515 $^{\circ}$C respectively and is attributed to the pyrolysis of the formatted polyene, resulting the formation of volatile aromatic compounds and carbon [173].

The curves reveal that the addition of Pd nanoparticles into the PVC matrix affects positively its thermal stability, it results in an increase of the onset decomposition temperature of the PVC polymer, while it does not change the PVC degradation mechanism. This is evidence that Pd nanoparticles act as barriers to impede the diffusion of heat, as well as the migration of the degraded volatile and as a result the decomposition rate decreases. Relevant curves for PVC and PVC-nanocomposites are available in the literature [114, 171, 173].
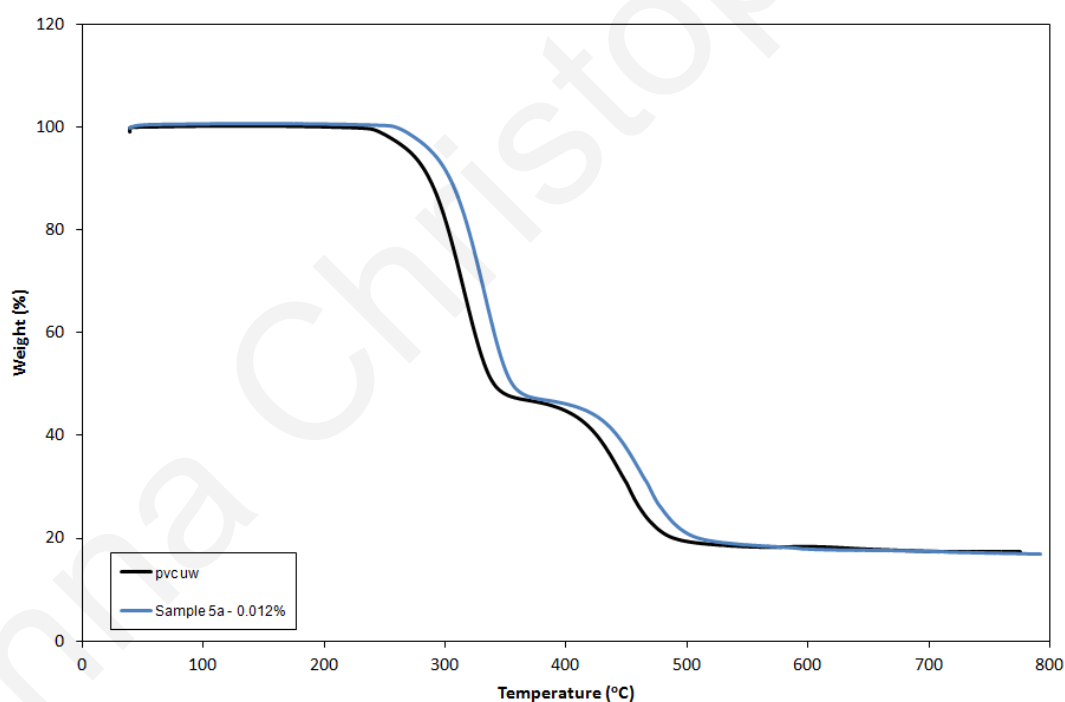
Figure 4.44 TGA curves of PVC foils and nanocomposite PVC foils containing Pd nanoparticles as a function of temperature - Sample 5

4.9 Conclusions of experimental part

Regarding the experimental results obtained from the characterization of polymer nanocomposites prepared by ultrasonic welding, one can conclude that the main objective of this research was achieved; this is the manufacturing of nanocomposite joints/seams with ultrasonic welding provision, with promising properties. The microscopic investigation of the nanocomposites revealed that the nanoparticles are not agglomerated significantly into micrometer structures when nanoparticle concentration is lower than 0.5 wt.%, while for higher concentrations agglomerations have been created with sizes approximately 200-500nm. In general for lower nanoparticle concentrations (0.1 - 0.5 wt.%) the nanoparticles are well and symmetrically dispersed all over the interface of the welded foils, however, by examining their concentration into the polymer matrix, it was shown that it decreases when moving from the interface (middle of nanocomposite) to outwards of the nanocomposite. For higher concentrations the aggregations appear to degrade the quality of the nanocomposites. Furthermore, it is believed that the mechanism of particle penetration into the polymer matrix changes after an optimum nanoparticle concentration, this is the 2 wt.%. The above mention statements agree when examining the other properties (i.e. magnetic, mechanical) of the nanocomposites. At last, it should be mentioned that the presence of TiO_2 particles into the nanocomposite matrixes also seems to degrade their properties, since their structure is a source of weakness.

According now to the other measured properties, almost all of the magnetic-containing series of nanocomposites resulted in a superparamagnetic behavior exhibiting high Ms values. This behavior was considered to be useful for further research and use in sewage pipes and underground cable protection by a local company namely Elysee Irrigation LTD, since due to their magnetic properties their position can be detected in the subsoil in order to avoid unnecessary excavations when there is a technical problem or a leak in these pipes. Finally the results obtained from the characterization of the mechanical properties of these materials, ensured that the lower concentrations of nanoparticles (0.1 - 0.5 wt.%) enrich the mechanical properties of the nanocomposites.

Part B. Computational

4.10 Computational analysis of nanoparticle movement into thermoplastic matrix

4.10.1 Introduction - Motivation

Based on the successful manufacturing of polymeric/thermoplastic nanocomposite materials by means of ultrasonic welding in the experimental part of this thesis, with regard of their interesting properties, as well as in order to better understand the phenomena occurs while producing those nanocomposites, an initial computational model is been proposed and is presented to the Computational Part of Chapter 4. The main aim of computational analysis is to understand the movement of nanoparticles into the weld affected zone. It is anticipated that the existence of an initial model will enable further simulated investigation of the manufacture process of nano-composites. In addition it could provide the basis for designing new nano-composites with properties tailored to specific needs.

A perquisite for building such a model is the understanding of important aspects of the manufacturing process itself. To this end, the next section prescribes the knowledge gained from the experimental work that is considered important for model creation and describes its relationship with the manufacturing method.

4.10.2 Specifies of the manufacturing process

The experimental cases studied in this research in association with the existing knowledge (literature) unveiled that the properties of the nano-composites are dilated by the following: (1) Nanoparticle mechanism of movement, (2) Nanoparticle distribution, (3) Nanoparticle width penetration and (4) agglomerations. These in turn as derive by the specific parameters of the manufacturing process such as for example are the welding

pressure, vibration frequency and formability between nanoparticles and polymer matrix. This relationship is depicted diagrammatically in more detail in the flowchart of Figure 4.45. In that flowchart the actual values of the parameters in (A) determine nanocomposite characteristics in (B) which finally determine the actual properties of (C).
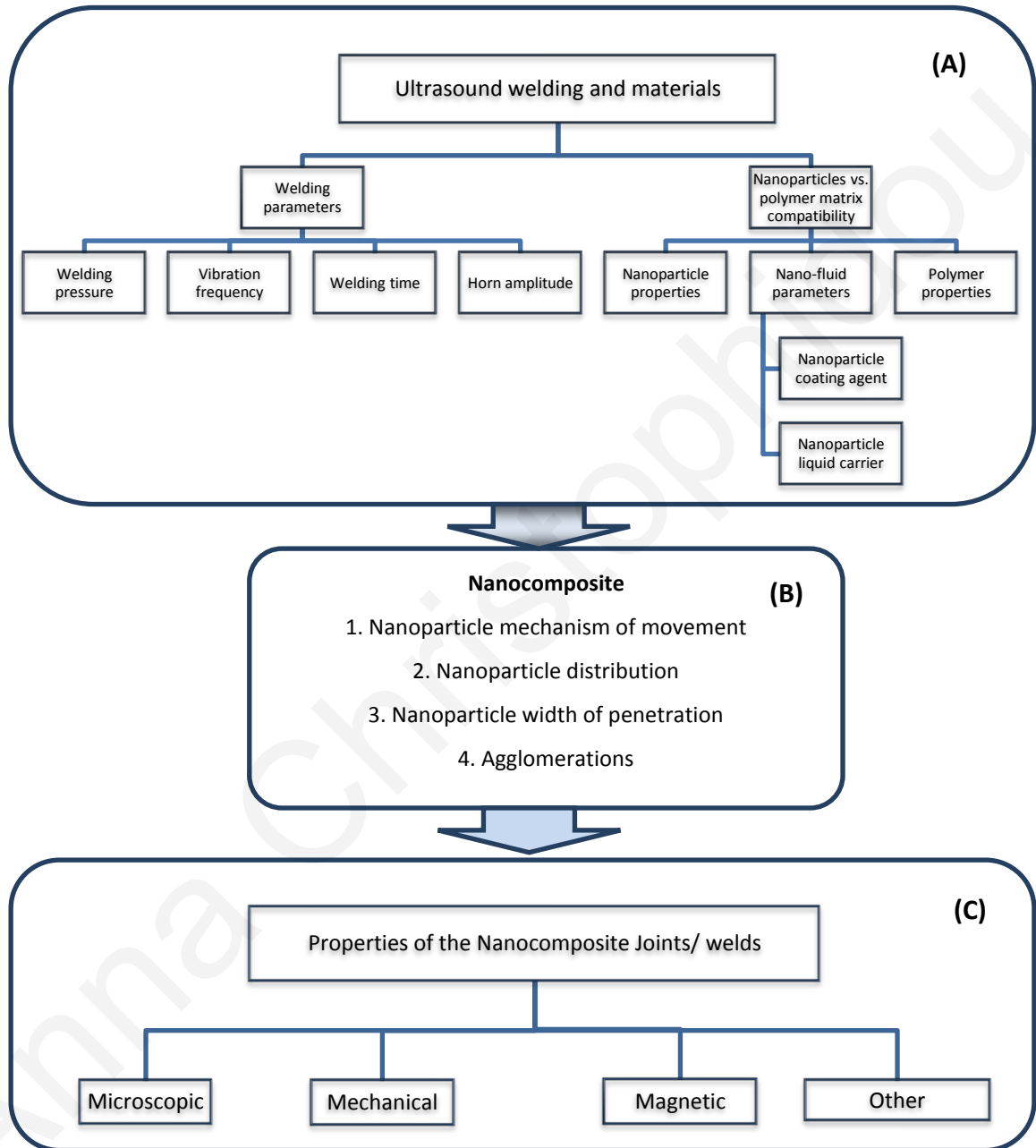
Figure 4.45 Aspects affecting the properties of nanocomposites prepared by means of ultrasonic welding

As a consequence of this procedure is proposed that simulates the dispersion movement and flow of nanoparticles into the polymer matrix due to the ultrasonic welding.

4.10.3 Modeling of the process

The main task of this study is to determine the mechanism of the distribution of Fe_3O_4 nanoparticles into the weld affected zone of PVC. This is actually a simulation of motion and it can be described as modelling of ultrasonic vibratory forced motion of nanoparticles.

The basic theory/principle behind ultrasonic welding of thermoplastic materials according to the knowledge gained, reveals that "*ultrasonic energy is applied, under pressure, to the area to be welded/bonded, the vibrations are then travel through polymeric materials where the mechanical energy is convert to thermal energy due to friction of polymeric chains, the polymer chains of the surfaces of the two parts are then diffuses and distributed to each other until the weld is done, ultrasonic vibration then stops, while pressure is holding the parts together for some fractions of second in order to give time to polymer to re-solidify*". This statement implies that the strength of the weld depends upon the total amount of energy that polymer matrices receive from the horn.

$$E = P \times T$$

Eq. 4-1

where, E is energy, P is power and is equal to $P = F \times U$ and T is time

resulting to:

$$E = F \times U \times T$$

Eq. 4-2

where, F is force and U is velocity.

Eq. 4-2 contains the four main welding parameters that affect the ultrasonically generated bond strength. In other words, energy which is transferred to the specimens to be welded, depends on welding force (which is the static pressure), welding velocity (which is the amplitude of ultrasonic vibration), as well as the weld and hold time of the procedure (Chapter 2.5). Different thermoplastics with various structures require different ultrasonic energy in order to bond together, concerning also their properties, such as glass transition temperature (Tg), flow temperature (Tf), melting temperature (Tm) and their crystallinity (Chapter 2.6 and 2.7).

During ultrasonic welding, the viscoelastic polymer dissipates energy into heat through intermolecular friction and weld affected zone is generated. A critical observation, that should be considered, is that welding of the thermoplastics begins only after Tg is reached. Moreover, in order to simplify the theoretical analysis (Figure 4.46), the following assumptions were employed: (a) spot ultrasonic welding occurs, (b) affected zone is equal to the thickness of the two foils to be joint together, and (c) a cell model based on the complementary vibration principle is designed.
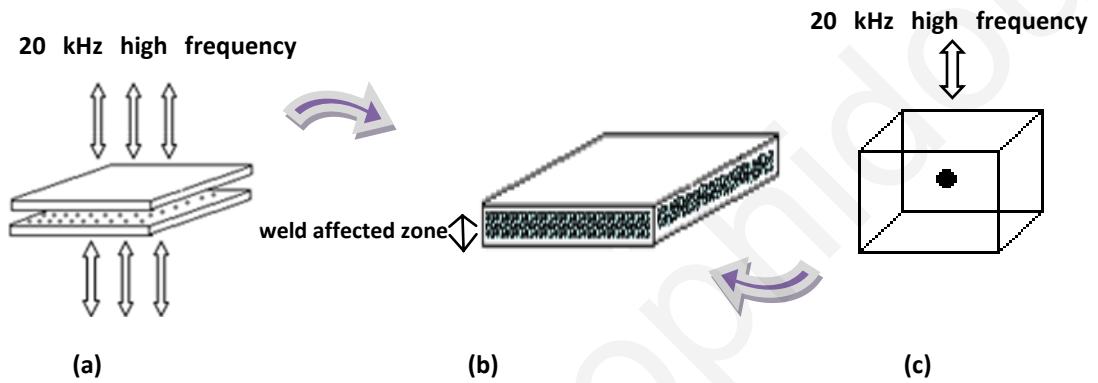
Figure 4.46 (a) Diagram of manufacturing polymer nanocomposites by means of ultrasonic welding procedure, (b) nanocomposite with dispersed nanoparticles, (c) cell model

According to Benatar [84] the power per unit volume dissipation of a typical plastic welt is governed by:

$$Q = \frac{\omega A_0^2 E''}{2}$$

Eq. 4-3

where, Q is internal heat generation (W/m^3), ω is the welding frequency (rad/s), A_0 is the amplitude and E'' is the loss modulus of the polymer, which is frequency (ω) and temperature dependent. Concerning the model, the loss modulus E'' during ultrasonic welding is that of the parental polymer matrix. Moreover:

$$E^* = E' + jE'' = \frac{\sigma}{\varepsilon}$$

Eq. 4-4

where, E^* is the complex modulus, E' is the storage modulus, σ is the stress and ε is the strain.

Dynamic loading - Oscillatory motion

Since polymer matrix is subjected to forced vibration, a sinusoidal stress is subjected to a viscoelastic material, the polymer, which melts. While nanoparticles are subjected to the same vibration forced motion. These nanoparticles cannot move until polymer softens and melt. The model is taking place in the cubic cell, as this has been designed in Figure 4.45c, while the instantaneous drag on a rigid spherical moving particle is equal to [174]:

$$-F_D = \frac{\pi d^2 \rho}{8} C_D U_R |U_R| + \frac{\rho V \Delta_A}{2} \frac{dU_R}{dt} + \frac{3d^2}{2} \Delta_H \sqrt{\pi \rho \mu} \int_0^t \frac{\dot{U}_R(s)ds}{\sqrt{t-s}} - \rho V \frac{dU_f}{dt}$$

Eq. 4-5

where, U_p is the velocity of the spherical nanoparticle, U_R is the velocity of the particle relative to the fluid and is equal to $U_R = U_p - U_f$, U_f is the velocity of the fluid, C_D is the drag coefficient, V is the volume of the spherical nanoparticle, Δ_A is the added mass coefficient, Δ_H is the history coefficient and s is the molecular speed radio. While Eq. 4-5 can be simplified according to the observation that the fluid oscillates in the direction of the vibrating force; this is the vertical direction, and velocities are positive downwards. The equation of motion for a freely moving particle is:

$$\left(\gamma + \frac{\Delta_A}{2}\right)\frac{dU_R}{dt} = (\gamma - 1)g - \frac{3C_D U_R |U_R|}{4d} - \frac{9\Delta_H}{d}\sqrt{\frac{\nu}{\pi}}\int_0^t \frac{\dot{U}_R(s)ds}{\sqrt{t-s}} - (\gamma - 1)\frac{dU_f}{dt}$$

Eq. 4-6

When particle Reynolds number (Re) is small, Eq. 4-6 becomes linear:

$$\left(\gamma + \frac{1}{2}\right)\frac{dU_p}{dt} = (\gamma - 1)g - \frac{18\nu U_R}{d^2} - \frac{9}{d}\sqrt{\frac{\nu}{\pi}}\int_0^t \frac{\dot{U}_R(s)ds}{\sqrt{t-s}} + \frac{3}{2}\frac{dU_f}{dt}$$

Eq. 4-7

and the velocities can be written as sums of mean values and variations from the mean, i.e.:

$$U_p = \bar{U}_p + u_p; \qquad U_f = \bar{U}_f + u_f; \qquad U_R = \bar{U}_R + u_R$$

Eq. 4-8

101

According also to Stokes terminal velocity, where: $\overline{U}_R = \Delta\rho g d^2 / 18\mu$; the Eq. 4-7 becomes:

$$\left(\gamma + \frac{1}{2}\right)\frac{du_p}{dt} = \frac{3}{2}\frac{du_f}{dt} - \frac{9}{d}\sqrt{\frac{\nu}{\pi}}\int_0^t \frac{\dot{u}_R(s)ds}{\sqrt{t-s}} - \frac{18\nu du_R}{d^2}$$

Eq. 4-9

When considering pure sinusoidal oscillations,

$$u_f = A\omega cos\,\omega t$$

Eq. 4-10

the **particle velocity (u_p)** is related to u_f by an amplitude ration η and phase shift β:

$$u_p = \eta\,A\omega cos(\omega t + \beta)$$

Eq. 4-11

where for rigid spheres entrained in oscillating fluids at low Reynolds numbers the Amplitude radio (η) and Phase shift (β) are respectively equal to:

$$Amplitude\ radio\ = \eta\ \sqrt{(1 + h_1)^2 + h_2{}^2}$$

Eq. 4-12

$$Phase\ shift = \beta\ =\ tan^{-1}[h_2/(1 + h_1)]$$

Eq. 4-13

while for full solution

$$h_1 = H_1(1 + H_2)$$

Eq. 4-14

$$h_2 = H_1 H_2(1 + 2\tau_0)$$

Eq. 4-15

and

$$H_1 = \frac{2(1-\gamma)/(2\gamma+1)}{H_2{}^2\left(1+\sqrt{2\tau_0}\right)^2 + (1+H_2)^2}$$

Eq. 4-16

$$H_2 = \frac{9}{(2\gamma+1)}\sqrt{\frac{\tau_0}{2}}$$

Eq. 4-17

$$\gamma = \frac{\rho_p}{\rho_f}$$

Eq. 4-18

$$\tau_0 = \nu/\omega\alpha^2$$

Eq. 4-19

The solution of equations Eq. 4-11 was achieved using the MATLAB, by substituting Eq. 4-12 to Eq. 4-19 and the material parameters that are listed in Table 4.6. Amplitude radio $\eta = 1$ and $\beta \approx 0$. Particle velocity (u_p). While this is an indication that the nanoparticles are distributed into the polymer matrix due to the movement of the polymer chains. Further investigation is needed in order to simulate the nanoparticles movement into the polymer matrix.

Table 4.6 Mechanical properties of Pd-PVC nanocomposites

Parameters	Values
PVC dynamic viscosity	ν = 10.000
PVC density	ρ_f = 1.370 kg/m^3
Amplitude frequency	f = 20.000 Hz
Omega	$\omega = 2\pi f$
Particle diameter	a = 500*10^{-9} m
Particle density	ρ_p = 2.510 Kg/m^3

Chapter 5.   Characterization of fiber and CNT based polymer nano and micro-composites, results and discussion

Part A. Experimental

5.1 Introduction - Characterization techniques

The experimental part of Chapter 5 deals with the characterization of the properties of the fiber and CNT based polymer nanocomposites; these are loaded with CNTs/PVC, as well as micro-fiber-CA, nano and micro-composites. All the composites were investigated initially by SEM in order to obtain the structure of the ultrasonic joint, as well as the distribution of the nano/micro-fibers into the cross-section of the polymer matrix. Further, they were analyzed according to their mechanical properties. The composites loaded with CNTs and fibers were produced at a later stage than those containing nano-particles.

5.2 Scanning electron microscopy

The SEM pictures were carried out using a Tescan Vega SEM in class 1000 clean room facilities.

5.2.1 CNT nanocomposites

Figure 5.1 illustrates a specimen of the cross-section of sh-MWCNT-PVC nanocomposites, Sample 6 series of Table 3.11, in low magnifications. The heat affected

zone is porous and clearly depicted, while it expands through the entire thickness of the nanocomposite. It is important to mention that both samples are thicker (≈ 800 μm) than the those measured below for the scope of this thesis and they are out of the successful range of nanoparticle concentrations, which was 0.1 to 0.3 wt.%. Concerning the above-mentioned one can notice the importance of the optimum nanoparticles loading as well as optimum welding conditions, since thicker polymer foils require more head/energy in order to weld together, resulting in downgraded materials for the purpose of this thesis. Moreover, sh-MWCNTs, used to prepare Sample 6 nanocomposites, are not coated with any surfactant, which may also be attributed to the porous structure that is illustrated in Figure 5.1. Short CNTs embedded in PVC could not be visualized with SEM. The samples are coated with a 5 to 10 nm gold thin films with an "Anatech Hummer Cold Deposition Sputter Coater".

(a)   (b)
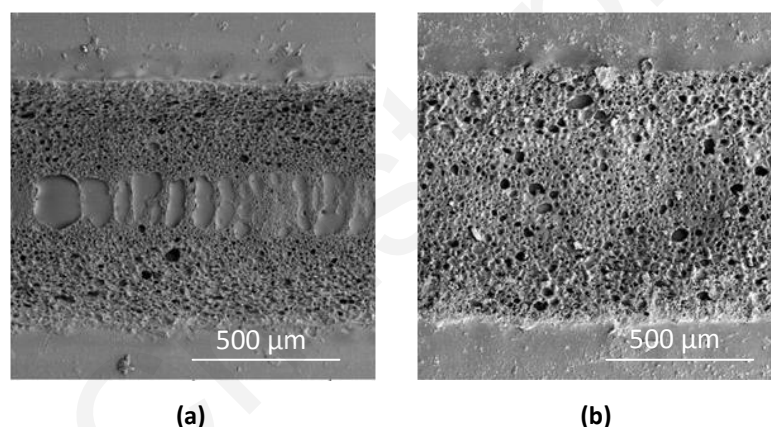
Figure 5.1 SEM micrographs of cross-section of (a) PVC/1 wt.% sh-MWCNT - Sample 6e, (b) PVC/2 wt.% sh-MWCNT - Sample 6f, nanocomposites manufactured by ultrasonic welding (thicker samples)

Finally, long-MWCNT of the Sample 7 series (Table 3.11) are visible in heat affected zone, in higher magnifications and discerned as thin dark shadows embedded into the PVC matrix, as illustrated in Figure 5.2. This can be explained with their structure and size, since the average length of long-MWCNTs is in the range of 1.5 μm. Moreover, the embedded long-MWCNTs into long-MWCNTs-PVC nanocomposites are coated with an anionic surfactant, resulting in smooth structures similar to those of ferro- and Pd-nanocomposites.
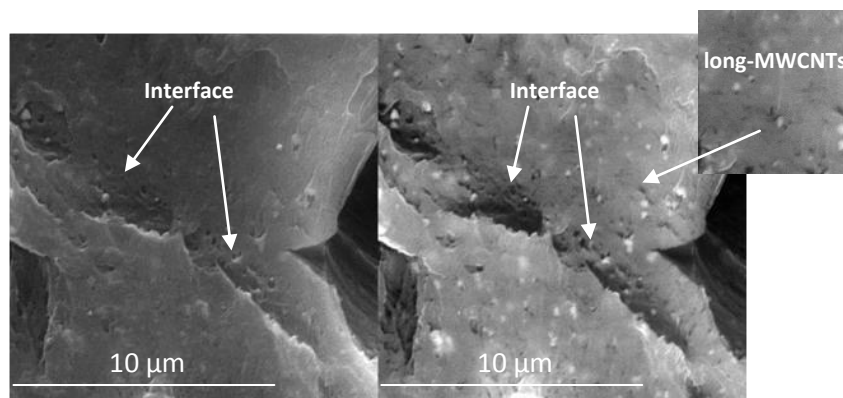
Figure 5.2 SEM micrographs of the heat affected zone of a cross-section of PVC/long-MWCNT nanocomposites manufactured by ultrasonic welding - Sample 7e

5.2.2 CA micro-composites

An identical procedure was also followed for cellulose acetate micro-composites. Figure 5.3 to Figure 5.7 illustrate the result of the ultrasonic welding process on the CA foils with the electrospun CA and CA/PAni fibrous membranes, manufactured under various spinning parameters as this described in Table 3.12. It should be noted that the welding conditions remained the same for all the prepared micro-composites. More precisely, Figure 5.3 presents the ultrasonically welded area of two plain CA foils. When compared to the PVC welded foils, the CA welds/joints do not flow evenly to produce solid weld affected zones. Moreover, it is important to mention that the weld affected zone is again expanding through the entire thickness of the material.

In Figure 5.3 to Figure 5.7 the sections present (a) the SEM micrograph of the electrospun membrane used, while (b) and (c) the SEM micrographs of the fabricated micro-composites. CA micro-composites have porous structures possibly due to the use of micro-fibers. The micro-fibers are visible in all the micro-composites (Figure 5.4 to Figure 5.7). Regarding Sample 8a (Figure 5.4), the CA/PAni fibrous membranes are homogeneously encapsulated into the cellulose acetate matrix and dispersed all over the nanocomposite. On the other hand, CA fibrous membranes embedded in series 9 (Figure 5.5 to Figure 5.7) of nanocomposites, keep their initial structure and the CA matrix flows around them. As a result, three different layers are observed; two external CA foils and in the middle one that consists of CA fibrous membranes surrounded by the CA matrix.
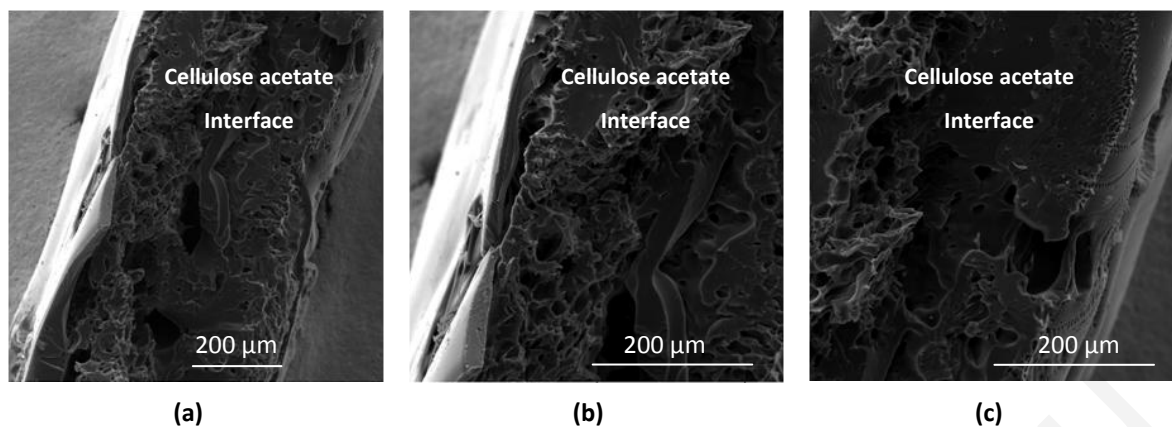
Figure 5.3 SEM micrographs of the two CA foils ultrasonically welded
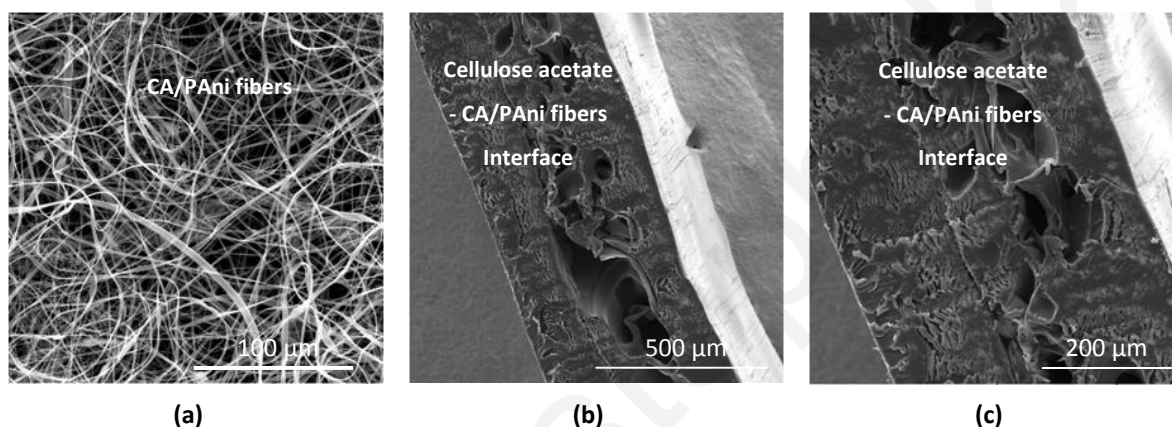
Figure 5.4 (a) SEM micrograph of CA/PAni fibers electrospun from a 12.5 w/v.% concentration solution (90 wt.% CA - 10 wt.% PAni), with a 100 µl/min feeding rate, using a 20-gauge needle, under a voltage of 15 kV and a tip-to-collector distance of 10 cm, (b) and (c) SEM micrograph showing the cross-section of the fabricated micro-composite - Sample 8a
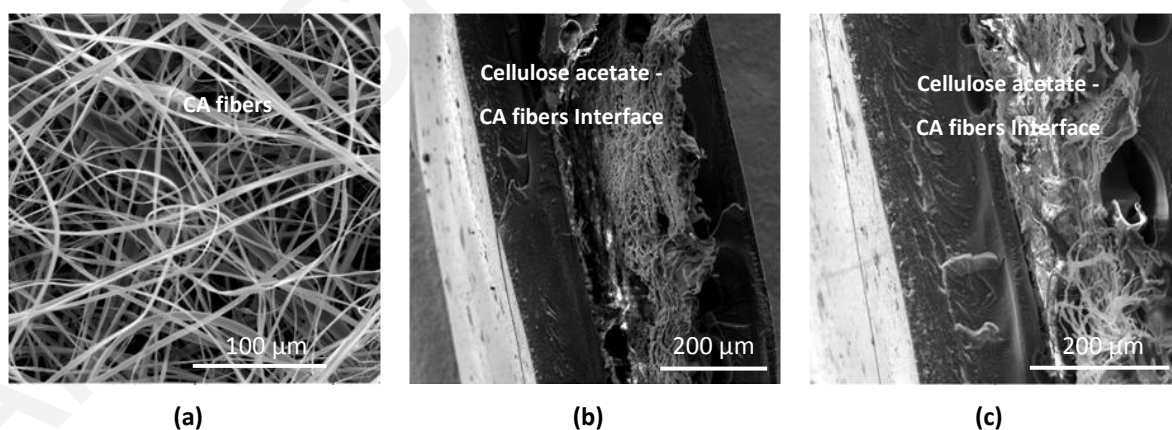
Figure 5.5 (a) SEM micrograph of CA fibers electrospun from a 12.5 w/v.% concentration solution, with a 1 ml/min feeding rate, using a 16-gauge needle, under a voltage of 10 kV and a tip-to-collector distance of 10 cm, (b) and (c) SEM micrograph showing the cross-section of the fabricated micro-composite - Sample 9a

(a)	(b)	(c)
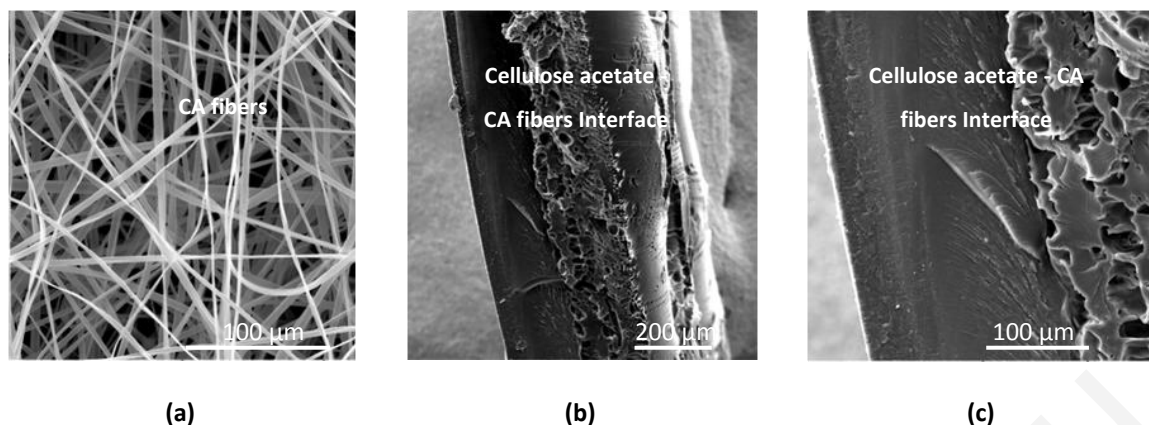
Figure 5.6 (a) SEM micrograph of CA fibers electrospun from a 12.5 w/v.% concentration solution, with a 1 ml/min feeding rate, using a 16-gauge needle, under a voltage of 15 kV and a tip-to-collector distance of 10 cm, (b) and (c) SEM micrograph showing the cross-section of the fabricated micro-composite - Sample 9b

(a)	(b)	(c)
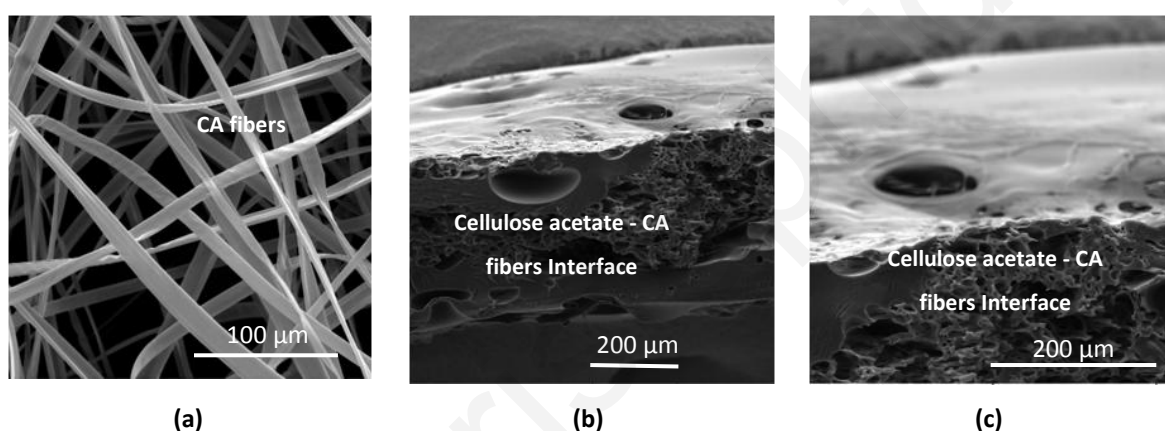
Figure 5.7 (a) SEM micrograph of CA fibers electrospun from a 15 w/v.% concentration solution, with a 1 ml/min feeding rate, using a 16-gauge needle, under a voltage of 20 kV and a tip-to-collector distance of 15 cm, (b) and (c) SEM micrograph showing the cross-section of the fabricated micro-composite - Sample 9c

5.3 Mechanical properties

The mechanical properties of all the fiber based nano/micro-composite samples prepared in Chapter 3 were investigated by tensile testing. The resulting tensile strength, Young's modulus, elongation at break and other properties are examined. A Universal Testing Machine (UTM), model LR 300K from Lloyds Instruments Ltd (UK), based on BS EN 10002-1 standards (Figure 5.8) was employed. The measurements were carried out at room temperature conditions of 23 ± 2 °C, with humidity 65 ± 5 % and accuracy ≤ 0.5 %. The clamping distances of the samples had 2 cm length, around 0.3 cm with and 0.045 cm thickness; the loading speed was 50 mm/min and preload 1 N. Measurements are presented in Table 5.1, Table 5.2 and Table 5.3.
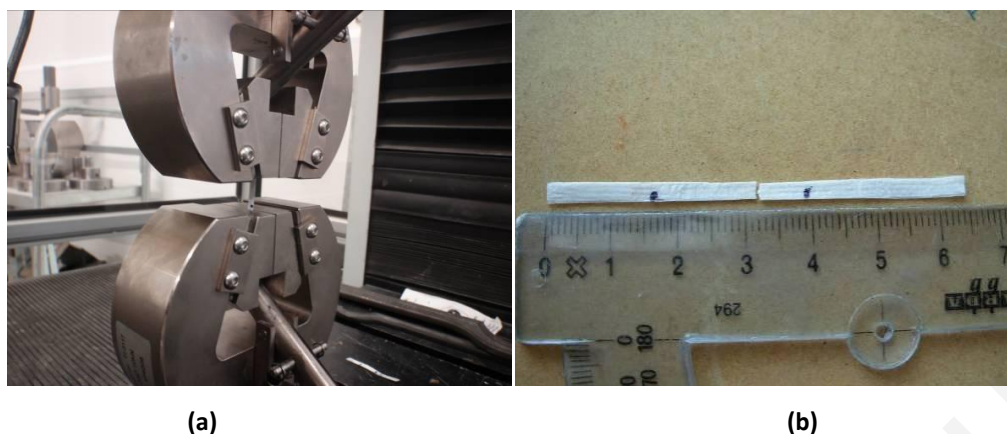
Figure 5.8 (a) General image of mounded nanocomposite which is held in PPMS tension mode, (b) general image of PVC/nanocomposite, after failure when measuring the mechanical properties with the PPMS

5.3.1 CNT-PVC nanocomposites

The mechanical properties of the sh-CNTs-PVC nanocomposite samples; these are the series 6 of Table 3.11, are listed at Table 5.1. The data show that the mechanical parameters initially increases to maximum values with the presence of the sh-CNTs up to loadings approximately equal to 0.2 to 0.3 wt.%. At higher CNTs concentrations they gradually decrease, but again most of them are higher than the plain PVC ultrasonically welded foils. When CNT concentration reaches 2 wt.% the mechanical properties decrease, an evidence that there is a maximum loading capability of this synthesis method, a similar phenomenon observed with the iron oxide nanoparticles. Corresponding references, where the tensile strength first increases while after an optimum concentration of CNTs and/or graphene decreases, also exist in the literature [175-178]. Figure 5.9 illustrates their load at max versus the CNTs concentration.

Table 5.1 Mechanical properties of the sh-CNTs-PVC nanocomposites

Sample number	sh-CNTs (wt.%)	Load at max (N)	Young modulus (GPa)	Tensile strength (MPa)
PVC UW	-	48.4 ± 1.2	0.9 ± 0.05	33.3 ± 0.5
6a	0.1	57.5 ± 1.6	0.96 ± 0.19	49 ± 4.2
6b	0.2	61.7 ± 1.3	0.96 ± 0.09	51.9 ± 0.1
6c	0.3	54.8 ± 4.9	1.13 ± 0.09	44.4 ± 1.7
6d	0.5	54.2 ± 6.6	0.57 ± 0.21	30.8 ± 1.9
6e	1	54.9 ± 0.3	0.55±0.04	42.1 ± 2.6
6f	2	47.2 ± 0.5	0.96 ±0.11	32.4 ± 2.2
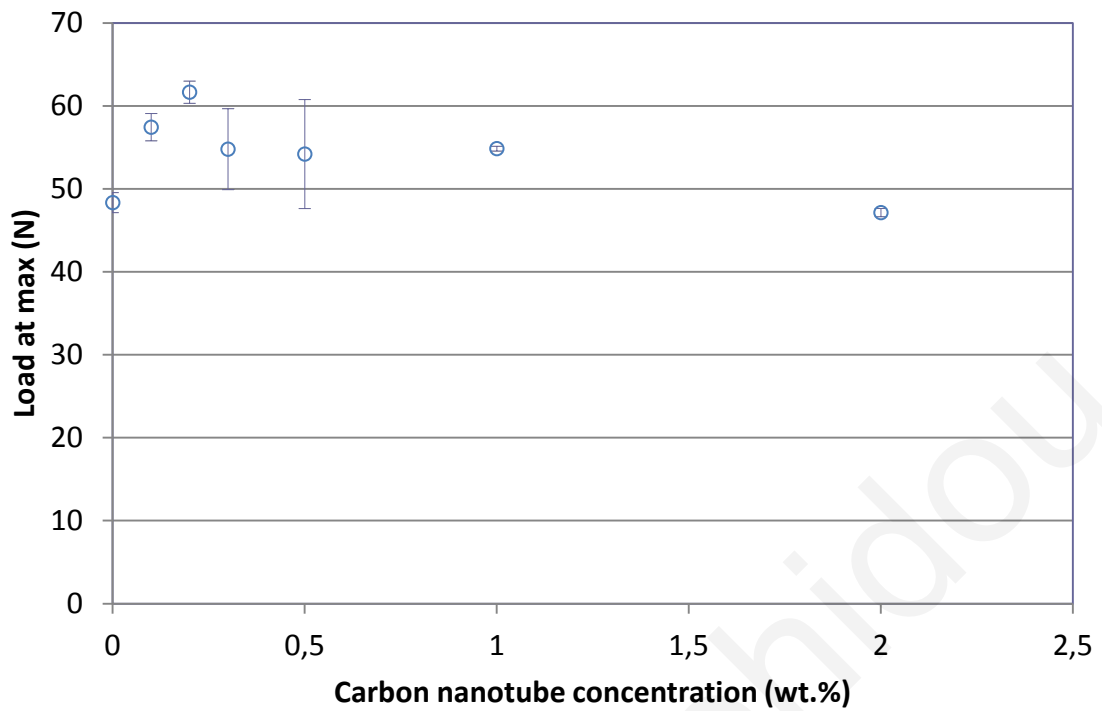
Figure 5.9 sh-CNTs-PVC load at max vs CNTs concentration - Sample 6

The mechanical properties of the long-CNT-PVC nanocomposites samples; these are the series 7 of Table 3.11, are listed in Table 5.2. According to the data, a similar response as in the case of the sh-MWCNTs occurs, since their properties decrease with the presence of CNTs, up to loadings equal to 0.2 wt.%. A further increase of the CNTs loading leads to a decrease of their mechanical properties equivalent to the parental material. Again the results are converging with the literature [175-178], while Figure 5.10 illustrates their load at max versus the CNTs concentration.

Table 5.2 Mechanical properties of the long-CNTs-PVC nanocomposites

Sample number	long-CNTs (wt.%)	Load at max (N)	Young modulus (GPa)	Tensile strength (MPa)
PVC UW	-	48.4 ± 1.2	0.9 ± 0.05	33.3 ± 0.5
7a	0.01	50.15	1.25	37.83
7b	0.05	50.73	1.05	33.8
7c	0.1	55.61	0.94	43.18
7d	0.2	59.97	0.82	44.25
7e	0.3	47.07	0.76	32.38
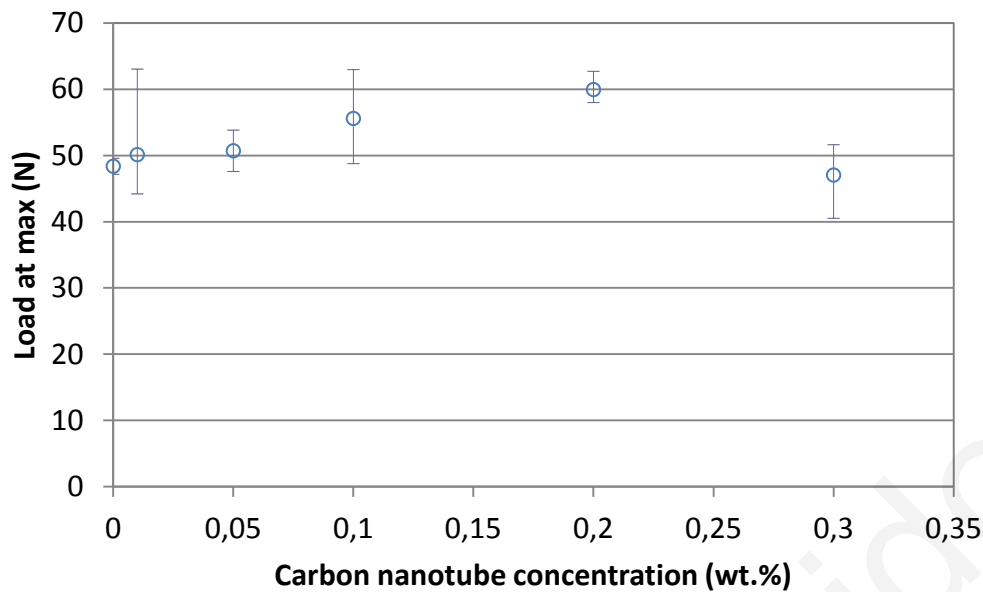
Figure 5.10 long-CNTs-PVC load at max vs CNTs concentration - Sample 7

Almost all the measured mechanical properties of the CNT nanocomposites were higher than the unloaded ultrasonically welded PVC, while by comparing sh-CNT and long-CNT nanocomposites there are observed behaviors that are consistent with each other. It is notable to mention that sh-CNTs at optimum loads (0.1 - 0.3 wt.%) show even better mechanic properties than long-CNTs, i.e. at 0.2 wt.% concentration the load at max is equal to 61.7 N for sh-CNTs versus 60 N for sh-CNTs, while tensile strength is equal to 51.9 MPa versus 44 MPa respectively.

5.3.2 CA/Pani and CA/CA nanocomposites

In Table 5.3 the mechanical properties of the CA-micro-composite foils are listed (Table 3.12), compared to the unloaded ones. The results show that their load to max and tensile strength basically are doubled with the loading of the micro-fibers. The results indicate that the composites exhibit better mechanical properties than the parental material.

Table 5.3 Mechanical properties of the CA/Pani and CA/CA microcomposites

Sample number	Morphology	Load at max (N)	Young modulus (GPa)	Stiffness (kN/m)	Tensile strength (MPa)
CA UW	-	20.4	0.42	30	12
8a	90 wt.% CA - 10 wt.% PAni 12.5 w/v.% CA/acetone solution Beads-on-string, quite uniform fibers	44.2	0.43	72.7	23.5
9a	12.5 w/v.% CA/acetone solution Rare beads-on-string, cylindrical fibers	40	0.35	53	25.2
9b	12.5 w/v.% CA/acetone solution Cylindrical uniform fibers	32	0.44	51.4	22.3
9c	15 w/v.% CA/acetone solution Non-uniform flat fibers, wrinkle in beads	42.4	0.44	62.5	24.8

By analyzing the morphology of the micro-composites, Samples 8a, 9a and 9c it has been shown that the morphology of the fibers affect the mechanical properties of the micro-composites and it can be concluded that they actually react like cross-links to the polymer chains, resulting in higher stiffness and load at max. Sample's 8a micro-fibers include 10 wt.% of PAni which further enhances the strength of the composite. Sample 9b also results in better mechanical properties, although when compared with the other has increased properties possibly due to the cylindrical uniform fibers. The Young's modulus on the other hand remains at the values since the embedded micro-fibers are synthesized with the same material as the polymer matrix; this is the cellulose acetate.

5.4 Conclusions of experimental part

With regard to their characterization results, one can conclude that the manufacturing of nano and micro-fiber composite joints/seams with ultrasonic welding provision was achieved, while again the distribution as well as the concentration of the

nano/micro-fibers into a polymer matrix is of critical importance for their potential properties. Almost all the CNT-based and all the microfiber-based composites demonstrated mechanical properties superior than the plain ultrasonically welded thermoplastics.

Part B. Computational

5.5 Molecular dynamics

5.5.1 Mathematical background

The matter is composed of atoms and all the macroscopic properties that experience in everyday life are a direct consequence of this fact. From the point of view of flow modeling, however, it is often more convenient to consider the flow as a continuum and assume variables like viscosity, diffusivity or density to be intrinsic properties of the fluid rather than the result of atomic dynamics. Sometimes, however, researchers are interested to phenomena occurring at the micro- or nano-scale and they cannot avoid to taking into account the 'granular' being of matter.

One of the key parameters, which characterize the modeling of flows, is represented by the so-called Knudsen number:

$$K_n = \frac{\lambda}{L}$$

Eq. 5-1

Where, λ is the molecular mean free path and L a typical length scale of the system.

According to the value of Kn, various flow regimes are possible [179]:

1. Continuum flow regime (Kn < 0.01), which can be modeled by the Navier–Stokes equation with no-slip boundary conditions.

2. Slip flow regime (0.01 ≤ Kn ≤ 0.1), where the no-slip boundary conditions cannot be applied to sub-layer on the order of one mean free path known as Knudsen layer. In this layer, the granular nature of the flow becomes dominant especially near the walls. For this reason, the flow in the Knudsen layer cannot be described, at least in theory, by the Navier–Stokes equation. This region, however, often covers less than 10 % of the channel height and the Navier–Stokes equation gives a reasonable description of the flow, provided that a slip-velocity is taken into account at the walls. This slip-velocity, however, must be calculated by other means like, for instance, molecular dynamics.

3. In the transition regime (Kn ≥ 0.1), finally, the continuum hypotheses definitely breaks down and 'granular' modeling (e.g. molecular dynamics) must be used.

The critical Kn numbers, which separated the aforementioned flow regimes, refer, strictly speaking, to gas flows. In the case of liquids or polymers, these values are expected to differ, but the general division in three regimes is still applicable.

5.5.2 Calculations of the experimental used carbon nanotubes

The median mass of short multi-wall CNTs ($M_{sh-MWCNT}$) have been used in order to manufacture Sample 6, series nanocomposites; these are sh-MWCNTs-PVC is calculated from Eq. 5-2, while there median volume ($V_{sh-MWCNT}$) from Eq. 5-3 respectively,

$$M_{sh-MWCNT} = \pi L n \big(D_{out} - 0.34(n-1) \big) k_1$$

Eq. 5-2

$$V_{sh-MWCNT} = \frac{\pi D_{out}{}^2 L}{4}$$

Eq. 5-3

where, $L = 280nm$ (length of sh-MWCNT), $D_{out} = 8.4nm$ (outer diameter of sh-MWCNT) and $D_{in} = 2.5nm$ (inner diameter of sh-MWCNT), as these have been measured

115

by typical X-Ray diffraction patterns and Micro-Raman spectra respectively [154]. Moreover, n equals to the number of layers and is calculated from Eq. 5-4, while $k_1 = 0.87 \times 10^{-21} g/nm^2$ is the estimated mass density of a flat graphene sheet of the sh-MWCNT,

$$n = 1 + (D_{out} - D_{in})/0.6$$

Eq. 5-4

by calculating the above, $n = 9$ layers, $M_{sh-MWCNT} = 3.9 \times 10^{-17} g$ and $V_{sh-MWCNT} = 1.55 \times 10^{-17} cm^3$.

The median density of the "median" short multi-wall carbon nanotubes ($d_{sh-MWCNT}$) is equal to $d_{sh-MWCNT} = 2.51 g/cm^3$, from equation Eq. 5-5, compared with the theoretical (Roentgen) density of graphite, which is $d_{sh-MWCNT\ theoretical} = 2.66 g/cm^3$, that is a bit less concluding that sh-MWNT have been used are well-graphitized.

$$d_{sh-MWCNT} = \frac{M_{sh-MWCNT}}{V_{sh-MWCNT}}$$

Eq. 5-5

5.5.3 Basics of molecular dynamics

In classical molecular dynamic simulations, atoms move according to the Newtonian equations of motion:

$$m_i \frac{\partial^2 \vec{r}_i}{\partial t^2} = -\frac{\partial}{\partial \vec{r}_i} U_{TOT}(\vec{r}_1, \vec{r}_2 ... \vec{r}_N), \quad i = 1,2...N,$$

Eq. 5-6

where m_i is the mass of atom i, r_i is its position, and U_{TOT} is the total potential energy that depends on all atomic positions. The potential energy is the most crucial part of the simulation because it must faithfully represent the interaction between atoms in the form of a simple mathematical function. Some of the most widely known MD-software are based on certain force-field packages like AMBER, GROMACS, CHARMM or OPLS, which have been studied and tested for certain typical applications. Conceptually,

the forces acting on atoms are divided into non-bonded and intra-molecular atomic forces.

5.5.3.1 Non-bonded atoms forces

Atoms can interact through electrostatic forces, attractive forces at long ranges (van der Waals force) and repulsive forces at short ranges (the result of overlapping electron orbital's) referred to as Pauli repulsion. The Lennard-Jones potential [180] is a simple mathematical model, which combines together van der Waals attraction and Pauli repulsion

$$U_{vdW}(r_{i,j}) = 4\varepsilon_{i,j}\left[\left(\frac{\sigma_{i,j}}{r_{i,j}}\right)^{12} - \left(\frac{\sigma_{i,j}}{r_{i,j}}\right)^{6}\right]$$

Eq. 5-7

where ε is the depth of the potential well and σ is the (finite) distance at which the potential is zero. Due to its simplicity, this potential is by far the most common in molecular dynamics simulations. The fast decay of the Lennard-Jones potential usually allows a truncation of the potential at a certain cutoff distance r_C (typically 9-12 Å).

The electrostatic force follows the known Coulomb law

$$U_{Coulomb}(r_{i,j}) = \frac{q_i q_j}{4\pi\varepsilon_0 r_{i,j}}$$

Eq. 5-8

where q_i and q_j are the electrostatic charges of atom i and j, $r_{i,j}$ the distance between them and ε_0 the dielectric constant. The decay of the electrostatic potential is not as sharp as in the previous case and it can create certain problems especially in connection with periodic boundary conditions. In order to tackle this problem, specific summation techniques such as the Ewald summation [181] or the Particle-Mesh Ewald summation [182] have been developed over the years.

5.5.3.2 Intra-molecular forces

The modeling of intra-molecular forces presents a larger variety of cases and different kinds of potentials. The expression used by NAMD [183] (the code used in the present work) is based on the following approximation.

$$U_{intramolecular} = U_{stretch} + U_{angle} + U_{dihedral}$$

Eq. 5-9

$$U_{stretch} = k_{stretch}(r - r_0)^2$$

Eq. 5-10

$$U_{angle} = k_{angle}(\theta - \theta_0)^2$$

Eq. 5-11

$$U_{dihedral} = k_{dihedral}\left[1 + \cos(n\phi - \phi_0)^2\right]$$

Eq. 5-12

where $U_{stretch}$ models the force exerted when the bond is stretched from its initial position r_0 to the new position r; U_{angle} models the force exerted when the angle Θ between two bonds changes with respect to its initial angle Θ_0; $U_{dihedral}$ describes the force that atoms separated by three covalent bonds exert when they are subject to a torsion angle ϕ. An improper dihedral force, which regards three planar atom bonds, also exists but it is not reported here because such a possibility does not appear in this case. In this work, the AMBER force field [184] for the C-C interaction in the grapheme sheet and the parameters reported in Smith et al. [185] for the PVC[1] was used. In order to distinguish between the carbon in the grapheme and the carbon in the PVC, the first was indicated as C* and the second as C.

---

[1] The $U_{dihedral}$ in Smith et al. has a form different from eq. 5-12 and a least squares fitting (error < 1 %) between the two functions was necessary. In Table 5.4, the parameter fitted for eq. 5-12 are reported.

Table 5.4 Force field parameters for bonded and non-bonded interactions

L-J (Eq. 5-7)	σ (Å)	ε (kcal/mol)
methyl group	4.1752	0.1419
C	3.9197	0.0540
Cl	3.9720	0.1608
H	3.2126	0.0086
C*	3.4000	0.086

Electrostatic (Eq. 5-8)	Partial Charge [e]	Electrostatic (Eq. 5-8)	Partial Charge [e]
C (methylene)	-0.1792	H (methylene)	0.0990
C (methine)	0.0313	H (methine)	0.1486
Cl	-0.1987	C*	0.0000

Stretch Eq. 5-10	$k_{stretch}$ (kcal/mol/Å^2)	r_0 (Å)
C-C	618	1.53
C-H	704	1.09
C-Cl	376	1.83
C*-C*	469	1.4

Bend Eq. 5-11	k_{angle} (kcal/mol/deg^2)	θ_0 (deg)
C-C-C methylene centered	170	112.0
C-C-C methine centered	170	108.2
C-C-H	104	106.3
H-C-H	108	109.0
C-C-Cl	126	106.3
Cl-C-H	126	103.0
C*-C*-C*	63	120.0

Torsion Eq. 5-12[1]	$k_{dihedr.}$ (kcal/mol)	ϕ_0 (deg)	n
C-C-C-C racemic	0.85	180	1/3
C-C-C-C meso	1.20	180	1/3
C*-C*-C*-C*	3.65	180	2

The mixing L-J parameters (Cl-C, C*-C etc.) are calculated according to the Lorentz-Berthelot rule.

$$\sigma_{AB} = \frac{1}{2}\left(\sigma_A + \sigma_B\right)$$

Eq. 5-13

$$\varepsilon_{AB} = \sqrt{\varepsilon_A \varepsilon_B}$$

Eq. 5-14

5.5.4 PVC - CNT interaction

As previously explained, under certain conditions, the flow can be modeled by the Navier–Stokes equation associated with a slip-velocity at the walls. In this section the CNT/PVC interaction was taken into consideration in order to calculate the slip velocity at the nanotube walls by means of molecular dynamics.

The flow of PVC between two graphite sheets under a gravity-like acceleration was simulated. The real nanotubes in the polymer have an average diameter of approximately 9 nm. It is a too large nanotube for molecular simulation, but, since only the PVC-wall interaction is of interest here, only two graphitic flat surfaces (distance 3 nm) stuffed with PVC can be taken into consideration. The graphite-PVC sandwich, used in the molecular dynamics simulations, is shown in Figure 5.11.
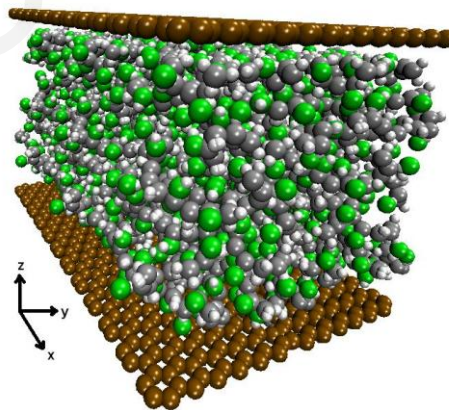
Figure 5.11 The graphite-PVC sandwich used in the molecular dynamics simulations

The PVC atoms were accelerated by the method of pseudo-gravity forces **a**, which has the advantage of low computational costs and it is frequently used for these kinds of problems (e.g. [186]). Three cases with the vector **a** pointing towards the x axis (|**a**|=1,

2.5 and $5 \cdot 10^8$) and two cases with **a** pointing towards y (|**a**|=1 and $5 \cdot 10^8$) were simulated. It must be noted that the hexagonal symmetry of the grapheme sheet changes in the x or y direction (see Figure 5.11) and, consequently, two sets of simulations are required. The simulations were carried out with the numerical code NAMD 2.6 developed by the Theoretical and Computational Biophysics Group in the Beckman Institute for Advanced Science and Technology at the University of Illinois at Urbana-Champaign [183]. Simulations were carried out at constant temperature of 400 K and with a time steps of 1 fs. There are certain issues concerning the equilibration phase and the initial polymer distribution that were solved following the procedure illustrated by Smith et al. [93].

The results show that the perfectly smooth graphene sheets do not cause any shear stress on the PVC. The PVC velocity profile obtained with a 10^8 m s^{-2} acceleration in the x direction is shown in Figure 5.12.
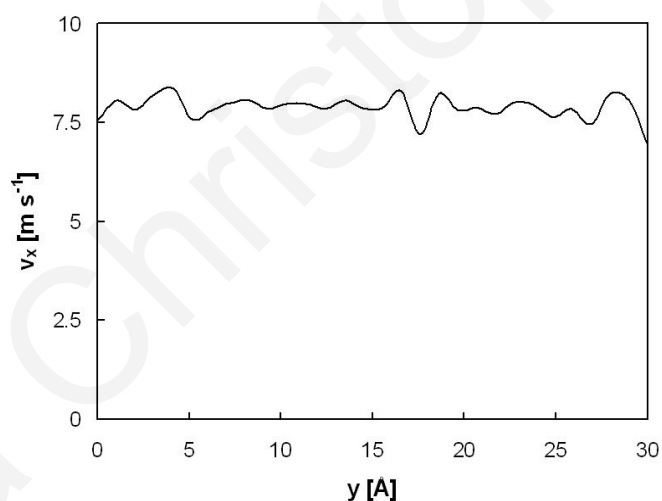
Figure 5.12 Velocity profile in the graphitic channel as a consequence of a 10^8 m/s^2 acceleration in the x direction

The profile in the graphitic channel, besides a certain statistical noise, which is typical of MD simulations, is approximately flat. This means that the flow in the channel is of the plug-flow type rather than Poiseuille-flow type. This behavior, although it can appear unusual to CFD people is not uncommon in systems of MD interest. Carbon nanotubes, in particular, show a similar behavior with water. Hanasaki et al. [187], for instance, demonstrated that water molecules move in a frictionless way inside a nanotube with, as in the case, a plug-flow velocity profile.

Chapter 6.   Conclusions and further work

6.1 Conclusions

The main aim of this research was achieved; this is the introduction of a new method for manufacturing various polymer foil nano- and microcomposites with different properties. The basis conclusions arising from this work are:

1. A novel, efficient, high speed and low cost polymer ultrasonic welding technique for manufacturing polymer-based nano- and microcomposite foils is introduced. Iron oxide (Fe_3O_4) and palladium (Pd) nanoparticles and carbon nanotubes (CNTs) in stabilized fluids, as well as cellulose acetate (CA) microfibrous membranes, were introduced to the interface of foils of poly(vinyl chloride) (PVC) and cellulose acetate (CA) matrices to prepare four different types of composite seams with various concentrations of embedded nanoparticles, CNTs and microfibers.

2. A uniform dispersion of the nanoparticles and micro-fibers all over the polymer matrices was achieved. This was the first critical stage of the proposed method.

3. The second stage of the proposed method comprises the proper joining of the polymer matrices, including the sandwiched layers of nanoparticles and micro-fibers and was also successfully achieved.

4. The research proceeded with the characterization of the nano- and micro-composites, demonstrating interesting mechanical and magnetic properties.

5. There is an optimum loading concentration of nanoparticles, CNTs and microfibers.

6. Finally, two mathematical models were analyzed, with the main purpose to understand different phenomena which occur during the fabrication of the aforementioned polymer-based nanocomposites. These are the vibrating forced motion of the nanoparticles into the weld and the molecular dynamic forces to the CNTs and PVC interface.

Conclusions concerning the microscopic characterization of the nano/micro-composite samples:

1. The microscopic analysis of the nanocomposites and CNTs-composites with low concentrations (up to ≈ 0.5 wt.%) showed that nanoparticles are uniformly dispersed all over the interface of the weld affected zone. Nanocomposites and CNTs-composites with higher concentrations resulted in structures with agglomerations.

2. The penetration of the nanoparticles into the welding zone depends mostly on three parameters: (a) the liquid carrier of the nano-suspensions, (b) the organic coating (stabilizing agent) of the nanoparticles, as well as (c) their concentration. In order to verify the previous statement, welding parameters as well as material selection were kept constant.

3. The width of the dispersed nanoparticles varies for the different nanocomposites.

4. The structures of the nanocomposites differs with the presence or the absence of the particle-surfactant.

Conclusions concerning the magnetic characterization of the nanocomposite samples:

1. Almost all of the composites prepared from the ferrofluids containing iron oxide nanoparticles (the Fe_3O_4-nanocomposites) exhibit superparamagnetic behavior, while

the rest demonstrated ferrimagnetic indicated by the presence of a small hysteresis.

2. Very promising magnetic properties were observed in the Sample 1 series of the Fe_3O_4-nanocomposites, produced by ferrofluids with hexanol-1 carrier liquid and double oleic acid stabilizing surfactant, since the samples exhibited very high saturation magnetization compared to similar composites produced with different nanofluids and techniques.

3. The saturation magnetization and the coercive field of the nanocomposites are strongly dependent on the nature of the liquid carrier, as well as the nature of surfactant double layer covering of magnetite nanoparticles. The coercive field remains constant until an optimum nanoparticle concentration ($\approx$ 2 wt.%).

Conclusions concerning the viscoelastic characterization of the nanocomposite samples:

1. No significant variations are observed in the viscoelastic properties of the nanocomposites with the addition of Fe_3O_4 nanoparticles into the PVC matrix. In particular, the storage modulus at 25°C for most of samples decreases with the increase of the Fe_3O_4 loading when compared with the pure ultrasonically welded PVC. The maximum of the loss modulus for the most of the series increases with the increase of the Fe_3O_4 nanoparticles, while the temperature range for the maximum changes independently from the nanoparticle loading. The Tg temperature is not influenced by the presence of the nanoparticles, while in general the nanocomposites have lower values of tanδ.

2. The change of the viscoelastic parameters has been explained in terms of a decrease of the molar mass, as well as by changes of the morphology of the manufactured nanocomposites due to the presence/embedding of with stabilizing layers coated nanoparticles between the polymer chains, which is believed that they act as plasticizers. The viscoelastic properties are mainly influenced by the distribution of nanoparticles into the nanocomposite matrix, their width into the polymer matrix, as well as the presence of agglomerations or not, the mechanism of nanoparticle penetration into the polymer matrix and possible chemical

interactions taking place between the nanoparticles and the nanoparticles with the polymer matrix. The combinations of surfactants used as stabilizing agents, as well as the carrier liquids of the nanoparticles also affect the final product.

3. The mechanism of penetration also changes after an optimum percentage of nanoparticles into the polymer matrix.

Conclusions concerning the mechanical characterization of the nanocomposite samples:

1. The distribution of nanoparticles and microfibers into the nanocomposite matrix, their concentration, their structure (coating, etc.), their depth into the polymer matrix, as well as the presence of agglomerations or not, the mechanism of nanoparticle penetration into the polymer matrix and possible chemical interactions all affect the mechanical properties of the nanocomposites.

2. The rigidity of Fe_3O_4/PVC and Pd/PVC nanocomposites is boosted because of the concentration of the nanocomposites to the welding zone, which may lead to the phase separation resulting to a slight decrease of the tensile strength. However, the inclusion of the surfactant-coated magnetic nanoparticles in low concentrations (0.1 - 0.3 wt.%) affect positively the mechanical behavior of the nanocomposites; most mechanical properties increase.

3. The mechanical properties of the CNTs/PVC, have been improved with the loading of the CNTs into to polymer matrix, until an optimum value of nanofiller concentration. Again, the optimum CNT concentrations are from 0.1 to 0.3 wt.%, while sh-CNTs seams to excel when compared with the long-CNTs.

4. CA/CA and CA/PAni micro-composites have also enhanced the mechanical properties of the polymer foils.

6.2 Further work

As further experimental work it is proposed to search for other combinations of polymer matrices with various embedded nanoparticles and nano-, microfibers, with different properties, in various concentrations. For example:

1. The idea of introducing clay-based nanoparticles seems to be very attractive, since there are good potentials according to the properties of the final products [58-61].

2. The inclusion of iron-oxide-containing nanofibers [188] seems to have also many potentials, since two different objectives can be reached; the magnetic properties provided from the iron-oxide nanoparticles, as well as the mechanical strength provided from the nano or micro fibers.

Attractive is also the study to prepare certain nano- and microcomposites by means of ultrasonic welding and change of the welding parameters which were kept constant in this thesis. This will help to optimize the process of manufacturing polymer nanocomposites and study further the penetration of nanoparticles and/or nano-microfibers into the polymer matrix [189].

Further work on the mathematic simulations is also of critical importance in order to explain in detail the phenomena occurring during the manufacturing of nano or micro-composites by means of ultrasonic welding. A multi-scale approach of the process in order to prevent the particle penetration into the polymer matrix, and further to prevent the properties of the nano/ micro-composites, seems very challenging. Further research is also needed on the molecular dynamics simulations to analyze the chemical bonds created at the interfaces of the composed parts.

Chapter 7.   Bibliography

[1]   M. F. Ashby, P. J. Ferreira, D. L. Schodek, Nanomaterials, Nanotechnologies and Design - An introduction for engineers and architects, UK: Elsevier Ltd, 2009.

[2]   Dr. M. Schulenburg, "Nanotechnology - Innovation for tomorrow's world," European Commission, Research DG, Cologne, 2004.

[3]   L. S. S. P. V. B. P. M. Ajayan, Nanocomposite Science and Technology, USA: Wiley-VCH Verlag GmbH & Co. KGaA, 2003.

[4]   P. S. Anton, R. Silberglitt, J. Schneider, "The global technology revolution - Bio/nano/materials trends and their synergies with information technology by 2015," RAND, CA, 2001.

[5]   A. D. Perrault, "Polymer nanocomposites are the future," University of Wisconsin-Stout, 2005.

[6]   W. E. Gacitua, A. A. Ballerini, J. Zhang, "Polymer nanocomposites: Synthetic and natural fillers a review," *Maderas. Ciencia y tecnologia,* vol. 7, no. 3, pp. 159-178, 2005.

[7]   R. A. Vaia, "Polymer nanocomposites open a new dimension for plastics and composites," *The AMPTIAC Newsletter,* vol. 6, no. 1, pp. 17-24, 2002.

[8]   A. I. Alateyah, H. N. Dhakal, Z. Y. Zhang, "Processing, properties, and applications

of polymer nanocomposites based on layer silicates: A review," *Advances in Polymer Technology,* vol. 32, no. 4, p. 21368, 2013.

[9] M. Soloviev, "Nanobiotechnology today: focus on nanoparticles," *Journal of Nanobiotechnology,* vol. 5, p. 11, 2007.

[10] Y. Sun, Y. Xia, "Shape-controlled synthesis of gold and silver nanoparticles," *Science,* vol. 298, no. 5601, pp. 2176-2179, 2002.

[11] J. Leadbitter, J. A. Day, J. L. Ryan, PVC - compounds, processing and applications, Shrewsbury, 1994.

[12] C. E. Wilkes, J. W. Summers, C. A. Daniels, M. T. Berard, PVC Handbook, Hanser Verlag, 2005.

[13] R. D. McMichael, R. D. Shull, L. J. Swartzendruber, L. H. Bennett, "Magnetocaloric effect in superparamagnets," *Journal of Magnetism and Magnetic Materials,* vol. 111, pp. 29-33, 1992.

[14] D. Lopez, I. Cendoya, F. Torres, J. Tejada and C. Mijangos, "Preparation and characterization of polystyrene-based magnetic nanocomposites. Thermal, mechanical and magnetic properties," *Polymer Engineering and Science,* vol. 41, pp. 1845-1852, 2001.

[15] Xu-J. Huang, F. Dong, L. Chen, Yi-Q. Li, "Nanopalladium immobilized on aminoethanol-functionalized poly(vinyl chloride): an easily prepared, air and moisture stable catalyst for Heck reactions," *Monatsh Chem,* vol. 139, pp. 1447-1451, 2008.

[16] C. Caliendo, G. Contini, I. Fratoddi, S. Irrera, P. Pertici, G. Scavia and M. V. Russo, "Nanostructured organometallic polymer and palladium/polymer hybrid: surface investigation and sensitivity to relative humidity and hydrogen in surface acoustic wave sensors," *Nanotechnology,* vol. 18, p. 125504, 2007.

[17] D. Meka, V. Onbattuvelli, S. Atre, S. Prasad, "Palladium/polymer nanocomposite

based chemiresistive SO2 sensor," in *Nanotech Conference Program Abstract 1*, 2008.

[18]   K. Scorczewska, D. Chmielewska, K. Piszczek, J. Tomaszewska, T. Sterzynski, "Obtaining PVC/CNT nanocomposites with the use of dispersing agents," *Chemic,* vol. 65, no. 4, pp. 337-342, 2011.

[19]   A. M. Kaushal, S. Garg, "An update on osmotic drug delivery patents," *Pharmaceutical Technology,* vol. 8, pp. 38-97, 2003.

[20]   Association, Global Acetate Manufacturers, "Environmentally degradable material made from a modified natural polymer (cellulose)," 2014. [Online]. Available: http://www.acetateweb.com/wp-content/uploads/2014/06/Att.10_GAMA-article-prf1.pdf.

[21]   S. Fischer, K. Thummler, B. Volkent, K. Hettrich, I. Schmidt, K. Fischer, "Properties and applications of cellulose acetate," *Macromolecular Symposia,* vol. 262, no. 5, pp. 89-96, 2008.

[22]   M. Hubbe, O. Rojas, L. Lucia and M. Sain, "Cellulosic nanocomposites: A review," *BioResources,* vol. 3, no. 3, pp. 929-980, 2008.

[23]   E. Entcheva, H. Bien, L. Yin, C-Y Chung, M. Farrell, Y. Kostov, "Functional cardiac cell constructs on cellulose-based scaffolding," *Biomaterials,* vol. 25, no. 26, pp. 5753-5762, 2004.

[24]   D. Han, P. I. Gouma, "Electrospun bio-scaffolds that mimic the topology of extracellular matrix," *Nanomedicine: Nanotechnology, Biology and Medicine,* vol. 2, pp. 37-41, 2006.

[25]   S. M. Phadke, Quality Engineering Using Robust Design, New Jersey: Prentice Hall, 1989.

[26]   C. Ageorges, L. Ye, M. Hou, "Advances in fusion bonding techniques for joining thermoplastic matrix composites: A review," *Composites: Part A,* vol. 32, pp. 839-

857, 2001.

[27]   S. M. Phadke, Quality Engineering Using Robust Design, New Jersey: Prentice Hall, 1989.

[28]   A. Benatar, T. Gutowski, "Ultrasonic welding of PEEK graphite APC-2 composites," *Polymer Engineering and Science,* vol. 29, pp. 1705-1721, 1989.

[29]   D. C. Montgomery, Design and Analysis of Experiments, New York: 3rd, Wiley & Sons, 1991.

[30]   G. S. Peace, Taguchi Methods, New York: Addison-Wesley, 1993.

[31]   S. Matsuoka, "Ultrasonic welding and characteristics of glass-fiber reinforced plastic: Comparison between the paper-making method and the impregnation method," *Journal of Materials Processing Technology,* vol. 55, pp. 427-431, 1995.

[32]   B. Harras, K. C. Cole, T. Vu-Khanh, "Optimization of the ultrasonic welding of PEEK-carbon composites," *Journal of Reinforced Plastics & Composites,* vol. 15, pp. 174-182, 1996.

[33]   C. A. Butler, R. L. Mc-Cullough, R. Pitchumani, and W. J. Gillespieet, "An analysis of mechanisms governing fusion bonding of thermoplastic composites," *Journal of Thermoplastic Composite Materials,* vol. 11, pp. 338-363, 1998.

[34]   S. Liu, I. Chang, "Optimizing the weld strength of ultrasonically welded nylon composites," *Journal of Composite Materials,* vol. 36, pp. 611-624, 2002.

[35]   A. P. Costa, E. C. Botelho1, M. L. Costa, N. E. Narita, J. R. Tarpani, "A Review of welding technologies for thermoplastic composites in aerospace applications," *Journal of Aerospace Technology and Management,* vol. 4, no. 3, pp. 255-265, 2012.

[36]   A. Christophidou, C. Doumanidis, "Ultrasonic welding of polymer nanocomposites," in *3th International Symposium on Nanomanufacturing*, Cyprus,

2005.

[37] A. Christophidou, D. Bica, N. Crainic, L. Vekas, C. Doumanidis, "Structural and dynamic mechanical analysis of magnetic nanocomposites by polymer ultrasonic welding," in *4th International Symposium on Nanomanufacturing*, Boston, 2006.

[38] A. Christophidou, Z. Viskadourakis, C. Doumanidis, "Structural, magnetic and dynamic mechanical analysis of magnetic nanocomposite foils by polymer ultrasonic welding," *Journal of Nano Research,* vol. 10, pp. 39-47, 2010.

[39] S. C. Tjong, "Structural and mechanical properties of polymer nanocomposites," *Materials Science and Engineering. A Review journal,* pp. 73-197, 2006.

[40] J. H. Koo, Polymer nanocomposites, processing, characterization and, applications, New York: McGraw-Hill Nanoscience and Technology Series, 2006.

[41] E. Manias, "Nanocomposites: stiffer by design," *Nature Materials,* vol. 6, no. 1, pp. 9-11, 2007.

[42] H. D. Wagner, "Nanocomposites paving the way to stronger materials," *Nature Nanotechnology,* vol. 2, pp. 742-744, 2007.

[43] M. Xanthos, Functional Fillers for Plastics. Chapter 1: Polymers and polymer composites, Wiley Online Library, 2007.

[44] V. Mittal, Optimization of Polymer Nanocomposite Properties, Wiley, 2010.

[45] A. Usuki, Y. Kojina, M. Kawasumi, A. Okada, Y. Fukushina, T. Kurauchi, and O. Kamigaito, "Synthesis of nylon 6-clay hybrid," *Journal of Materials Research,* vol. 8, p. 1179, 1993.

[46] J. K. Pandey, K. R. Reddy, A. K. Mohanty, M. Misra, Handbook of polymernanocomposites. Processing, performance and application: Volume A: Layered silicates, New York: Springer Science & Business Media, 2014.

[47] C. Edser , "Auto applications drive commercialization of nanocomposites," *Plastics, Additives and Compounding,* vol. 4, no. 1, pp. 30-33, 2002.

[48] M. Mohseni, B. Ramezanzadeh, H. Yari and M. Gudarzi, "The role of nanotechnology in automotive industries," Intech, 2012.

[49] J. Njugama, "Polymer nanocomposites with corbon nanotubes in aerospace and defence," in *Polymers in Defence and Aerospace*, Toulouse, France, 2007.

[50] D. Wood, "Challenges for lightweight design aircraft structure," in *Polymers in Defence and Aerospace*, Toulouse, France, 2007.

[51] I. Dinca, C. Ban, A. Stefan, G. Pelin, "Nanocomposites as advanced materials for aerospace industry," *Incas Bulletin,* vol. 4, no. 4, pp. 73-83, 2012.

[52] D. King, O. Inderwildi, C. Carey, "Advanced aerospace materials: past, present and future," Oxford University's Smith School of Enterprise and the Environment, UK, 2009.

[53] Boeing, "787 Commercial transport - Historical snapshot," 2009. [Online]. Available: http://www.boeing.com/history/products/787.page.

[54] Boeing, "Air tahiti nui finalizes order for two 787-9 Dreamliners," 2013. [Online]. Available: http://www.boeing.com/commercial/customers/air-tahiti-nui/air-tahiti-nui-finalize-order-for-two-787-9-dreamliners.page.

[55] O. Rodrıguez-Fernandez, C. Rodrıguez-Calzadıaz, I. Yanez-Flores, S. Montemayor, "Preparation and characterization of magneto-polymeric nanocomposite: Fe3O4 nanoparticles in a grafted, cross-linked and plasticized poly(vinyl chloride) matrix," *Journal of Magnetism and Magnetic Materials,* vol. 320, pp. 81-84, 2008.

[56] I. Yanez-Flores, R. Betancourt-Galindo, J.Matutes-Aquino, O. Rodrıguez-Fernandez, "Preparation and characterization of magnetic PVC nanocomposites," *Journal of Non-Crystalline Solids,* vol. 353, pp. 799-801, 2007.

[57]   M. Vazquez, C. Luna, M. Morales, R. Sanz, C. Serna, C. Mijangos, "Magnetic nanoparticles: synthesis, ordering and properties," *Physica B,* vol. 354, pp. 71-79, 2004.

[58]   X. L. Xie, Q. X. Liu, R. K. Y. Li, X. P. Zhou, Q. X. Zhang, Z. Z. Yu, Y. W. Mai, "Rheological and mechanical properties of PVC/CaCO3 nanocomposites prepared by in situ polymerization," *Polymer,* vol. 45, pp. 6665-6673, 2004.

[59]   Y. Yoo, S.S. Kim, J.C. Won, K.Y. Choi, J.H. Lee,, "Enhancement of the thermal stability, mechanical properties and morphologies of recycled PVC/clay nanocomposites," *Polymer Bulletin,* vol. 52, pp. 373-380, 2004.

[60]   T. Krasia-Christoforou, "Chapter 2. Organic–inorganic polymer hybrids: Synthetic strategies and applications," in *Hybrid and Hierarchical Composite Materials*, Switzerland, Springer, 2015, pp. 11-64.

[61]   B. Chen, "Polymer-clay nanocomposites: an overview with emphasis on interaction mechanisms," *British Ceramic Transactions,* vol. 103, pp. 241-249, 2004.

[62]   A. Brody, ""Nano, nano" Food packaging technology," *Food Technology,* pp. 52-54, 2003.

[63]   A. Zihlif, G. Ragosta, "A study on the physical properties of rock wool fibe - Polystyrene composite," *Journal of Thermoplastic Composite Materials,* vol. 16, no. 3, pp. 273-283, 2003.

[64]   V. K. Stokes, S. Y. Hobbs, "Strength and bonding mechanisms in vibration-welded polycarbonate to polyetherimide joints," *Polymer Engineering and Science,* vol. 29, no. 23, pp. 1667-1676, 1989.

[65]   S. H. McKnight, S. T. Holmes, J. W. Gillespie, C. T. Lambing, J. M. Marine, "Scaling issues in resistance-welded thermoplastic composite joints," *Advances in Polymer Technology,* vol. 16, no. 4, p. 279–295, 1997.

[66]   A. Yousefpour, M. Hojjati, J-P. Immarigeon, "Fusion bonding/welding of thermoplastic composites," *Journal of Thermoplastic Composite Materials,* pp. 303-341, 2004.

[67]   V. K. Stokes, "Joining methods for plastics and plastic composites: An overview," *Polymer Engineering and Science,* vol. 29, no. 19, pp. 1310-1324, 1989.

[68]   M. J. Troughton, Handbook of Plastics Joining-A Practical Guide, 2nd ed., William Andrew Inc., 2008.

[69]   J. L. Jellison, C. E. Albright, J. Devine, G. Harmon, G.A. Knorovsky, V. H. Winchell, Welding Handbook, 8th ed., Vols. Chapter 25, Ultrasonic welding, American Welding Society, 1991.

[70]   H. V. Wijk, A. G. Luiten, G. P. Engen, and J. C. Nonhof, "Process optimization of ultrasonic welding," *Polymer Engineering and Science,* vol. 36, no. 9, pp. 1165-1176, 1996.

[71]   J. C. Nonhof, A. G. Lutten, "Estimates for process conditions during the ultrasonic welding of thermoplastics," *Polymer Engineering and Science,* vol. 36, no. 9, pp. 1177-1183, 1996.

[72]   L. E. Chemistry, "Ultrasonic welding," [Online]. Available: https://techcenter.lanxess.com/scp/americas/en/techServscp/77022/article.jsp?docId=86732.

[73]   Graftech Coorporation, "Ultrasonic welding - Sonic welding," 2015. [Online]. Available: http://www.craftechcorp.com/ultrasonic-welding/.

[74]   Z. Mao, C. B. Goswami, "Studies on the process of ultrasonic bonding of nonwovens: Part 1 – Theoretical analysis," *International Nonwovens Journal,* vol. Part 1, pp. 38-47, 2001.

[75]   Z. Mao, C. B. Goswami, "Studies on the process of ultrasonic bonding of nonwovens: Part 2 – Experiments and results," *International Nonwovens Journal,*

vol. 2, pp. 17-28, 2001.

[76]   J. Hornstein , "Ultrasonic assembly of plastic parts," in *Proceedings of the Regional Technical Conference on Decorating*, 1996.

[77]   A. Benatar, Z. Cheng, "Ultrasonic welding of thermoplastics in the far-field," *Polymer Engineering and Science,* vol. 29, no. 23, pp. 1699-1704, 1989.

[78]   W. Shi, T. Little, "Mechanisms of ultrasonic joining of textile materilas," *International Journal of Clothing Science and Technology,* vol. 12, no. 5, pp. 331-350, 2000.

[79]   R. Rashli, E. A. Bakar, S. Kamaruddin, A. R. Othaman, " A review of ultrasonic welding of thermoplastic composites," *Caspian Journal of Applied Sciences Research,* vol. 2, no. 3, pp. 1-16, 2013.

[80]   N. M. Tolunary, R. P. Dawson, K. K. Wang, "Heating and bonding mechanisms in ultrasonic welding of thermoplastics," *Polymer Engineering and Science,* vol. 23, pp. 726-733, 1983.

[81]   Y. Ming, S. L. Fu, S. Zheng, "A new optimization method for horn designs in ultrasonic welding systems," 2002.

[82]   G. Coffignal, M. Touratieer, "A computer aided program for the tuning of ultrasonic machining tools using the finite element method," in *Proceedings of Ultrasonics International*, 1986.

[83]   A. Benatar, R. V. Eswaran, S. K. Nayar, "Ultrasonic welding of thermoplastics in the near-field," *Polymer Engineering and Science,* vol. 29, no. 23, pp. 1689-1698, 1989.

[84]   D. Grewell, A. Benatar, "Welding of plastics: Fundamentals and new developments," *International Polymer Processing XXII,* pp. 43-60, 2007.

[85]   PhD Craig Freudenrich, "How ultrasonic welding works," 22 March 2011. [Online]. Available: http://science.howstuffworks.com/ultrasonic-welding2.htm.

[86]   L. W. Land, "Investigations into the process of ultrasonic welding," *Kunststoffe,* vol. 68, no. 4, pp. 16-18, 1978.

[87]   P. Rempp, E. W. Merrill, Polymer Synthesis, New York: Huthig & Wepf, 1991.

[88]   A. D. Maher, P. Walkin, "Ultrasonic welding of thermoplastics," *British Plastics,* vol. 38, no. 7, p. 436, 1965.

[89]   H. P. Daniells, "Welding of metals and plastic foils," *Ultrasonics,* p. 220, 1966.

[90]   Branson, "Characteristics and compatibility of thermoplastics for ultrasonic assembly," Branson Ultrasonics Corporation, USA, 1995.

[91]   S. Thomas, G. E. Zaikov, S. V. Valsaraj, A. P. Meera, Recent Advances in Polymer Nanocomposites: Synthesis and Characterisation, Taylor and Francis Group, 2010.

[92]   Q. Xiaoyun, H. Shuwen, ""Smart" materials based on cellulose: A review of the preparations, properties, and applications," *Materials,* vol. 6, pp. 738-781, 2013.

[93]   J. R. Smith et al., Scientific and technical assessment report on vinyl chloride and polyvinyl chloride, Washington: U.S. Environmental Protection Agency; Office of Research and Development, 1975.

[94]   S. G. Patrick, Practical Guide to Polyvinyl Chloride, UK: Rapra Technology Ltd, 2005.

[95]   K. Kamide, Cellulose and Cellulose Derivatives, USA: Elsevier, 2005.

[96]   D. Bica, L. Vekas, M. V. Avdeev, M. Balasoiu, O. Marinica, F. D. Stoian, D. Susan-Resiga, G. Torok, L. Rosta, "Magnetizable colloids on strongly polar carriers - preparation and manifold characterization," *Progress in Polymer Science,* vol. 125, pp. 1-9, 2004.

[97]   D. Bica, "Preparation of magnetic fluids for various applications," *Romanian Reports in Physics,* vol. 47, pp. 265-272, 1995.

[98] D. Bica, L. Vekas, M. Rasa, "Preparation and magnetic properties of concentrated magnetic fluids on alcohol and water carrier liquids," *Journal of Magnetism and Magnetic Materials,* vol. 252, pp. 10-12, 2002.

[99] D. Bica, L. Vekas, M. V. Avdeev, O. Marinica, V. Socoliuc, M. Balasoiu, V. M. Garamus, "Sterically stabilized water based magnetic fluids: synthesis, structure and properties," *Journal of Magnetism and Magnetic Materials,* vol. 311, pp. 17-21, 2007.

[100] S. Odenbach, "Ferrofluids/magnetically controlled suspensions," *Colloids and Surfaces A: Physicochemical and Engineering Aspects,* vol. 217, pp. 171-178, 2003.

[101] X. L. Xie, Y. W. Mai, X.P.Zhou, "Dispertion and alignment of carbon nanotubes in polymer matrix: A review," *Materials Science and Engineering,* vol. 49, pp. 89-112, 2005.

[102] J. P. Salvetat, G. Desarmot, C. Gauthier and P. Poulin, "Mechanical properties of individual nanotubes and composites," *Lecture Notes in Physics,* vol. 677, pp. 439-493, 2006.

[103] P. Liu, "Modifications of carbon nanotubes with polymers," *European Polymer Journal,* vol. 41, p. 2693–2703, 2005.

[104] C. Velasco-Santos, A. L. Martinez-Hernandez and V. M. Castano, "Carbon nanotube-polymer nanocomposites: The role of interfaces. A Review," *Composite Interfaces,* vol. 11, no. 8-9, p. 567–586, 2005.

[105] S. K. Swain, I. Jena, "Polymer/carbon nanotube nanocomposites: A novel material (review)," *Asian Journal of Chemistry,* vol. 22, no. 1, pp. 1-15, 2010.

[106] Y. S. Song, J. R. Youn, "Influence of dispersion states of carbon nanotubes on physical properties of epoxy nanocomposites," *Carbon,* vol. 43, pp. 1378-1385, 2005.

[107] L. Mau, A. Dai, "Controlled synthesis and modification of carbon nanotubes and C60: Carbon nanostructures for advanced polymeric composite materials," *Advanced Materials,* vol. 13, pp. 899-913, 2001.

[108] Y. Mamunya, A. Boudenne, N. Lebovka, L. Ibos, Y. Candau, M. Lisunova, "Electrical and thermophysical behaviour of PVC-MWCNT nanocomposites.," *Composites Science and Technology,* vol. 68, p. 1981–1988, 2008.

[109] S. Sathyanarayana, C. Hübner, "Thermoplastic nanocomposites with carbon nanotubes," *Structural Nanocomposites,* pp. 19-60, 2013.

[110] M. S. Vasanthkumar, B. Ravi, P. A. Ved, I. Sameera, V. Prasad, H. S. Jayanna, "Characterization, charge transport and magnetic properties of multy-walled carbon nanotube-polyvinyl chloride nanocomposites," *Physica E,* vol. 56, pp. 10-16, 2014.

[111] V. Mittal, Polymer nanotube nanocomposites: Synthesis, properties, and applications, Chapter 4, Willey, 2010, pp. 83-113.

[112] S. Thomas,G. E. Zaikov, Polymer nanocomposite research advances, Chapter 7, New York: Nova Science Publisher, 2008, p. 229.

[113] P. Mukhopadhyay, R. K. Gupta, Graphite, graphene, and their polymer nanocomposites, Chapter 10, New York: Taylor & Francis Group, 2013, pp. 367-372.

[114] R. Jung, H. S. Kim, H. J. Jin, "Multiwalled carbon nanotube-reinforced poly(vinyl chloride)," *Macromolecular Symposia,* pp. 259-264, 2007.

[115] G. Broza, K. Piszczek, K. Schulte, T. Sterzynski, "Nanocomposites of poly(vinyl chloride) with carbon nanotubes (CNT)," *Composites Science and Technology,* vol. 67, pp. 890-894, 2007.

[116] M. Chipara, et al, "Polyvinylchloride-single-walled carbon nanotube composites:

Thermal and spectroscopic properties," *Journal of Nanomaterials,* pp. 1-6, 2012.

[117] A. Aljaafari, M. A. Abdeen and M. Aljaafari, "Mechanical and electrical properties of poly(vinyl chloride) loaded with carbon nanotubes and carbon nanopowder," *Journal of Thermoplastic Composite Materials,* vol. 25, no. 6, pp. 679-699, 2012.

[118] A. Dufrense, M. R. Vignon, "Improvement of starch film performances using cellulose microfibrils," *Macromolecules,* vol. 31, pp. 2693-2696, 1988.

[119] A. Dufresne, J. Y. Cavaille, M. R. Vignon, "Mechanical behavior of sheets prepared from sugar beet cellulose microfibrils," *Journal of Applied Polymer Science,* vol. 64, pp. 1185-1194, 1997.

[120] C. J. Nonhof, G. A. Lutten, "Estimates for process conditions during the ultrasonic welding of thermoplastics," *Polymer Engineering and Science,* vol. 36, no. 9, pp. 1177-1183, 1996.

[121] V. H. Wijk, A. G. Luiten, G. P. Engen, J. C. Nonhof, "Process optimization of ultrasonic welding," *Polymer Engineering and Science,* vol. 36, no. 9, pp. 1165-1176, 1996.

[122] Y. K. Chuah, L. H. Chien, B. C. Chang, S. J. Liu, "Effects of the shape of the energy director on far-field ultrasonic welding of thermoplastics," *Polymer Engineering and Science,* vol. 40, no. 1, pp. 157-167, 2000.

[123] A. Tsai, "Mechanical and thermal modeling of plastic ultrasonic welding based on variable pressure curves," Tufts University, 2002.

[124] K. S. Suresh, M. R. Rani, K. Prakasan, R. Rudramoorthy, "Modeling of temperature distribution in ultrasonic welding of thermoplastics for various joint designs," *Journal of Materials Processing Technology,* vol. 186, p. 138–146, 2007.

[125] A. Levy, S. Le Corre, A. Poitou, E. Soccard, "Time homogenization for the modeling and simulation of the ultrasonic welding of thermoplastic composites," in *The 9th International Conference on Flow Processes in Composite Materials*, Canada, 2008.

[126] A. Levy, S. L. Corre, N. Chevaugeon, A. Potiou, "A level set based approach for finite element simulation of a forming process involving multiphysics coupling: Ultrasonic welding of thermoplastic composites," *European Journal of Mechanics / A Solids,* vol. 30, no. 4, pp. 501-509, 2011.

[127] A. Levy, S. L. Corre, I. F. Villegasc, "Modeling of the heating phenomena in ultrasonic weldingof thermoplastic composites with flat energy directors," *Journal of Materials Processing Technology,* vol. 214, pp. 1361-1371, 2014.

[128] Fermi, Pasta and Ulam, "Studies in non-linear problems," *American Mathematical Monthly,* vol. 74, no. 1, 1967.

[129] B. Arash, Q. Wang, V. K. Varadan, "Mechanical properties of carbon nanotube/polymer composites," *Scientific Reports,* vol. 4, pp. 6479-6486, 2014.

[130] Y. Li, G. D. Seidel, "Multyscale modeling of the effects of nanoscale load transfer on the effective elastic properties of unfuctionalized carbon nanotube-polyethylene nanocomposites," *Modeling and Simulation in Materials Science and Engineering,* vol. 22, p. 28, 2014.

[131] K. C. Lo, S. Y. Li, W. K. Chan, "Photoconductivity enhancement and charge transport properties in a conjugated polyelectrolyte/carbon nanotube hybrid studied by scanning probe microscopy," *Royal Society of Chemistry,* vol. 2, pp. 7739-7751, 2014.

[132] Y. Han, J. Elliott, "Molecular dynamics simulations of the elastic properties of polymer/carbon nanotube composites," *Computational Materials Science,* vol. 39, no. 2, p. 315–323, 2007.

[133] E. Zaminpayma, K. Mirabbaszadeh, "Interaction between single-walled carbon nanotubes and polymers: A molecular dynamics simulation study with reactive force field," *Computational Materials Science,* vol. 58, pp. 7-11, 2012.

[134] C. Hall, Polymer Materials - An introduction for technologists and scientists,

Appendix B, London: Macmillan, 1989.

[135] I. L. Gomez, Engineering with rigid PVC: Processability and applications, New York: Marcel Dekker, 1984, pp. 1-12.

[136] W. V. Titow, PVC Technology, Fourth Edition ed., USA: Elsevier Applied Science Publishers, 1986, p. Chapter 1.

[137] J. Leadbitter, J. A. Day, J. L. Ryan, PVC - Compounds, processing and applications, vol. 7, Rapra Technology Ltd, 1994, pp. 5-16.

[138] H. K. Lonsdale, U. Merten, R. L. Riley, "Transport properties of cellulose acetate osmotic membranes," *Journal of Applied Polymer Science,* vol. 9, no. 4, pp. 1341-1362, 1965.

[139] Goodfellow, "Data report," Goodfellow Cambridge Limited, England, 2012.

[140] J. E. Mark, Polymer Data Handbook, Oxford University Press, Inc., 1999.

[141] R. Klein, Laser Welding of Plastics, Wiley-VCH Verlag GmbH & Co. KGaA, 2011, p. Chapter 1: Material Properties of Plastics.

[142] L. Vekas, D. Bica, M. Avdeev, "Magnetic nanoparticles and concentrated magnetic nanofluids: Synthesis, properties and some applications," *China Particuology,* vol. 5, pp. 43-49, 2007.

[143] J. A. Lopez, F. González, F. A. Bonilla, G. Zambrano, M. E. Gómez, "Synthesis and characterization of Fe3O4 magnetic nanofluid," *Revista Latinoamericana de Metalurgia y Materiales,* vol. 30, pp. 60-66, 2010.

[144] L. L. Vatta, R. D. Sanderson, K. R. Koch, "Magnetic nanoparticles: Properties and potential applications," *Pure and Applied Chemistry ,* vol. 78, p. 1793–1801, 2006.

[145] L. Merhari, "Chapter 11. Polymer-iron oxide based magnetic nanocomposites," in *Hybrid nanocomposites for nanotechnology: Electronic, optical, magnetic and*

biomedical applications, Springer Science & Business Media, 2009, pp. 454-506.

[146] L. Vekas, D. Bica, O. Marinica, "Magnetic nanofluids stabilized with various chain length surfactants," *Romanian Reports in Physics,* vol. 58, no. 3, p. 257–267, 2006.

[147] L. R. Arco, A. G. Ramírez, J. D.G. Durán, M. T. L. López, "Chapter 17. New perspectives for magnetic fluid-based devices using novel ionic liquids as carriers," in *Intech*, 2012, pp. 445-464.

[148] Pubchem, "Open chemistry database. Oleic acid," 2015. [Online]. Available: http://pubchem.ncbi.nlm.nih.gov/compound/oleic_acid.

[149] B. Sampedro, A. Hernando, "Magnetic behaviour of Pd nanoparticles," *Physica Status Solidi,* vol. 12, p. 3670–3672, 2004.

[150] A. M. Schmidt, "Thermoresponsive magnetic colloids," *Colloid & Polymer Science,* vol. 258, pp. 953-966, 2007.

[151] M. Zervos, M. Demetriou, T. Krasia-Christoforou, A. Othonos, R. P. Turcu, "Synthesis of hybrid polymethacrylate-noble metal (M = Au, Pd) nanoparticles for the growth of metal-oxide semiconductor nanowires," *RSC Advances,* vol. 2012, no. 2, pp. 4370-4376, 2007.

[152] K. Iliopoulos, G. Chatzikyriakos, M. Demetriou, T. Krasia-Christoforou, S. Couris, "Preparation and nonlinear optical response of novel palladium-containing micellar nanohybrids," *Optical Materials,* vol. 33, pp. 1342-1349, 2011.

[153] V. A. Ryzhkov , "Carbon nanotube production by a cracking of liquid hydrocarbons," *Physica B,* vol. 323, no. 1-4, 2002.

[154] Rosetter Holdings Ltd, "Nanotube products," 2001. [Online]. Available: http://www.e-nanoscience.com/products.html#.

[155] S.A. Nanocyl, "Aquacyl 0101 material safety data sheet," Nanocyl S.A., Belgium, 2008.

[156] S. A. Nanocyl, "Nanocyl NC7000 series - Product datasheet - Thin multi-wall carbon nanotubes," Nanocyl S.A., Belgium, 2009.

[157] T. Christoforou, "Biodegradable cellulose acetate nanofiber fabrication via electrospinning," Department of Mechanical and Manufacturing Engineering, University of Cyprus, Cyprus, 2009.

[158] T. Subbiah, G. S. Bhat, R. W. Tock, S. Parameswaran, S. S. Ramkumar, "Journal of Applied Polymer Science," *Electrospinning of nanofibers,* vol. 96, p. 557–569, 2005.

[159] C. H. Hong, S. J. Ki, J. H. Jeon, H. L. Che, I. K. Park, C. D. Kee, I. K. Oh, "Electroactive bio-composite actuators based on cellulose acetate nanofibers with specially chopped polyaniline nanoparticles through electrospinning," *Composites Science and Technology ,* vol. 87, pp. 135-141, 2013.

[160] F. Rodrı guez, M. M. Castillo-Ortega, J. C. Encinas, H. Grijalva, F. Brown, V. M. Sa nchez-Corrales, V. M. Castano, "Preparation, characterization, and adsorption properties of cellulose acetate-polyaniline membranes," *Journal of Applied Polymer Science,* vol. 111, no. 3, pp. 1216-1224, 2009.

[161] M. Benz, "Superparamagnetism: Theory and applications," 2012.

[162] M. Hanson, C. Johanssoon, M. S. Pedersen, S. Morup, "The infuence of particle size and interactions on the magnetization and susceptibility of nanometre-size particles," *Journal of Physics: Condensed Matter,* vol. 7, pp. 9269-9277, 1995.

[163] R. Sanz, C. Luna, M. H. Velez, M. Vazquez, D. Lopez, C. Mijangos, "A magnetopolymeric nanocomposite: Co80Ni20 nanoparticles in a PVC matrix," *Nanotechnology,* vol. 16, pp. S278-S281, 2005.

[164] I.G. Flores, R. B. Galindo, J. A. Aquino, O. R. Fernandez, "Preparation and characterization of magnetic PVC nanocomposites," *Journal of Non-Crystalline Solids,* vol. 353, pp. 799-801, 2007.

[165] O. S. R-Fernandez, C. A. R-Calzadiaz, I. G. Y-Flores, S. M. Montemayor, "Preparation and characterization of a magneto-polymeric nanocomposite: Fe3O4 nanoparticles in a grafted, cross-linked and plasticized poly(vinyl chloride) matrix," *Journal of Magnetism and Magnetic Materials,* vol. 320, pp. e81-e84, 2008.

[166] T. Sabu, Z. Gennady, Valsaraj, Meera, Recent Advances in Polymer Nanocomposites: Synthesis and Characterisation, U.S.: Taylor & Francis Group, 2010, pp. 137-154.

[167] J. Loffler, H. V. Swygenhoven, W. Wagner, J. Meier, B. Doudin, J. P. Ansermet, "Influence of grain size and oxidation on the magnetic properties of nanostructured Fe and Ni," *Nanostructured Materials,* vol. 9, pp. 523-526, 1997.

[168] W. D. Callister, Materials Science and Engineering. An Introduction, New York: John Wiley & Sons, Inc, 2007.

[169] K. P. Menard, Dynamic Mechanical Analysis. A practical introduction, New York: Taylor & Francis Group, LLC, 2008.

[170] A. Jelen, V. Bukosek, J. Dolinsek, "Viscoelastic properties and reinforcement performance of the MoS2 nanotubes-polymer composite," *International Journal of Material Science,* vol. 2, no. 1, pp. 20-26, 2012.

[171] X. Yan, Q. He, X. Zhang et all, "Magnetic polystyrene nanocomposites reinforced with magnetite nanoparticles," *Macromolecular Materials and Engineering,* vol. 299, pp. 485-494, 2014.

[172] S. Chen, S. Zhang, Y. Li, G. Zhao, "Synthesis and properties of novel UV - curable hyperbranched waterborne polyurethane/Fe3O4 nanocomposite films excellent magnetic properties," *Royal Society of Chemistry,* vol. 5, pp. 4355-4363, 2015.

[173] B. Yalcin, M. Cakmak, "Nanocomposites based on poly(vinyl chloride)," in *Recent Advances in Polymer Nanocomposites: Synthesis and Characterisation*, FL, Taylor & Francis Group, 2010, pp. 137-154.

[174] R. Clift, J. R. Grace and M. E. Weber, Bubbles, Drops and Particles, vol. Chapter 11, New York: Academic Press, 1978.

[175] M. Hasan, M. Lee, "Enhancement of the thermo-mechanical properties and efficacy of mixing technique in the preparation of graphene/PVC nanocomposites compared to carbon nanotubes/PVC," *Progress in natural science: Materials international,* vol. 24, no. 6, p. 579–587, 2014.

[176] C. Liu, Y. F. Luo, Z. X. Jia, B. C. Zhong, S. Q. Li, B. C. Guo, D. M. Jia, "Enhancement of mechanical properties of poly(vinyl chloride) with polymethyl methacrylate-grafted halloysite nanotube," *eXPRESS Polymer Letters,* vol. 5, no. 7, p. 591–603, 2011.

[177] Song BJ1, Ahn JW, K.K. Cho, J. S. Roh, D. Y. Lee, Y. S. Yang, J. B. Lee, D. Y. Hwang, H. S. Kim , "Electrical and mechanical properties as a processing condition in polyvinylchloride multi walled carbon nanotube composites," *Journal of Nanoscience and Nanotechnology,* vol. 13, no. 11, pp. 7723-7727, 2013.

[178] A. R. Zanjanijam, M. Bahrami, M. Hajian, "Poly(vinyl chloride)/single wall carbon nanotubes composites: Investigation of mechanical and thermal characteristics," *Journal of Vinyl & Additive Technology,* p. 10.1002, 2014.

[179] Karniadakis, Beskok, Aluru, Microflows and Nanoflows Fundamentals and Simulation, Springer, 2004.

[180] J. E. Lennard-Jones, "Cohesion," *Proceedings of the Physical Society,* vol. 43, pp. 461-482, 1931.

[181] P. P. Ewald, *Annual Physics,* no. 64, pp. 253-287, 1921.

[182] T. Darden, D. York, L. Pedersen, "Particle mesh Ewald: An N· log (N) method for Ewald sums in large systems," *Journal of Chemical Physics,* vol. 98, p. 10089–10092, 1993.

[183] J. C. Phillips et al., "Scalable molecular dynamics with NAMD," *Journal of Computational Chemistry,* vol. 26, p. 1781–1802, 2005.

[184] D. A. Pearlman et. al, "AMBER, a package of computer programs for applying molecular mechanics, normal mode analysis, molecular dynamics and free energy calculations to simulate the structural and energetic properties of molecules," *Computer Physics Communications,* vol. 91, pp. 1-41, 1995.

[185] G. D. Smith, R. L. Jaffe, D. Y. Yoon, "Conformations and order in atactic poly(vinyl chloride) melts from molecular dynamics simulations," *Macromolecules,* vol. 26, no. 2, pp. 298-304, 1993.

[186] V. P. Sokhan, D. Nicholson, N. Quirke, "Fluid flow in nanopores: Accurate boundary conditions for carbon nanotubes," *Journal of Chemical Physics,* vol. 117, p. 8531–8539, 2002.

[187] I. Hanasaki, A. Nakatani, "Flow structure of water in carbon nanotubes: Poiseuille type or plug-like?," *Journal of Chemical Physics,* vol. 124, no. 14, p. 144708, 2006.

[188] E. Ghasemia, H. Ziyadia, A. M. Afshara, M. Sillanpää, "Iron oxide nanofibers: A new magnetic catalyst for azo dyes degradation in aqueous solution," *Chemical Engineering Journal,* pp. 146-151, 2015.

[189] Herrmann Electronics, "Ultrasonic welding technology. Basics of plastics," Herrmann Ultrasonics, Inc., USA, 2014.